

Role of Integrin-linked kinase in extracellular matrix  
remodeling and cell fate decisions

Inaugural-Dissertation

zur

Erlangung des Doktorgrades

der Mathematisch-Naturwissenschaftlichen Fakultät

der Universität zu Köln

vorgelegt von

Jessica Morgner

aus Düsseldorf

Berichterstatter: Dr. Sara A. Wickström  
Prof. Dr. Matthias Hammerschmidt  
Prüfungsvorsitzender: Prof. Dr. Mats Paulsson  
Tag der mündlichen Prüfung: 25.11.2014



<b>ABSTRACT</b>	<b>7</b>
<b>ZUSAMMENFASSUNG</b>	<b>9</b>
<b>1 INTRODUCTION</b>	<b>11</b>
<b>1.1 THE EXTRACELLULAR MATRIX</b>	<b>11</b>
1.1.1 COLLAGENS	12
1.1.2 GLYCOPROTEINS	13
1.1.3 ELASTIC FIBERS	13
1.1.4 FIBRONECTIN	14
1.1.5 PROTEOGLYCANS	14
1.1.6 HEPARAN SULFATE PROTEOGLYCANS	15
<b>1.2 THE BASEMENT MEMBRANE</b>	<b>16</b>
1.2.1 LAMININS	16
<b>1.3 THE INTEGRIN RECEPTOR FAMILY</b>	<b>18</b>
1.3.1 INTEGRIN STRUCTURE AND ACTIVATION	18
1.3.2 INTEGRIN SIGNALING	21
1.3.2.1 Inside-out signaling	21
1.3.2.2 Outside-in signaling	21
1.3.3 FOCAL ADHESION MATURATION	22
<b>1.4 INTEGRIN-LINKED KINASE</b>	<b>23</b>
1.4.1 PROTEIN STRUCTURE OF ILK	24
1.4.2 ILK IS A PSEUDOKINASE THAT FUNCTIONS AS AN ESSENTIAL ADAPTOR PROTEIN	25
1.4.3 THE ILK-PINCH-PARVIN COMPLEX	26
1.4.4 ILK REGULATES THE ACTIN CYTOSKELETON	28
<b>1.5 MAMMALIAN SKIN</b>	<b>29</b>
1.5.1 EPIDERMAL ARCHITECTURE AND HOMEOSTASIS	29
1.5.2 HAIR FOLLICLE MORPHOGENESIS AND CYCLING	32
1.5.3 HAIR FOLLICLE STEM CELLS AND CYCLING	33
1.5.4 HAIR FOLLICLE STEM CELL NICHE	37
<b>1.6 THE SKIN BASEMENT MEMBRANE</b>	<b>38</b>
1.6.1 LAMININS IN THE SKIN	39
<b>1.7 THE EXTRACELLULAR MATRIX OF THE DERMIS</b>	<b>41</b>
<b>1.8 INTEGRIN-LINKED KINASE IN THE SKIN</b>	<b>42</b>
1.8.1 ILK IN THE EPIDERMIS	42
1.8.2 ILK IN DERMAL FIBROBLASTS	44
<b>2 AIMS OF THE THESIS</b>	<b>46</b>
<b>3 MATERIALS AND METHODS</b>	<b>47</b>
<b>3.1 CHEMICALS AND REAGENTS</b>	<b>47</b>
<b>3.2 ANIMAL EXPERIMENTS</b>	<b>47</b>
3.2.1 BREEDING SCHEMES AND ANIMAL PROCEDURES	47
3.2.2 TWO-STAGE CARCINOGENESIS EXPERIMENT	50
3.2.3 BRDU AND EDU INJECTIONS	50
<b>3.3 HISTOLOGICAL ANALYSES</b>	<b>51</b>
3.3.1 EQUIPMENT AND MATERIALS	51
3.3.2 HISTOLOGICAL METHODS	51
3.3.2.1 Preparation of paraffin sections	52
3.3.2.2 Preparation of cryosections	54
3.3.2.3 Hematoxylin and eosin staining	54
3.3.2.4 $\beta$ -galactosidase staining	55
3.3.2.5 Alkaline phosphatase staining	56

<b>3.4</b>	<b>IMMUNOLOGICAL METHODS</b>	<b>57</b>
3.4.1	MATERIALS	57
3.4.1.1	Primary antibodies	57
3.4.1.2	Secondary antibodies	58
3.4.2	IMMUNOFLUORESCENCE STAINING OF PARAFFIN SECTIONS	58
3.4.3	IMMUNOFLUORESCENCE STAINING OF CRYOSECTIONS	59
3.4.4	IMMUNOFLUORESCENCE STAINING OF ADHERENT CELLS	60
3.4.5	IMMUNOHISTOCHEMISTRY	60
3.4.6	BRDU STAINING	62
3.4.7	EDU STAINING	62
3.4.8	TUNEL STAINING	63
<b>3.5</b>	<b>CELL CULTURE METHODS</b>	<b>63</b>
3.5.1	EQUIPMENT AND MATERIALS	63
3.5.2	CELL CULTURE OF IMMORTALIZED MOUSE FIBROBLASTS	64
3.5.3	GEL CONTRACTION ASSAY	65
3.5.4	ISOLATION OF PRIMARY KERATINOCYTES	65
3.5.5	CELL SUBSTRATE ADHESION ASSAY	67
3.5.6	COVERSLIP ACTIVATION	68
<b>3.6</b>	<b>BIOCHEMICAL METHODS</b>	<b>68</b>
3.6.1	EQUIPMENT AND MATERIALS	68
3.6.2	PREPARATION OF CELL EXTRACTS FROM ADHERENT CELLS	69
3.6.3	PREPARATION OF ECM EXTRACTS FROM MOUSE SKIN	70
3.6.4	DETERMINATION OF PROTEIN CONCENTRATION	71
3.6.5	ONE-DIMENSIONAL SDS-POLYACRYLAMIDE-GEL ELECTROPHORESIS	71
3.6.6	WESTERN BLOTTING AND IMMUNODETECTION	73
<b>3.7</b>	<b>MOLECULAR BIOLOGY METHODS</b>	<b>74</b>
3.7.1	EQUIPMENT AND MATERIALS	74
3.7.2	EXTRACTION OF MOUSE TAIL DNA	75
3.7.3	EXTRACTION OF MOUSE EPIDERMIS	75
3.7.4	MAGNETIC-ACTIVATED CELL SEPARATION	76
3.7.5	POLYMERASE CHAIN REACTION	77
3.7.6	AGAROSE GEL ELECTROPHORESIS	80
3.7.7	RNA ISOLATION	81
3.7.8	QUANTITATIVE REAL-TIME POLYMERASE CHAIN REACTION	82
3.7.8.1	Analysis of qRT-PCR	83
3.7.9	FLOW CYTOMETRY	84
<b>3.8</b>	<b>MICROSCOPY</b>	<b>85</b>
3.8.1	LIGHT MICROSCOPY	85
3.8.2	LASER SCANNING CONFOCAL MICROSCOPY	85
3.8.3	TRACTION FORCE MICROSCOPY	86
<b>3.9</b>	<b>STATISTICAL ANALYSIS</b>	<b>88</b>
<b>4</b>	<b>RESULTS</b>	<b>89</b>
<b>4.1</b>	<b>ILK PROMOTES FORCE GENERATION AND MATRIX ASSEMBLY</b>	<b>89</b>
4.1.1	ILK-DEFICIENT FIBROBLASTS SHOW A DISORGANIZED ACTIN CYTOSKELETON AND ALTERED FA STRUCTURES	89
4.1.2	ILK IS REQUIRED FOR FORCE GENERATION	90
4.1.3	ILK IS REQUIRED FOR MATRIX ASSEMBLY AND REMODELING	91
<b>4.2</b>	<b>ILK IS REQUIRED FOR THE MAINTENANCE OF HFSCs</b>	<b>93</b>
4.2.1	EPIDERMAL DELETION OF ILK CAUSES PROGRESSIVE LOSS OF HFSCs	94
<b>4.3</b>	<b>LOSS OF HFSCs IN ILK-DEFICIENT EPIDERMIS OCCURS INDEPENDENTLY FROM MORPHOGENESIS</b>	<b>100</b>

<b>4.4</b>	<b>ILK-DEFICIENCY LEADS TO LOSS OF BULGE SCs THROUGH ENHANCED DIFFERENTIATION</b>	<b>101</b>
<b>4.5</b>	<b>ILK IS REQUIRED TO ESTABLISH AND MAINTAIN THE BULGE SC NICHE</b>	<b>107</b>
4.5.1	ILK-DEFICIENCY LEADS TO ALTERATIONS IN LN-332 AND LN-511 DEPOSITION	107
4.5.2	ILK-DEFICIENCY LEADS TO ALTERATIONS IN THE EPITHELIAL-MESENCHYMAL CROSSTALK	110
4.5.3	NO ALTERATIONS IN THE IMMUNE CELLS WITHIN THE HF MICROENVIRONMENT	112
<b>4.6</b>	<b>SC FATE-DETERMINING PATHWAYS ARE ALTERED UPON ILK-DEFICIENCY</b>	<b>114</b>
<b>4.7</b>	<b>LN-332 AND LN-511 REGULATE SC FATE DETERMINING PATHWAYS</b>	<b>118</b>
4.7.1	LN-332 REGULATES WNT AND LN-511 REGULATES TGF-B SIGNALING	118
4.7.2	A WILD TYPE MATRIX RESCUES THE ALTERED SIGNALING ACTIVITY IN ILK-DEFICIENT KERATINOCYTES	120
<b>4.8</b>	<b>ABERRANT SC ACTIVATION CAUSES REPLICATION STRESS AND PREDISPOSES TO SKIN CARCINOGENESIS</b>	<b>122</b>
<b>5</b>	<b>DISCUSSION</b>	<b>129</b>
<b>5.1</b>	<b>ILK PROMOTES FORCE GENERATION AND MATRIX ASSEMBLY</b>	<b>129</b>
<b>5.2</b>	<b>ILK IS REQUIRED FOR HFSC QUIESCENCE AND MAINTENANCE</b>	<b>131</b>
<b>5.3</b>	<b>ILK-DEFICIENCY LEADS TO LOSS OF BULGE SCs THROUGH ENHANCED DIFFERENTIATION</b>	<b>134</b>
<b>5.4</b>	<b>ILK IS REQUIRED TO ESTABLISH AND MAINTAIN THE BULGE SC NICHE</b>	<b>135</b>
<b>5.5</b>	<b>FUNCTIONAL CONSEQUENCES OF THE ALTERED NICHE</b>	<b>137</b>
<b>5.6</b>	<b>ABERRANT SC ACTIVATION CAUSES REPLICATION STRESS AND PREDISPOSITION TO SKIN CARCINOGENESIS</b>	<b>138</b>
	<b>REFERENCES</b>	<b>140</b>
	<b>APPENDIX</b>	<b>158</b>
	<b>ABBREVIATIONS</b>	<b>159</b>
	<b>ACKNOWLEDGEMENTS</b>	<b>163</b>
	<b>PUBLICATIONS</b>	<b>164</b>
	<b>ERKLÄRUNG</b>	<b>165</b>
	<b>LEBENS LAUF</b>	<b>166</b>

## Abstract

The extracellular matrix (ECM) functions as a structural scaffold for tissues and regulates signaling by interacting with specific receptors and by providing a reservoir for growth factors. This multitude of functions makes the ECM an essential regulator of organ development and maintenance. The deposition and remodeling of the ECM into a precise configuration is a cell-dependent process that requires integrin adhesion receptors and the generation of cellular forces. However, it is not clear how integrins transduce force necessary for ECM remodeling. In addition, the role of ECM remodeling in directing cell fate decisions *in vivo* is not completely understood. Integrin-linked kinase (ILK) is an essential adaptor protein that binds to  $\beta$ 1- and  $\beta$ 3-integrin cytoplasmic tails and links them to the actin cytoskeleton. The aim of this study was to analyze the function of ILK in ECM remodeling and the role of this process in the regulation of stem cell (SC) fate. *In vitro* experiments revealed that ILK is required for cellular force generation, cell-matrix adhesion maturation, and subsequent remodeling of a fibronectin matrix. Using various strategies to delete ILK in murine epidermis, it was further shown that ILK regulates SC fate within hair follicles (HFs). Deletion of ILK led to gradual loss of HFSCs due to their aberrant activation and enhanced differentiation. Furthermore, ILK was observed to regulate the precise composition of the basement membrane (BM) SC niche. The inverse gradients of laminin-(LN) 511 and LN-332 present in the skin of wild type mice was lost upon deletion of ILK. As a consequence, Wnt and Tgf- $\beta$  signaling pathways that were shown to be modulated by LN-511 and LN-332, were dysregulated causing aberrant SC activation. Consequently, reconstituting a wild type ECM restored the activities of Wnt and Tgf- $\beta$  pathways in ILK-deficient cells to the level of controls. The aberrant SC activation was observed to cause replication stress and accumulation

of DNA damage, which predisposed ILK-deficient mice to skin carcinogenesis. Taken together, this study identifies a critical role for ILK in ECM remodeling and highlights the importance of reciprocal cell-ECM interactions in cell fate decisions and tissue homeostasis.

## Zusammenfassung

Die extrazelluläre Matrix (EZM) dient als Gerüst für Gewebe, sowie als Reservoir für Wachstumsfaktoren und reguliert Signalwirkungen durch die Interaktion mit spezifischen Rezeptoren. Diese Vielzahl an Funktionen macht sie zu einem wesentlichen Regulierer von Organentwicklung und –erhalt. Die Ablagerung und Umgestaltung der EZM in eine konkrete Struktur ist ein zell-abhängiger Prozess, der Integrin Adhäsionsrezeptoren und die Generierung von Zellkräften benötigt. Allerdings ist es unklar, wie Integrine die erforderliche Kraft für die EZM Umgestaltung übertragen. Des Weiteren ist die Rolle der EZM in der Regulation von Zell-Schicksalen *in vivo* nicht komplett verstanden. Integrin-linked Kinase (ILK) ist ein entscheidendes Adapterprotein, dass an die zytoplasmatischen Anteile der  $\beta$ 1- und  $\beta$ 3-Integrine bindet und diese mit dem Aktin Zytoskelett verbindet. Das Ziel dieser Studie war es, die Funktion von ILK bezüglich seiner Rolle in der EZM Umgestaltung und in der Regulation von Stammzell (SZ)-Schicksalen zu untersuchen. Durch *in vitro* Experimente konnte gezeigt werden, dass ILK für die Generierung der Zellkraft, der Reifung von Zell-Matrix Adhäsionen und die darauffolgende Umgestaltung einer Fibronectin Matrix notwendig ist. Durch den Gebrauch von unterschiedlichen epidermalen ILK-defizienten Mausmodellen konnte ferner gezeigt werden, dass ILK das Schicksal von SZ im Haarfollikel (HF) reguliert. Die Deletion von ILK führte zu einem Verlust von HFSZ aufgrund von veränderter Aktivierung und erhöhter Differenzierung. Des Weiteren konnte festgestellt werden, dass ILK die präzise Zusammensetzung der Basalmembran (BM) der SZ Nische regelt. Der inverse Gradient aus Laminin-(LN) 511 und LN-332 in der Haut von Kontrollmäusen war in ILK-defizienten Mäusen nicht vorzufinden. Daraus folgte, dass die Signalwege Wnt und Tgf- $\beta$ , die durch LN-511 und LN-332 reguliert werden, missreguliert waren, was

zu einer veränderten Aktivierung von SZ führte. Durch die Verwendung einer Wildtyp-EZM konnten die Signalwege in ILK-defizienten Keratinozyten wieder auf Kontrollniveau zurückgesetzt werden. Die veränderte Aktivierung hatte zur Folge, dass replikativer Stress entstand, der zur Anhäufung von DNA Schädigung führte, wodurch die ILK-defizienten Mäuse anfälliger für Haut Karzinogenese waren. Zusammenfassend hat die Studie eine entscheidende Rolle von ILK in der EZM Umgestaltung ermittelt und hebt die Wichtigkeit der gegenseitigen Zell-Matrix Kommunikation im Zusammenhang mit Zell-Schicksalsentscheidungen und Gewebemöostase hervor.

# 1 Introduction

Tissues in our body are organized into complex multicellular structures. Their formation and maintenance is determined by cellular interactions governed by cell-cell and cell-matrix adhesions. Interactions between cells and their environment not only provide the tissue their shape and proper architecture, but they also regulate fate decisions of individual cells. Cell-matrix interactions have the potential to generate signals that regulate proliferation, differentiation, and migration, which is essential to ensure coordinated growth during development and tissue homeostasis (Daley and Yamada, 2013). Cells in turn actively remodel the extracellular matrix (ECM) thereby engaging in dynamic crosstalk with their environment. Most adult tissues contain stem cells (SCs) that provide the tissue the capability to regenerate. The ability to mobilize SCs upon demand, and on the other hand to maintain a stable pool of SCs throughout the lifetime of an individual, requires the tight regulation of SC quiescence and activation (Gattazzo et al., 2014; Hsu and Fuchs, 2012; Hsu et al., 2014; Scadden, 2006). In this respect it is critical to understand how cell-ECM interactions are able to regulate SC fate.

## 1.1 The extracellular matrix

The ECM is a complex non-cellular network present within tissues. It serves as a physical scaffold and as a regulator of intercellular communication. The ECM is mainly composed of fibrous proteins and proteoglycans, which determine the biochemical and mechanical properties of the tissue. The ECM also provides an anchoring platform for cells and serves as a reservoir for growth factors. Therefore the composition and organization of the ECM and ECM-associated proteins is a

## Introduction

critical determinant of cellular fate during development, homeostasis and disease (Frantz et al., 2010; Gattazzo et al., 2014; Watt and Fujiwara, 2011). The basement membrane (BM) is a specialized type of ECM and unique to metazoans (Breitkreutz et al., 2013; LeBleu et al., 2007). The following chapters will introduce the main components of the ECM and BMs and highlight the constituents relevant for this thesis.

### 1.1.1 Collagens

Collagens play an important role in structuring and shaping the tissue and determine its mechanical properties such as tensile strength or rigidity. The collagen superfamily comprises of 28 members that are all characterized by their triple helical structure. Three collagen  $\alpha$ -chains can form either hetero- or homotrimers resulting in a structural triple helix. Collagens are classified into fibril-forming, network-forming, microfibrillar, fibril-associated collagens with interrupted triple helix (FACIT) and transmembrane collagens (Bruckner, 2010; Kadler et al., 2007; Ricard-Blum, 2011). Collagen synthesis is a complex stepwise process. mRNA transcription leads to the synthesis of precursor polypeptides ( $\alpha$ -chains). Pre-pro-collagen forms in the endoplasmatic reticulum by post-translational modifications. It undergoes further modifications including glycosylation and prolyl hydroxylation leading to the formation of procollagen. Procollagen undergoes its last modifications in the Golgi apparatus before it is secreted into the extracellular space. Outer membrane-bound collagen peptidases process procollagen into collagen molecules. Lysyl oxidase then crosslinks collagen molecules leading to fibril formation. The subsequent interaction with other collagens and macromolecules of the ECM defines the specific structure and biological activity of the tissue (Gordon and Hahn, 2010).

### 1.1.2 Glycoproteins

Glycoproteins are proteins that contain covalently bound oligosaccharide chains. They are highly abundant in the ECM and comprise of a variety of different subgroups with different properties. For instance, LNs, elastic fibers, fibronectin (FN), tenascins, thrombospondins and matrilins can be found ubiquitously or in a tissue-restricted manner (Naba et al., 2012). LNs will be discussed in the context of the BM. Also FN and its assembly will be introduced in the next sections. Finally, elastic fibers are of interest as they regulate the bioavailability of certain growth factors.

### 1.1.3 Elastic fibers

The elastic fiber network consists of fibrillins, fibulins, microfibril-associated glycoproteins (MAGPs) and latent Tgf- $\beta$ -binding proteins (LTBPs) (Ramirez and Dietz, 2007). These proteins are especially interesting, as they regulate Tgf- $\beta$  bioavailability. Tgf- $\beta$  is associated with small latent associated proteins (LAPs) and LTBP and together they are secreted as the large latent complex. Binding of the growth factor to its receptor is inhibited by LAPs, rendering it inactive. LTBP interacts with fibrillin-1 and fibulin 4/5, which then anchor the latent growth factor to the ECM. Binding of  $\alpha$ v-integrins to LAPs and the subsequent induction of adhesion-mediated cellular forces lead to the release and activation of the growth factor (Munger et al., 1998). Mutations in fibrillin causes Marfan syndrome that is associated with increased Tgf- $\beta$  signaling, providing compelling evidence for the importance of ECM-association to confer latency to Tgf- $\beta$  (Ramirez and Dietz, 2007; Ramirez and Sakai, 2010).

## Introduction

### 1.1.4 Fibronectin

FN is a ubiquitously expressed glycoprotein that is secreted as a dimeric protein. FN contains multiple binding domains for protein interactions. It interacts with the cell surface by binding to integrins or syndecans, and with other ECM proteins such as thrombospondin-1, tenascin-C, fibrillin-1 as well as extracellular enzymes (Schwarzbauer and DeSimone, 2011). FN is essential for development and deletion of FN in mice leads to embryonic lethality (George et al., 1993). The expression and local assembly of FN-containing ECM is crucial for morphogenesis and differentiation (Sakai et al., 2003a). Mice with functional null mutations in FN or deletion of FN initiate gastrulation, but mutant embryos fail to form mesodermally derived tissues such as the notochord and somites. It is suggested that FN acts as a guidance cue for ECM remodeling and subsequent organogenesis (George et al., 1993; Georges-Labouesse et al., 1996b). FN fibrillogenesis is a cell-dependent process wherein FN binding to integrins induces integrin clustering and the compaction of FN. Upon exertion of cellular forces, FN assembles into fibrils, where it undergoes conformational changes and becomes extended, exposing cryptic self-assembly sites that promote fibrillogenesis (Baneyx et al., 2002; Pankov et al., 2000).

### 1.1.5 Proteoglycans

Proteoglycans consist of a core protein and glycosaminoglycan (GAG) chains. According to their GAG chains, they can be grouped into proteoglycans containing dermatan sulfate, heparan sulfate, chondroitin sulfate and keratin sulfate chains. Proteoglycans can be membrane-bound where they can act as co-receptors of growth factor receptors or as adhesion receptors. Secreted into the ECM space, they bind to a variety of other ECM molecules and regulate morphogenic gradients of growth

factors and chemokines (Esko et al., 2009). In light of their function as adhesion receptors and regulator of growth factor bioavailability, the group of heparan sulfate proteoglycans will be described in more detail.

### **1.1.6 Heparan sulfate proteoglycans**

Heparan sulfate proteoglycans (HSPGs) contain one to four HS chains that are connected to the core protein. HSPG biosynthesis is a stepwise process that is initiated by the attachment of xylose to the core protein in the ER. Chain elongation occurs in the Golgi apparatus and is mediated by enzymes of the exostoses (EXT) family, which link glucuronic acids to *N*-acetylglucosamines giving rise to repetitive polysaccharide chains. Chain modifications such as *N*-deacetylation and sulfation are carried out by various sulfotransferases and epimerases (Bulow and Hobert, 2006). Deletion of key enzymes for HSPG synthesis results in embryonic or perinatal lethality, highlighting their importance in organogenesis (Fan et al., 2000; Lin et al., 2000). Syndecans and glypicans are the main membrane-bound HSPGs in epithelial cells, whereas perlecan, agrin and collagen XVIII are an integral part of the BM (Sarrazin et al., 2011). Syndecan-1 and syndecan-4 can regulate the activation of integrins at the cell surface, which then act synergistically to induce cell spreading (McQuade et al., 2006; Okina et al., 2009). In addition, HSPGs have been shown to have an essential role in regulating growth factor signaling. Morphogens like Wnts or Hedgehogs are transferred from one HSPG to the next along a path that is defined by the interacting ligands, thereby restricting diffusion (Yan and Lin, 2009). Cell surface HSPGs such as glypicans can act on morphogens by capturing those and presenting them to their appropriate receptors (Fico et al., 2011).

### 1.2 The basement membrane

BMs are thin, specialized layers of ECM that serve as an extension of the plasma membrane, protecting tissues from mechanical stress and providing an interactive interface between cells and their local environment by mediating signals between these compartments. The composition of BMs is specific to each developmental stage and tissue type. However, all BMs consist of at least one type of laminin (LN), nidogen, HSPGs such as perlecan or agrin and type IV collagen (Murray and Edgar, 2000; Yurchenco, 2011). On a structural level two distinct layers are present - the electron-dense *lamina densa* that is separated from the plasma membrane by the electron-lucent *lamina lucida* (McMillan et al., 2003). The assembly of the BM is a stepwise process and depends on binding of LNs to LN-binding competent cell surfaces. Cell surface anchorage of LNs and their interconnection facilitates the accumulation of nidogen, type IV collagen and perlecan, building a nascent scaffold that further matures by proteolytic processing of LNs, crosslinking of type IV collagens and rearrangement of cell surface receptors to strengthen the binding of the cell to the BM (Colognato et al., 1999; McKee et al., 2009).

#### 1.2.1 Laminins

LNs are heterotrimeric proteins consisting one of five  $\alpha$ , one of four  $\beta$  and one of three  $\gamma$  subunits. 16 different heterotrimers have been identified. Their distribution is tissue-specific and depends additionally on the developmental or pathophysiological state of the tissue (Aumailley et al., 2005). LN trimers assemble intracellularly. The  $\beta$ - and  $\gamma$  subunits form and are retained in the cytoplasm until trimerization with the  $\alpha$ -subunit drives their secretion (Yurchenco et al., 1997). At a structural level, all LNs show an arrangement of their chains into a cross-shape pattern with a central  $\alpha$ -

subunit surrounded by the  $\beta$ - and  $\gamma$  subunits. They differ from each other by the basis of their short arm composition, the binding affinity in the LN globular (LG) domain of the  $\alpha$  subunit as well as their posttranslational proteolytic processing. In general, LNs interact via their C-terminal ends of the  $\alpha$ -subunit with cell surface receptors, thereby mediating biochemical and mechanical cues between intra- and extracellular networks. Through the N-terminus, LNs interact with other ECM proteins to facilitate BM assembly and stability (Figure 1.2.1) (Aumailley, 2013).

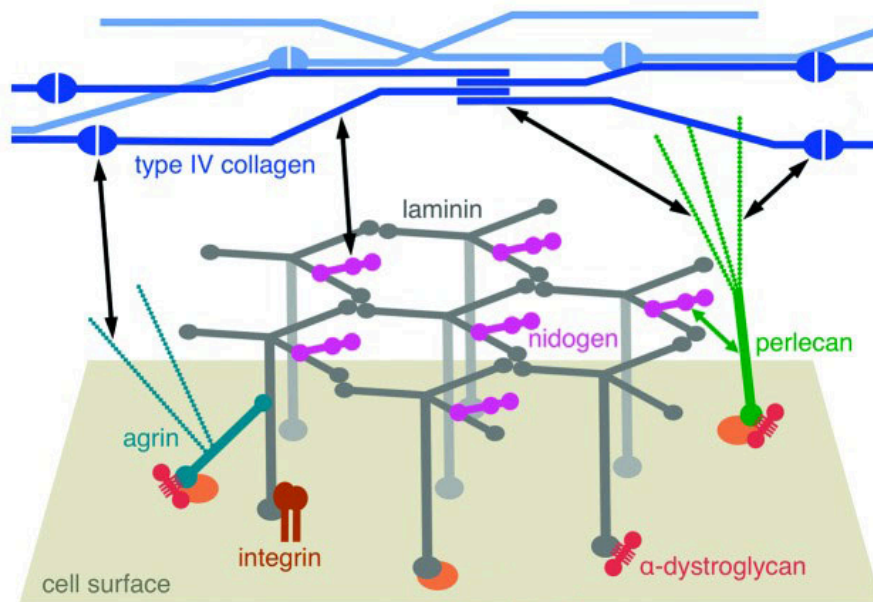


**Figure 1.2.1. Schematic representation of the BM.** During BM assembly, LNs bind to a binding-competent surface and form a network with interacting HSPGs (perlecan, agrin). An assembled network of type IV collagen interacts with LN-associated nidogen and HSPGs leading to BM formation (Hohenester and Yurchenco, 2013).

### **1.3 The integrin receptor family**

The search for molecules by which cells interact with the ECM protein FN led to the discovery of integrins that were named according to their structure: integral membrane protein complex linking the ECM to the cytoskeleton (Tamkun et al., 1986). Integrins are the major ECM receptors in all metazoans. Accordingly, their main task is to mediate the interactions of cells with the ECM. In addition, they are tightly connected to the actin and intermediate filament cytoskeletons, allowing them to generate traction forces. Finally, they are able to assemble large intracellular signaling platforms termed focal adhesions (FAs) that activate multiple signaling cascades. Together these three features make integrins essential for most cellular processes (Legate et al., 2009; Wickström et al., 2011).

#### **1.3.1 Integrin structure and activation**

Integrins are a family of heterodimeric type I transmembrane proteins comprising of 18  $\alpha$  and 8  $\beta$  subunits that assemble non-covalently into 24 distinct heterodimers (Hynes, 2002). The specific subunit combination determines their binding affinity and ligand specificity. Each integrin  $\alpha$  and  $\beta$  subunit consists of a large (~750-1000 amino acids) extracellular ectodomain, a short (~20 amino acids) membrane-spanning domain and a short (10-70 amino acids) flexible cytoplasmic domain (Campbell and Humphries, 2011). The  $\alpha$  subunit ectodomain comprises 4-5 extracellular domains: a  $\beta$ -propeller, a thigh, two calf domains, and 9 out of 18  $\alpha$  subunits contain an  $\alpha$ -I domain. The  $\beta$ -propeller with its  $\text{Ca}^{2+}$  binding sites (metal ion-dependent adhesion site; MIDAS) and the  $\alpha$ -I domain are important to define ligand-binding specificity (Larson et al., 1989; Oxvig and Springer, 1998). The  $\beta$  subunit ectodomain comprises seven domains: a  $\beta$ -tail domain connected to four epidermal growth factor (EGF)

domains, a plexin-semaphorin-integrin (PSI) domain and a hybrid domain connected to the  $\beta$ -I domain, which contains ion-binding sites for  $Mn^{2+}$  and  $Mg^{2+}$  (ADMIDAS; adjacent to metal-ion dependent adhesion site) and SyMBS (synergistic metal ion binding site) for  $Ca^{2+}$ -binding, involved in fine-tuning ligand-binding affinities (Campbell and Humphries, 2011; Hynes, 2002; Zhu et al., 2008).

Integrins receptors can switch between a bent and an extended conformation. The bent confirmation with closed headpieces of  $\alpha$  and  $\beta$  subunits represents an “inactive” state with very low ligand binding affinity. Upon ligand binding, the head domains undergo conformational changes and “open” as the integrin extracellular domain extends. In this primed state, the cytoplasmic adaptor protein talin binds to the  $\beta$ -integrin cytoplasmic domain and enables further recruitment of integrin co-activators. The stepwise recruitment of co-activators results in a fully “active” conformation with high ligand binding affinity (Zhu et al., 2008).

Integrins can be classified according to their ligand-binding and tissue-specific expression patterns (Figure 1.3.1). One group comprises integrins that bind to RGD (arginine, glycine, aspartate) motif-containing matrix proteins, such as FN. These contain the family of  $\alpha$ v-integrins, platelet-binding  $\alpha$ Ib $\beta$ 3 integrin and  $\alpha$ 5 $\beta$ 1 and  $\alpha$ 8 $\beta$ 1. A second group consists of integrins  $\alpha$ 4 $\beta$ 1 and  $\alpha$ 9 $\beta$ 1 that can bind to RGD and additionally recognize VCAM (vascular cell adhesion molecule), a member of the Ig-superfamily counter receptors. Another class of integrin heterodimers interacts with LNs ( $\alpha$ 3 $\beta$ 1,  $\alpha$ 6 $\beta$ 1,  $\alpha$ 7 $\beta$ 1 and intermediate filament binding integrin  $\alpha$ 6 $\beta$ 4). The fourth class of  $\beta$ 1-containing integrins forms dimers with  $\alpha$ 1-,  $\alpha$ 2-,  $\alpha$ 10- or  $\alpha$ 11-integrin and binds to collagens. The fifth class of  $\beta$ 2-containing integrins and  $\alpha$ E $\beta$ 7 integrin are leukocyte-specific integrin receptors involved in cell-cell adhesion (Humphries et al., 2006; Hynes, 2002).

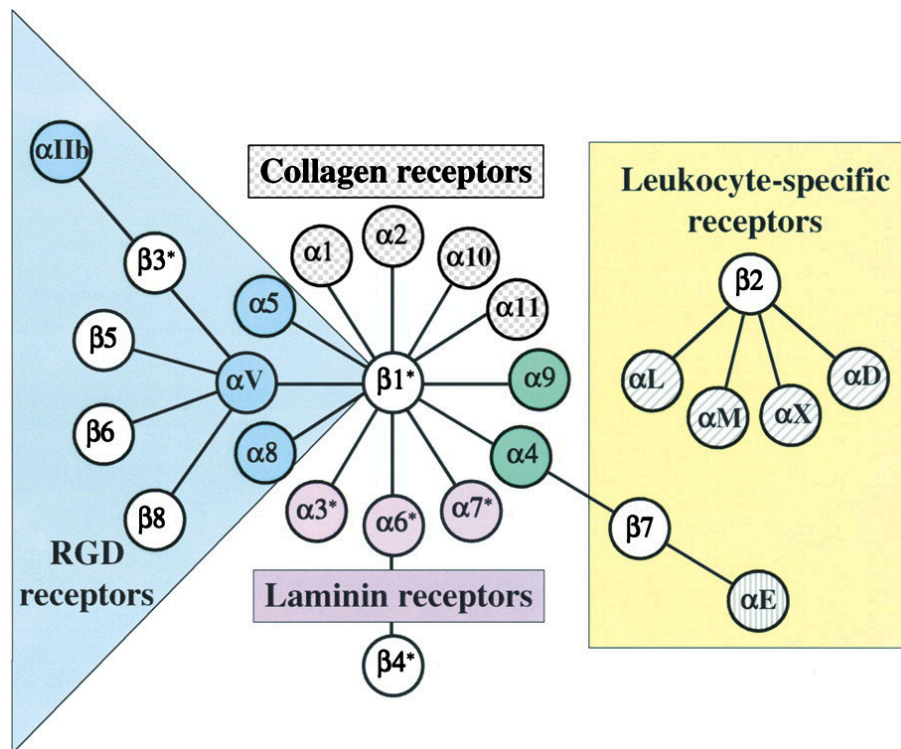


**Figure 1.3.1. The integrin receptor family.** Based on their recognition specificity integrin heterodimers can be subdivided into different groups (Hynes, 2002).

Knockout studies in mice have revealed the importance of different integrin subunits and their tissue-specific functions. Defects caused by the loss of integrins range from embryonic lethality and perinatal lethality to no obvious or very mild phenotypes. Deletion of integrin subunits  $\alpha 4$ ,  $\alpha 5$  or  $\beta 1$  in mice leads to embryonic lethality caused by severe impairment of ECM remodeling during embryogenesis (Fässler et al., 1995; Stephens et al., 1995; Yang et al., 1993, 1995). Perinatal lethality is found in mice with deletions for integrins that have tissue-restricted expression or that recognize non-ubiquitously expressed molecules such as specific LNs or collagens (Georges-Labouesse et al., 1996a). Collagen receptors have overlapping ligand-binding specificity, so that knockout of one  $\alpha 1$ -,  $\alpha 2$ -,  $\alpha 10$ - or  $\alpha 11$ - integrin subunit in mice is compensated by another  $\alpha$ -subunit and causes any drastic phenotype (Bouvard et al., 2013; Hynes, 2002).

### **1.3.2 Integrin signaling**

A hallmark of integrin receptors is their ability to mediate bi-directional signaling. “Inside-out” signaling regulates the ligand binding properties of integrins and is induced by non-integrin mediated signaling pathways. “Outside-in” signaling regulates cellular responses induced by ligand binding to integrin receptors that regulate cell spreading, migration and proliferation. Upon ligand binding, integrins cluster at the plasma membrane and a large number of integrin-binding proteins are recruited to the cytoplasmic tails of  $\beta$ -integrins. Adaptor proteins subsequently initiate the link to the actin cytoskeleton, thereby connecting the ECM with the cytoskeleton of the cell (Legate et al., 2009; Wickström et al., 2011).

#### **1.3.2.1 Inside-out signaling**

Binding of intracellular proteins to the integrin cytoplasmic tails in response to an integrin-independent stimulus is termed inside-out signaling. Integrin-independent signals initiate the translocation of talin and kindlin to  $\beta$ -integrin cytoplasmic tails and thereby activate integrins. The initial binding of these proteins leads to the subsequent recruitment of further adhesion associated proteins, thus enabling the link of integrins to the cytoskeleton, increasing the binding affinity towards its ligand (Margadant et al., 2011; Wickström et al., 2011).

#### **1.3.2.2 Outside-in signaling**

Binding of integrins to their ECM ligands initiates outside-in signaling. In the first step, binding of talin to  $\beta$ -integrin initiates the formation of a link between integrins and the actin cytoskeleton. Talin can bind actin directly but it also provides a binding platform for vinculin that stabilizes the integrin-actin connection. Recruitment of  $\alpha$ -

## Introduction

actinin to talin and vinculin further strengthens the integrin-cytoskeleton linkage. Paxillin is also recruited into early FAs where it can bind to vinculin and integrin-linked kinase (ILK). ILK together with its binding partners PINCH and parvin is also an early component of FAs. ILK might directly bind integrins, whereas parvin provides an additional contact to the actin cytoskeleton (Ghatak et al., 2013). In addition to direct recruitment, kindlins can also target ILK to integrin-adhesion sites (Huet-Calderwood et al., 2014). ILK will be discussed in more detail later in this thesis.

The core FA components subsequently recruit a large number of actin-modulatory proteins and signaling molecules allowing actin stress fiber formation, FA maturation, and propagation of intracellular signaling cascades (Harburger and Calderwood, 2009; Legate et al., 2009; Morse et al., 2014).

Recent mass-spectrometry analyses have identified a large number (200 different) of proteins found to be directly or indirectly bound to integrins (Zaidel-Bar et al., 2007). An even larger number of direct interactors (~700), including scaffolding and regulatory interactors, have been identified as components of integrin adhesions in the so-called “adhesome” (Zaidel-Bar and Geiger, 2010).

### **1.3.3 Focal adhesion maturation**

The assembly and remodeling of integrin adhesion complexes is a highly dynamic process that requires the recruitment of adaptor proteins and myosin II-containing actin networks to adhesion sites (Vicente-Manzanares and Horwitz, 2011). Upon cell attachment, integrins bind to the underlying substrate and focal complexes (FCs), or nascent adhesions, assemble at the contact site of the cell with the ECM, the lamellipodium. The maturation of small FCs (~100 nm in size) into large FAs (~1

$\mu\text{m}$ ) is driven by active myosin II that enables further recruitment of adhesion-associated proteins, such as vinculin or paxillin, along polymerizing actin. The integrin-actin cytoskeleton connection is strengthened leading to formation of stress fibers, antiparallel myosin II-containing actin bundles. Polymerizing actin creates a flow and mature FAs form behind lamellipodium, in the lamella (Vicente-Manzanares and Horwitz, 2011; Zamir and Geiger, 2001).

Fibroblasts adhering to a FN matrix develop a special type of cell-matrix adhesion called fibrillar adhesions (FB) (Pankov et al., 2000; Zamir et al., 2000). During FA maturation, specific FN-bound integrins, such as  $\alpha 5\beta 1$  integrins are segregated along the actin cytoskeleton. The subsequent generation of cellular forces and recruitment of tensin induces FB formation (Pankov et al., 2000). The cellular force that is applied on FN leads to conformational changes and self-assembly, resulting in FN fibrillogenesis (Ohashi et al., 2002; Zamir et al., 2000).

#### **1.4 Integrin-linked kinase**

ILK is a central component of  $\beta 1$ - and  $\beta 3$ -integrin adhesion complexes. It is ubiquitously expressed, consists of 452 amino acids and has a molecular weight of 52 kDa. ILK was originally identified in a yeast two-hybrid screen as a direct binding partner of  $\beta 1$ -integrin (Hannigan et al., 1996). Due to its sequence homology to other protein kinases as well as in vitro observations showing that ILK is capable of phosphorylating several substrates including GSK-3 $\beta$  and PKB/AKT and  $\beta 1$ -integrin, it was initially believed to be a serine/threonine kinase.

## Introduction

### 1.4.1 Protein structure of ILK

ILK is composed of five N-terminal ankyrin repeat (ANK) domains, followed by a pleckstrin homology (PH)-like domain and an N-terminal kinase domain (KD). Each of the five ANK domains forms an antiparallel  $\alpha$ -helix and together they form a superhelical spiral, giving rise to an “ankyrin groove” that serves as the binding domain for the LIM domain of PINCH (Chiswell et al., 2008). The PH-like domain of ILK is integrated into the P-loop structure of the ILK-KD and is not capable of binding the second messenger PIP3. A short 14-amino acid long unstructured linker domain connects the N-terminal ANK repeats with the C-terminal KD. The KD of ILK contains the binding domain for the calponin homology 2 (CH2) domain of  $\alpha$ -parvin (Fukuda et al., 2009; Stiegler et al., 2013). Despite the initial in vitro observations of weak kinase activity, sequence and crystal structure analyses of the ILK-KD demonstrated the lack of catalytic activity and validated ILK as a pseudokinase. During phosphotransfer, the DFG (Asp-Phe-Gly) motif conserved in most eukaryotic kinases mediates the alignment of the  $\gamma$ -phosphate, but in ILK this motif is replaced by DVK (Asp-Val-Lys). Phosphotransfer also requires the proton acceptance from the hydroxyl group catalyzed by the aspartate residue in the HRD (His-Arg-Asp) motif that is also lacking in ILK (Wickström et al., 2010). The presence of both DFG and HRD motif are required to fulfill kinase activity (Boudeau et al., 2006).

The crystal structure of the ILK-KD bound to the CH2 domain of  $\alpha$ -parvin showed that ILK-KD folds into a typical bilobial kinase structure but has a dramatically different catalytic core compared to known kinases. The P-loop structure that is essential for ATP-binding contains a non-flexible motif in ILK, which is unable to receive non-transferable phosphates of ATP. Due to the DVK motif the  $\gamma$ -phosphate is

abnormally aligned and lies far away from the putative catalytic site. Hence, bound ATP remains in an unhydrolyzed state (Figure 1.4.1) (Fukuda et al., 2009). Taken together, both sequence as well as structural analysis of ILK showed that ILK has no kinase activity. It was further shown that the observed activity observed in vitro was due to contaminants of the purified protein (Fukuda et al., 2009).

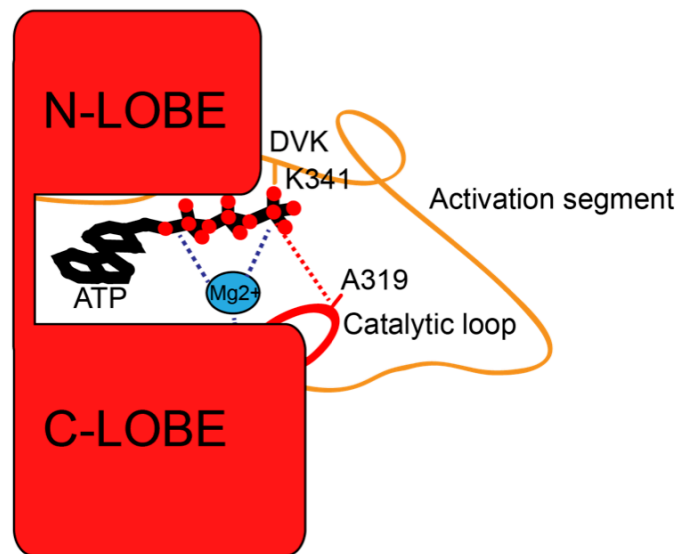


**Figure 1.4.1. Structure of the ILK-KD.** The ILK-KD folds into a kinase-typical bilobal structure. Conformational differences to known kinases are the DVK motif that replaces the DFG and, the untypical orientation of the non-hydrolyzed ATP with its  $\gamma$ -phosphate far away from the catalytic loop and forming a salt bridge with DVK. Additionally, ILK-KD contains just one  $Mg^{2+}$ , instead of two in typical kinases, and the activation segment has a rigid conformation (Ghatak et al., 2013).

#### 1.4.2 ILK is a pseudokinase that functions as an essential adaptor protein

Genetic studies further supported the role of ILK as a pseudokinase with adaptor function. The deletion of *ILK* in *Drosophila melanogaster* leads to embryonic lethality with failure in muscle attachment. Expression of ILK containing a mutation in the kinase domain (E359K) (corresponding to human kinase dead ILK), in these mutant flies is able to completely rescue the phenotype, indicating that ILK fulfills its

## Introduction

function independent of kinase activity (Zervas et al., 2001). Similarly, the knockout of *pat-4* (paralyzed, arrested elongation at two-fold; *C. elegans* homolog of ILK) in *Caenorhabditis elegans* leads to the inability of actin and myosin filament recruitment in embryonic muscle cells and the phenotype is rescued by the expression of a kinase dead ILK (Mackinnon et al., 2002). The constitutive deletion of *ILK* in mice is embryonic lethal (Sakai et al., 2003b). ILK-deficient mouse embryos die due to peri-implantation defects, and they fail to form a polarized epiblast due to impaired F-actin rearrangement and BM remodeling (Sakai et al., 2003b).

Knock-in mice that carry either a R211A mutation within the PH-domain leading to a kinase-dead ILK, or a mutations within the putative autophosphorylation site leading to a kinase-dead (S343A) or hyperactive (S343D) ILK are viable and healthy with no differences in phosphorylation of AKT or GSK-3 $\beta$  (Lange et al., 2009), supporting the kinase-independent function of ILK. Knock-in mice with mutations in the ATP-binding site, K220A or K220M, die shortly after birth due to renal dysgenesis (Lange et al., 2009). This mutation in ILK interferes with its ability to bind to  $\alpha$ -parvin, demonstrating that ILK- $\alpha$ -parvin interaction is crucial for the function of ILK (Lange et al., 2009).  $\alpha$ -parvin knockout mice develop similar kidney phenotype as that observed in ILK K220A/M mutants (Montanez et al., 2009), which suggests that ILK acts via  $\alpha$ -parvin to link integrins to the actin cytoskeleton at least during kidney development. Together, all these studies support the pseudokinase and adapter function of ILK.

### **1.4.3 The ILK-PINCH-parvin complex**

ILK forms a trimolecular protein complex with two other adaptors, PINCH and parvin (Figure 1.4.3). PINCH binds the ANK repeats and regulates actin dynamics by binding other downstream signaling proteins such as Ras suppressor protein 1

(RSU1), which activates the small GTPase Rac1, essential for cell spreading (Ito et al., 2010). Two PINCH isoforms are described in mammals. Both, PINCH1 and PINCH2, contain five LIM domains and a nuclear export signal. PINCH binds to ILK via its first LIM domain to the “ankyrin groove” of ILK (Chiswell et al., 2008; Yang et al., 2009).

As discussed above, parvin binds the KD of ILK. Three parvin isoforms exist in mammals. While  $\alpha$ -parvin is ubiquitously expressed,  $\beta$ -parvin is expressed in skeletal muscles and in the heart and  $\gamma$ -parvin expression is restricted to the hematopoietic system (Nikolopoulos and Turner, 2000; Olski et al., 2001; Tu et al., 2001; Yamaji et al., 2001). Parvins consist of a flexible N-terminal polypeptide chain followed by two CH domains at the C-terminus. The second CH domain binds to the KD domain of ILK (Fukuda et al., 2009; Tu et al., 2001). The IPP complex is presumed to assemble in the cytoplasm and is then recruited to integrin-containing adhesion sites (Zhang et al., 2002).

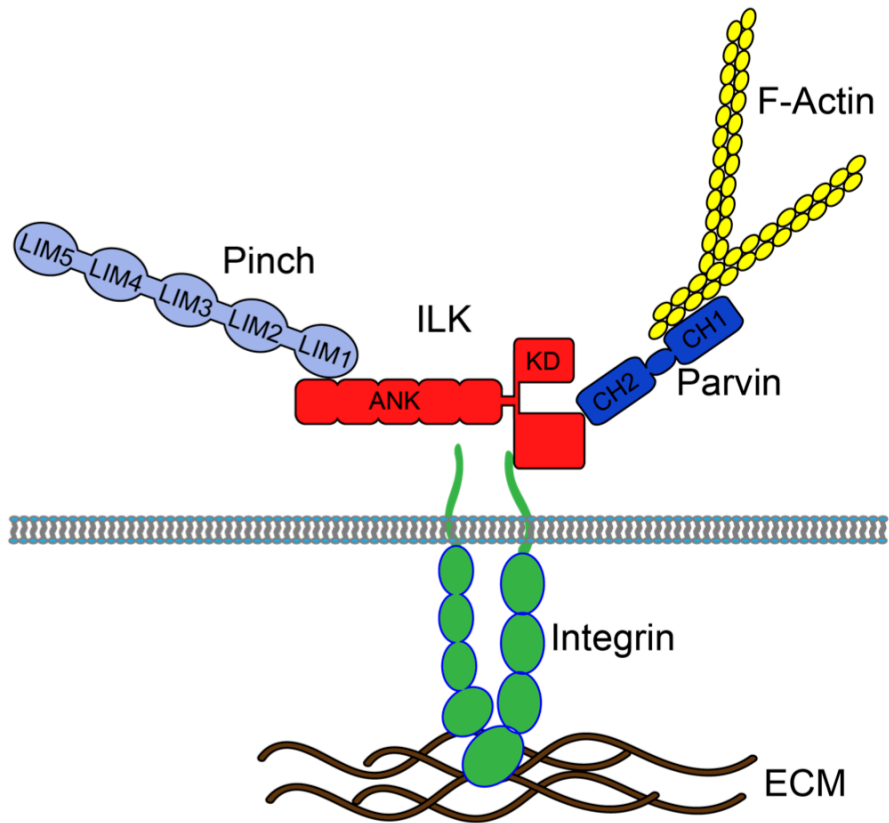


**Figure 1.4.3** Schematic representation of the IPP complex. ILK consists of an N-terminal ANK domain and a C-terminal KD. The interaction with parvin via its CH2 domain with the ILK-KD facilitates the connection of integrins to the actin cytoskeleton. Pinch binds with its LIM1 domain to the “ankyrin groove” of ILK. ILK might bind  $\beta$  integrins directly, although also indirect binding has been reported (Ghatak et al., 2013).

#### 1.4.4 ILK regulates the actin cytoskeleton

Tissue-specific ILK knockout mouse models have been generated to study the function of ILK. Mice with a chondrocyte-specific deletion of ILK show chondrodysplasia with abnormal chondrocyte shape, adhesion defects due to reduced FAs and actin stress fiber formation as well as decreased proliferation (Grashoff et al., 2003). Loss of ILK in skeletal muscle of mice leads to progressive muscle dystrophy with muscle detachment from the BM and subsequent development of fibrosis (Gheyara et al., 2007; Wang et al., 2008). Tissue-specific deletions in the kidney (El-

Aouni et al., 2006), liver (Gkretsi et al., 2007), immune system (Liu et al., 2005), central nervous system (Belvindrah et al., 2006; Mills et al., 2006; Niewmierzycka et al., 2005) or cardiovascular system (Friedrich et al., 2004) are reported. In most cases, deletion of ILK leads to disorganization of the actin cytoskeleton and subsequently defects in cell shape and migration. Collectively these studies indicate that ILK is an essential regulator of actin reorganization, linking the cytoskeleton to FA sites. In addition, ILK has important functions in ECM remodeling, and, depending on the tissue type, it is often required for proliferation, migration and/or polarity.

## **1.5 Mammalian skin**

Mammalian skin is a multilayered organ that covers the surface of the entire body. It serves as a barrier to protect the body from internal water loss and external insults caused by toxins, pathogens or temperature changes. The skin is comprised of the outer epithelial compartment - the epidermis, the underlying mesenchymal compartment - the dermis, and an adipose subcutis underneath. A BM separates epidermis and dermis.

In order to fulfill its function as a barrier, the epidermis undergoes constant self-renewing. Multiple distinct SC populations within the epidermis fuel the regeneration under homeostatic conditions and upon wound repair.

### **1.5.1 Epidermal architecture and homeostasis**

The epidermis is a stratified epithelium composed mainly of keratinocytes. It can be separated into pilosebaceous units comprising the hair follicle (HF), the sebaceous gland (SG) and the interfollicular epidermis (IFE) (Figure 1.5.1). Keratinocytes within the basal layer of the epidermis are in direct contact with the basement membrane

## Introduction

(BM) and can proliferate and give rise to differentiating daughter cells. During the process of stratification these differentiating cells translocate from the basal layer upwards into the suprabasal layers. While entering the terminal differentiation program, keratinocytes downregulate the expression of integrins and become post-mitotic. This stepwise process enables the formation of a multilayered epidermis consisting of the suprabasal spinous and granular layers and the stratum corneum. From here the terminally differentiated corneocytes are finally shed from the epidermal surface. Basal and suprabasal keratinocytes can be discriminated by their differential expression of keratins. While basal keratinocytes are marked by the expression of keratin 5 (K5) and K14 (Moll et al., 1982), suprabasal keratinocytes express K10 and K1 (Winter and Schweizer, 1983). Cells within the granular layer and stratum corneum are marked by their expression of loricrin and filaggrin, respectively (Steinert and Marekov, 1995).

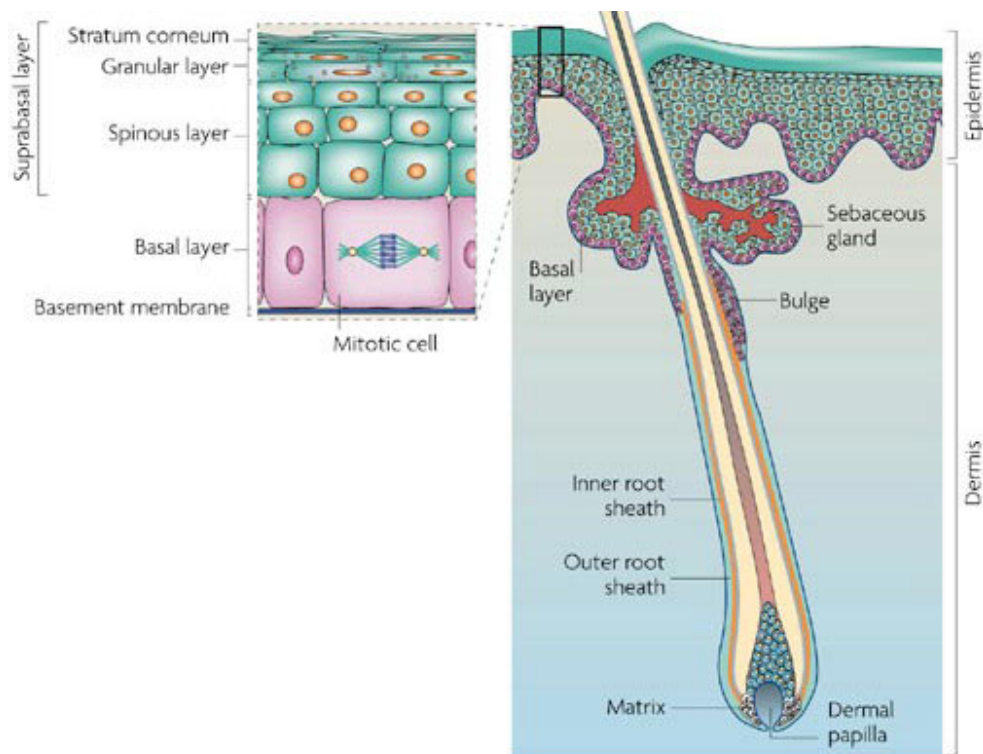


**Figure 1.5.1. The architecture of the skin and epidermis.** The skin can be subdivided into epidermis and dermis, which are separated by the BM. The pilosebaceous unit consists of a HF, SG and the surrounding IFE. Proliferating cells are located in the basal layer of the epidermis, adjacent to the BM. The differentiated suprabasal layers can be subdivided into the spinous and granular layers and the stratum corneum (Jones and Simons, 2008)

How epidermal multilayering and stratification is achieved is still not completely clear. Four different models to describe this process have been proposed: asymmetric cell division, delamination, epidermal proliferative units and a single-cell progenitor model. The asymmetric cell division model describes early embryonic skin development, where a single-layered epidermis expands first by symmetric cell division. Asymmetric cell divisions drive the onset of stratification, wherein the mitotic spindle orientates perpendicular to the BM and the resulting daughter cell directly translocates into the developing suprabasal layer (Lechler and Fuchs, 2005). However, it is not clear whether this occurs in the adult epidermis, as symmetric and

## Introduction

asymmetric cell divisions are found to occur randomly (Clayton et al., 2007). The delamination model describes a process in which basal keratinocytes weaken their adhesion to the BM and are subsequently pushed into the suprabasal layer by cellular contractions of neighboring keratinocytes (Vaezi et al., 2002; Watt and Green, 1982). The epidermal proliferative unit model (EPU) suggests that slow cycling basal layer keratinocytes give rise to transit-amplifying cells (TACs) that have a limited capacity of cell divisions and that are maintained in clusters within the epidermis (Potten, 1981). The single-cell progenitor model has challenged this idea. By tracing the fate of epidermal progenitors *in vivo* it was demonstrated that a single population of progenitors that undergoes stochastic cell division to provide daughters with progenitor or differentiated fate, is capable of maintaining epidermal homeostasis (Clayton et al., 2007; Jones et al., 2007). The asymmetric division model and the EPU model would require the presence of a distinct, bona fide epidermal SCs population. However, such cells have not yet been clearly identified.

### **1.5.2 Hair follicle morphogenesis and cycling**

HF morphogenesis is a tightly controlled process that relies on the precise signaling crosstalk between epidermis and the underlying mesoderm. HF morphogenesis starts at embryonic day (E) 14, when a dermal condensate of specialized fibroblasts forms in the dermis adjacent to the yet undifferentiated epidermis. Inductive epidermal signals act on the dermal condensate, which subsequently signals back to the epidermis leading to placode formation. A complex signaling network of activating and inhibitory signals secreted and received by the placodes and the dermal condensate allows further HF morphogenesis. In addition, it promotes neighboring cells to adopt IFE fate resulting in coordinated HF spacing (Sennett and Rendl, 2012).

By E16, the placode further develops into a hair germ (HG) and the dermal condensate differentiates into the dermal papilla (DP). During organogenesis the HG grows downwards and forms a peg that subsequently engulfs the dermal papilla at around E18. HF keratinocytes that are in direct contact with the DP become hair matrix cells. Hair matrix cells proliferate and move upwards to differentiate into six cylindrical layers of inner root sheath (IRS) and the hair shaft (HS). The outer layer of the HF, the outer root sheath (ORS) forms a continuum with the IFE and is surrounded by the BM (Botchkarev and Paus, 2003; Schmidt-Ullrich and Paus, 2005; Schneider et al., 2009).

There are different kinds of HFs in murine skin: guard hairs, awl/auchenne hairs and zig-zag hairs, which are formed in 3 specific waves of HF development during embryogenesis. After the third HF placode wave at E18 that gives rise to zig-zag hairs that represent the majority of the adult mouse hair coat (Schlake, 2007), HF morphogenesis continues with the full downgrowth of all three hair types until postnatal day (P) 14. Fully formed HFs undergo the first regression phase (catagen) between P17 and P19 followed by the first resting phase (telogen) around P21 (Cotsarelis et al., 1990). HF growth and regression appears cyclic and synchronous during the first two postnatal hair cycles. After this the HF continue cycling asynchronously (Blanpain and Fuchs, 2006).

### **1.5.3 Hair follicle stem cells and cycling**

Hair follicle stem cells (HFSCs) drive HF cycling. HFSCs identity is first established by distinct transcription factors. Sox9 (Nowak et al., 2008; Vidal et al., 2005) maintains HFSC identity and specifies the ORS lineage. The transcription factor nuclear factor of activated T cells c1 (Nfatc1) regulates SC quiescence in HFSCs

## Introduction

(Horsley et al., 2008), and Lhx2 balances HFSC maintenance and activation (Rhee et al., 2006). At the end of HF morphogenesis, the quiescent HFSC niche, the bulge, is formed below the SG at the base of the non-cycling part of the HF (Cotsarelis et al., 1990). It contains SCs that are marked by their expression of keratins (K15, K5, K14), the cell surface markers CD34 and Leucine-rich repeat-containing G protein-coupled receptor 5 (Lgr5), integrins ( $\alpha 6\beta 4$  and  $\alpha 3\beta 1$ ) and the transcription factors mentioned above.

To initiate the hair cycle and to start cell proliferation, HFSCs need to become activated. SC activation relies on the regulation of two critical signaling pathways: activation of Wnt pathway and inhibition of Bone Morphogenetic Proteins (BMPs). The Transforming Growth Factor  $\beta$  (Tgf- $\beta$ ) pathway plays an important role in initiating this regulation (Figure 1.5.3) (Blanpain and Fuchs, 2006).

### **Signaling during telogen-anagen transition**

Tgf- $\beta$  ligands (Tgf- $\beta$  1, 2 and 3) form dimers that bind to heterodimeric receptor complexes of serine/threonine kinases consisting of type I and type II receptor subunits. Upon ligand binding, the type II receptor phosphorylates and activates the type I receptor, initiating a Smad-dependent signaling cascade that regulates transcriptional activity (Dong et al., 2002). Tgf- $\beta$  signals through the receptor-regulated Smad2 and Smad3 (R-Smads) (Owens et al., 2008).

During the telogen-anagen transition, Tgf- $\beta 2$  is produced and secreted by the DP that acts on epithelial Tgf- $\beta 2$  receptors. This leads to the induction of transmembrane protein with EGF-like and two follistatin-like domains 1 (TMEFF1) that mediates the inhibition of the BMP pathway (Oshimori and Fuchs, 2012).

Furthermore, the DP secretes Wnt ligands and the BMP inhibitor noggin, which activates TACs in the hair matrix (Botchkarev et al., 2001; Greco et al., 2009). These TACs, characterized by P-cadherin expression (Muller-Rover et al., 1999), activate the Wnt/ $\beta$ -catenin pathway leading to cell proliferation and formation of the new hair (Deschene et al., 2014; Lowry et al., 2005). Wnt ligands bind to the frizzled receptor leading to the inactivation of a downstream destruction complex, thus enabling  $\beta$ -catenin to accumulate in the cytosol and to enter the nucleus to activate transcription of Wnt target genes (Clevers and Nusse, 2012). The epidermal deletion of  $\beta$ -catenin or its downstream mediator Lef-1 leads to hair loss (Huelsken et al., 2001; van Genderen et al., 1994).  $\beta$ -catenin is the master regulator of HF differentiation. In the absence of  $\beta$ -catenin, HFSCs fail to differentiate into follicular keratinocytes and adopt epidermal fate (Huelsken et al., 2001). Additionally, epidermal overexpression of  $\beta$ -catenin and thus a constitutively activated Wnt pathway, leads to de novo HF formation in these transgenic mice (Gat et al., 1998).

After dividing, HFSCs exit the bulge and migrate downwards along the ORS, where they further divide and expand the newly forming hair (Rompolas et al., 2013). The DP is pushed downward during this process and as it becomes more distant, the upper ORS becomes quiescent and lower ORS cells convert into TACs within the matrix (Rompolas et al., 2013). SC progeny or TACs that have not fully differentiated into a HF lineage but have migrated out of the bulge can return to their niche and serve as functional SCs during the next hair cycle (Hsu et al., 2014; Hsu et al., 2011).

Lgr5-positive HFSCs can be found in the lower part of the bulge and in the HG during telogen (Jaks et al., 2008). Upon anagen induction, these cells contribute to the lower ORS and replenish the pool of differentiating matrix cells. A proportion of these cells actively cycles and does not differentiate. Cells from the HG of the anagen

## Introduction

HF return to the HF bulge in the following telogen and provide the SC source for the next hair cycle. A small amount of Lgr5-progeny is additionally able to repopulate the HF isthmus (Jaks et al., 2008).

## Catagen

When matrix cells have exhausted their proliferative potential, the onset of catagen is initiated (Figure 1.5.3). Catagen is marked by a decrease in keratinocyte proliferation and the lower, non-permanent part of the HF degenerates by apoptosis. The DP remains attached to the BM at the HF tip while entering catagen and telogen.

By the onset of catagen, Wnt/ $\beta$ -catenin signaling in the HF is downregulated and apoptosis is initiated. Epidermal Growth Factor (EGF) receptor signaling (Mak and Chan, 2003; Murillas et al., 1995) and Tgf- $\beta$ 1 (Foitzik et al., 2000) have been shown to be key players during this process. However, it is not clear what initiates this cascade.

## Telogen

After the regression phase HFSC enter the quiescent telogen state (Figure 1.5.3). This phase is characterized by high BMP pathway activity. BMPs belong to the Tgf- $\beta$  superfamily and upon binding to their receptor they signal through R-Smads, Smad1, -5 and -8 (Owens et al., 2008). Mice with an inducible epidermis or HFSC-specific knockout of BMP receptor-1 have a defect in HFSC quiescence. The BMP receptor-deficient HFSCs show molecular characteristics of HG cells and they differentiate prematurely (Kandyba et al., 2013; Kobiela et al., 2007). Long-range BMPs, which are produced and secreted in cycles by the subcutaneous fat tissue, have also been

implicated in the regulation of SC quiescence (Plikus et al., 2008). After the quiescent phase, HFSCs become activated again and undergo the next round of cycle.

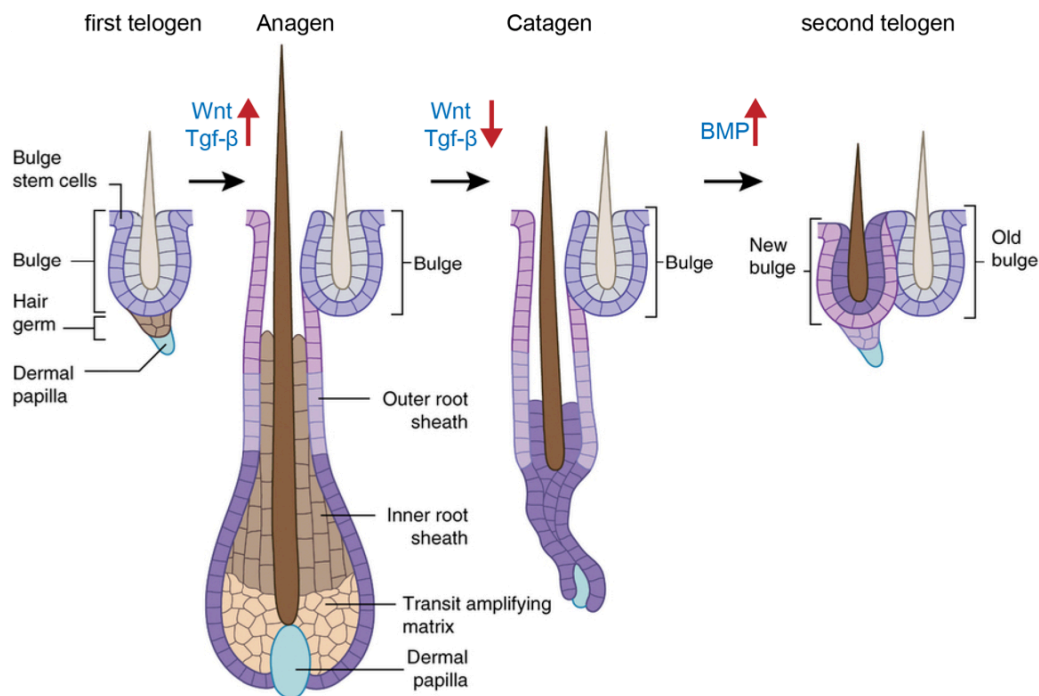


**Figure 1.5.3. The hair cycle.** The HF undergoes cyclic bouts of hair growth and regression. A pool of bulge HFSCs drives HF cycling. HFSCs are activated by the upregulation of Wnt and Tgf- $\beta$  signaling pathways upon anagen entry and downregulated when the HF regresses. Upregulation of the BMP pathway is required to establish and maintain SC quiescence during telogen (adapted from Hsu and Fuchs, 2014).

#### 1.5.4 Hair follicle stem cell niche

The term “niche” was first introduced in 1978 by Schofield as he described the functionality of hematopoietic cells in a local environment (Schofield, 1978). This local environment consisting of neighboring cells and ECM regulates SC behavior and is essential for their function (Fujiwara et al., 2011; Hsu and Fuchs, 2012; Scadden, 2006). SCs in the HF are localized within their distinct niches. Despite their intrinsic chronobiology that determines HF cycling in a temporal manner, the HFSC also participates in the regulation of SC activation and quiescence (Paus and Foitzik,

## Introduction

2004). Components of the HFSC niche consist of their local BM microenvironment, the DP as part of the dermal niche, and the subcutaneous fat tissue as part of the macroenvironment (Hsu and Fuchs, 2012). The cooperation of all niche components ensures proper HFSC function.

The BM is a central component of the HFSC niche. The BM provides a specific adhesion platform and determines growth factor bioavailability, thereby regulating SC function (Kerever et al., 2007; Nistala et al., 2010). Profiling of adult K15-positive HFSCs revealed that a large number of ECM genes are differentially expressed by bulge SCs compared to other basal keratinocytes (Morris et al., 2004). Furthermore, transcription profiling of genes that determine stemness identified  $\beta$ 1-integrin and  $\alpha$ 6-integrin to be upregulated in SCs compared with their progeny (Ivanova et al., 2002; Ramalho-Santos et al., 2002). Studies on epidermal  $\beta$ 1-integrin hypomorphic mice further showed that keratinocytes expressing  $\beta$ 1-integrins *in vivo* expanded more than  $\beta$ 1-low or  $\beta$ 1-null cells (Piwko-Czuchra et al., 2009), indicating that  $\beta$ 1 integrin expression is essential for epidermal SC function.

### **1.6 The skin basement membrane**

The epidermis and dermis are physically separated by a BM. It serves as an anchoring platform for keratinocytes, stabilizes the tissue and controls the release and diffusion of growth factors. Stable anchorage of the epidermis to the BM is mediated by hemidesmosomes (see below). As all BMs, the skin BM consists of LNs, type IV collagen, glycoproteins, nidogen and perlecan (Behrens et al., 2012; Mokkalapati et al., 2008). The BM is anchored to the underlying dermis via type VII collagen, produced by fibroblasts (Breitkreutz et al., 2013).

### 1.6.1 Laminins in the skin

Both keratinocytes as well as fibroblasts express and deposit LNs into the epidermal BM (Marinkovich et al., 1993). The most relevant LNs in the BM of the skin are LN-332 and LN-511. Mice lacking the LN- $\alpha$ 5 (*LAMA5*) chain die by E16.5 due to severe defects including syndactyly, failure in neural tube closure and placentopathy (Miner et al., 1998). To study the role of LN-511 in hair development, skin from E16.5 LN- $\alpha$ 5 deficient mice was transplanted onto nude mice, revealing a failure in HF organogenesis resulting in HF regression (Li et al., 2003). Further analysis showed that epidermis-derived LN-511 is important for the crosstalk with the DP, and consequently for HF downgrowth (DeRouen et al., 2010; Gao et al., 2008). The expression of LN-332 during HF morphogenesis occurs at later stages compared to LN-511 (Imanishi et al., 2014). Deletion of the LN- $\alpha$ 3 gene (*LAMA3*) results in neonatal lethality (Ryan et al., 1999). Deletions or mutations in *LAMA3*, *LAMB3* and *LAMC2* genes encoding for the chains of LN-332 lead to perturbation of LN-332 function in humans. Lack of functional LN-332 leads to a skin blistering disease termed junctional epidermolysis bullosa, characterized by disruption of the BM, diminished dermal-epidermal adhesion, and subsequent blister formation (Bruckner-Tuderman and Has, 2012).

Expression analyses of LN-332 and LN-511 during HF cycling showed that when anagen is induced by hair plucking, the expression of LN-511 remains constant whereas LN-332 expression is transiently downregulated during the peak phase of anagen (Sugawara et al., 2007). Furthermore, adding recombinant LN-511 to HF cultures in vitro promoted hair growth, whereas adding recombinant LN-332 suppressed this (Sugawara et al., 2007), supporting the hair growth-promoting role of LN-511. The opposing effect of the two LNs was further analyzed during catagen. At

## Introduction

this stage LN-332 levels were unchanged whereas LN-511 expression was gradually downregulated (Tateishi et al., 2010). Application of recombinant LN-332 had no effect on catagen progression, whereas LN-511 caused a prolonged catagen (Tateishi et al., 2010). A model that emerges from these studies is that LN-511 is highly expressed during the growth phase of the HF and it has a growth-promoting effect, whereas LN-332 suppresses HF growth and is subsequently involved in HF regression.

### **1.6.2 Laminins and their integrin receptors**

Both LN-332 and LN-511 bind to  $\alpha 3\beta 1$  integrins, although LN-511 binds with a higher affinity to  $\alpha 3\beta 1$  integrin compared to LN-332 (Nishiuchi et al., 2003). LN-332 also binds to the hemidesmosome-forming integrin  $\alpha 6\beta 4$ . Besides  $\alpha 6\beta 4$  integrin, skin hemidesmosomes contain type XVII collagen and tetraspanin CD151, and they are connected to intermediate filament network inside the cell. Disturbances in hemidesmosome formation lead to skin blistering due to BM instability (Wickström et al., 2011).

Proteolytical processing of the LN  $\alpha 3$  chain alters its binding affinity to integrin receptors. While the long, more immature isoform of the  $\alpha 3$ -chain mainly binds to  $\alpha 3\beta 1$  integrins, the shorter processed  $\alpha 3$ -chain binds preferentially to  $\alpha 6\beta 4$  integrins. The interaction of LN-332 with  $\alpha 3\beta 1$  integrin is mainly implicated in keratinocyte migration (Frank and Carter, 2004), where the cleavage in the  $\alpha 3$ -chain appears to be a prerequisite for hemidesmosome formation, enabling  $\alpha 6\beta 4$  integrin clustering and thereby promoting keratinocyte adhesion and BM stabilization (Baudoin et al., 2005).

## 1.7 The extracellular matrix of the dermis

The dermis is the connective tissue layer between the epidermis and the subcutaneous fat layer. In addition to ECM, it contains ECM-producing fibroblasts, immune cells (lymphocytes, neutrophils, monocytes and mast cells), blood and lymphatic vessels. It is subdivided into two parts: the papillary dermis (*stratum papillare*) adjacent to the epidermis and the BM, and the reticular dermis (*stratum reticulare*) underneath. The papillary dermis is composed of loose, small diameter collagen fibers and immature elastic fibers. The reticular dermis contains large-diameter collagen fibers and mature elastic fibers that are decorated with proteoglycans and fibril-associated macromolecules. Fibril-forming collagens including collagen type I, III and V are the most abundant collagens in the dermis. They interact with FACIT collagens type XII and XIV and assemble together into large, parallel fibril bundles. Non-fibril-forming collagens, including type IV, VI and VII are found in the BM (collagen type IV), intercalated into fibril bundles (type VI) or anchoring epidermis and dermis (type VII). Proteoglycans in the skin include HSPGs, chondroitin-6-sulfate proteoglycans, which are associated with the BM, whereas chondroitin sulfate (versican) or dermatan sulfate proteoglycans (lumican, decorin, biglycan) are found in the dermis. Decorin and biglycan contribute to collagen fibrillogenesis by connecting type I collagen and FACIT collagens. Lumican controls collagen fibril diameter and fibril spacing (Aumailley and Gayraud, 1998; Eckes and Krieg, 2004; Krieg and Aumailley, 2011).

The elastic fiber network in the dermis consists of fibrillins, fibulins, MAGPs and LTBP, which regulate the bioavailability of Tgf- $\beta$  and BMPs. Under physiological conditions, fibroblasts produce little ECM but upon tissue injury, Tgf- $\beta$  causes fibroblasts to differentiate into myofibroblasts, thus enabling ECM remodeling (Tomasek et al., 2002).

## **1.8 Integrin-linked kinase in the skin**

The expression of ILK in the epidermis is restricted to the basal layer keratinocytes of the IFE and the HF, where keratinocytes are anchored to the BM. In the dermis, ILK is expressed by all cell types present, including the dermal fibroblasts. To investigate the role of ILK in the skin, different conditional knockout mouse models with either epidermis- or dermis-specific deletions of ILK have been generated (Blumbach et al., 2010; Lorenz et al., 2007; Nakrieko et al., 2011; Nakrieko et al., 2008).

### **1.8.1 ILK in the epidermis**

Three different epidermal ILK-deficient mouse models have been described so far (Lorenz et al., 2007; Nakrieko et al., 2011; Nakrieko et al., 2008). Nakrieko and coworkers (2008) bred transgenic mice that express Cre recombinase under the K14 promoter with mice carrying loxP sites flanking exons 4 and 12 of ILK (Terpstra et al., 2003). The resulting ILK-K14 knockout mice were born with no detectable ILK protein in the epidermis at birth and the pups survived until P4 (Nakrieko et al., 2008). Lorenz and coworkers (2007) deleted ILK in the epidermis by crossing mice that overexpress Cre under the K5 promoter with mice that carry a floxed exon 2 including the transcription start site of ILK (Sakai et al., 2003b). These mice that are also used in this thesis work were viable and ILK was still present in the epidermis at birth, but became undetectable two days after birth (Lorenz et al., 2007). The differences in viability and HF morphogenesis (discussed below) between ILK-K14 and ILK-K5 mice are probably caused by the differential onset of Cre recombinase expression. K14-Cre expression is first detectable at E11.5 (Turksen et al., 1992) therefore leading to an earlier gene deletion as K5 promoter-driven Cre that starts to express Cre from E15.5 onwards (Ramirez et al., 2004).

ILK-K14 mice displayed a 55 % reduction in HF number. This was associated with reduced proliferation within the HFs, whereas proliferation within the IFE was not affected (Nakrieko et al., 2008). The epidermal-dermal junction showed presence of microblisters with discontinuous expression patterns of  $\alpha 6$ - and  $\beta 4$ -integrins at the BM. In addition, some  $\beta 1$ -integrin expressing cells were present in the suprabasal layer. The expression patterns for differentiation markers K14 and K15 were mostly similar between knockouts and controls (Nakrieko et al., 2008).

In a later study, the same authors investigated ILK-K14 animals during different stages of embryonic HF morphogenesis (Rudkouskaya et al., 2014). They found a downregulation of the Wnt signaling pathway during HF development and linked this finding to impairment in HF matrix formation and IRS lineage specification in ILK-K14 mice. The authors attributed the phenotype to a loss of keratinocyte apical-basal polarity in ILK-deficient HFs caused by impaired assembly of an intact LN-511-rich BM at the HF tip. The exogenous addition of LN-511 in *ex vivo* embryonic tissue explants rescued hair matrix formation indicated by a structural reorganization of P-cadherin expressing cells. However, it was not sufficient to rescue HF organogenesis. In conclusion, although some finding of this study were contradictory to their previous findings where they reported upregulation of Wnt, Hedgehog and Tgf- $\beta$  pathways, the authors concluded that ILK is required for the assembly of LN-511 in order to ensure functional epithelial-mesenchymal crosstalk, which is essential for hair matrix formation (Judah et al., 2012; Rudkouskaya et al., 2014).

The K5-Cre driven conditional ILK knockout mouse model (ILK-K5) used in this thesis was described by Lorenz and colleagues (Lorenz et al., 2007). At birth, the ILK-deficient mice are indistinguishable from their control littermates. They develop a hair coat with partial alopecia containing a mixture of fully developed and shortened

## Introduction

HF. After the first telogen phase (P21) ILK-K5 mice progressively lose their hair, resulting in complete alopecia at 6-8 weeks. During the first 3 weeks of postnatal development, the skin becomes hyperplastic (from P7 onwards) and microblisters develop into macroscopically visible skin blisters. Skin blistering is associated with compromised keratinocyte adhesion and BM integrity detected by irregular deposits of LN-332 containing BM fragments at the dermo-epidermal junction. Electron microscopy revealed no change in hemidesmosome number in intact parts of the BM. Furthermore, the expression levels of the  $\alpha 6$ -,  $\beta 4$ -, and  $\alpha v$ -integrins were unchanged in ILK-K5 keratinocytes, whereas  $\alpha 3$ - and  $\alpha 2$ -integrin chains were slightly upregulated and  $\beta 1$ -integrin was slightly downregulated. Hyperplasticity of the epidermis was associated with an increase in proliferation with abnormal localization of proliferating cells in the suprabasal layer. Increased proliferation was also observed in ORS cells that accumulated and led to ORS thickening. Differentiation within the IFE was impaired as K14-expressing cells were present in the suprabasal layer. However, the mechanism for the progressive hair loss was not uncovered in this study.

### **1.8.2 ILK in dermal fibroblasts**

To study the role of ILK in the dermis, ILK floxed mice were crossed with mice carrying Cre recombinase fused to a tamoxifen-sensitive estrogen receptor (Cre<sup>ERT</sup>) under the control of a fibroblasts-specific regulatory fragment of the pro- $\alpha 2(I)$  collagen gene (*Colla2*) (Blumbach et al., 2010; Sakai et al., 2003b). The authors found that ILK plays an important role in myofibroblast formation during skin repair. Myofibroblasts play critical role in regenerative processes in the skin (Hinz, 2007). *In vitro* experiments further showed that deletion of ILK in fibroblasts leads to increased

RhoA-ROCK activity, causing abnormal cell morphology, impaired cell motility and cell contraction. Reduced Tgf- $\beta$ 1 secretion by ILK-deficient fibroblasts as well as decreased exogenous Tgf- $\beta$ 1 activity was insufficient to induce  $\alpha$ -smooth muscle actin ( $\alpha$ -SMA) production, which consequently led to failure in myofibroblast differentiation.

## 2 Aims of the thesis

ILK is an essential adaptor protein linking  $\beta$ 1- and  $\beta$ 3-integrins to the actin cytoskeleton. It thereby regulates cellular processes that depend on integrin-driven actin dynamics such as migration and polarity. On the other hand, cell-matrix interactions are crucial for ECM remodeling that requires the generation of cellular tension. The precise composition of the ECM in turn determines cellular behavior through the modulation of various signaling activities. This study aimed to understand the role of ILK in cellular force generation and subsequent ECM remodeling.

Furthermore, the project was directed to investigate the importance of these processes *in vivo* and in particular to unravel the roles of cell-ECM interactions in regulating the SC niche and subsequently SC behavior.

The specific questions asked were:

1. Does ILK have a function in cellular force generation and ECM remodeling?
2. What is the role of ILK in SC fate regulation?
3. Does ECM remodeling by ILK impact SC behavior? What are the molecular mechanisms?

### 3 Materials and methods

#### 3.1 Chemicals and reagents

Unless denoted explicitly, common chemicals and reagents used in this study were purchased from the following suppliers: Merck (Darmstadt, Germany), Carl Roth (Karlsruhe, Germany), Sigma Aldrich (Munich, Germany).

#### 3.2 Animal experiments

All experiments were performed in compliance to guidelines and animal licenses of the State Office North Rhine-Westphalia and Bavaria, Germany. All mouse strains (except for ILK-Lgr5) were maintained and bred in the specific-pathogen-free mouse facility of the Center of Molecular Medicine Cologne, Germany. ILK-Lgr5 mice were housed in the animal facility of the Department for Pharmacology, Cologne, Germany. Mice for the two-stage carcinogenesis experiment were bred and maintained in the animal facility of the Max-Planck-Institute for Biochemistry (Martinsried, Germany). In all cases, mice were given *ad libitum* access to standard rodent diets and water. Breeding of mice started at 8-10 weeks of age. Mice were weaned between postnatal day (P) 18 and 22. Tail clips were taken for subsequent DNA isolation and genotyping. Genders were distributed randomly between genotypes in all mouse experiments.

##### 3.2.1 Breeding schemes and animal procedures

###### Epidermis-specific ILK-K5 mice

To generate epidermis-specific ILK knockout mice, homozygous female mice with loxP sites inserted to flank exon 2 and the transcription start site of the *Ilk* gene (*ILK flox/flox*; (Sakai et al., 2003b) were intercrossed with heterozygous male mice (*ILK*

## Materials and methods

*flox/wt*) that additionally carried a transgene to express the Cre recombinase under the control of the keratin 5 (K5) promoter (Ramirez et al., 2004). *ILK flox/flox, K5-Cre* (from here on ILK-K5) knockout mice were compared to *ILK flox/wt, K5-Cre* (from here on controls) littermates.

### **Inducible epidermis-specific ILK-iK14 mice**

To generate mice with an inducible deletion of the *Ilk* gene within the epidermis heterozygous female *ILK flox/wt* mice additionally carrying the tetracycline-controlled transactivator protein (rtTA) transgene under the control of the Keratin-14 promoter (*K14rtTA*) were crossed with homozygous *ILK flox/flox* male mice additionally carrying a Cre recombinase transgene under the control of a tetracycline-responsive promoter element (*tet-O-Cre*) (Nguyen et al., 2006). Cre recombinase expression was induced by administration of doxycycline (for details see below). *ILK flox/flox, K14rtTA, tet-O-Cre* knockout mice (from here on ILK-iK14) were compared to control littermates carrying the following genotypes: *ILK flox/flox tet-O-Cre*; *ILK flox/wt, K14rtTA, tet-O-Cre* (controls).

ILK-iK14 mice were fed with doxycycline containing chow (1 g/ kg; ssniff, Germany) from 3 weeks of age onwards in order to induce Cre expression and the deletion of the *Ilk* gene. Deletion of ILK was induced by the tetracycline-controlled transcriptional activation (Tet-on) system, which activates the expression of a transgene that is dependent on the activity of a transcriptional activator and the presence of tetracycline or its derivate doxycycline. In brief, the basis for the Tet-on system is the reverse tetracycline-controlled transactivator (rtTA), a fusion protein comprising of a Tet repressor DNA binding protein (isolated from the tetracycline-resistance operon of *Escherichia coli*) fused to the transactivating domain of VP16 from Herpes simplex virus. In the presence of doxycycline, rtTA induces the

expression of target transgenes that contain a tetracycline-responsive promoter element. This element consists of a Tet operator (tetO) sequence fused to a minimal promoter. In this study, rtTA expression was driven by the Keratin 14 (K14) promoter and the tetO was coupled to the Cre transgene. Hence, expression of Cre in K14-positive cells was induced by administration of doxycycline, leading to the excision of the floxed *Ilk* allele within these cells.

### **HFSC-specific ILK-Lgr5 mice**

To achieve inducible deletion of the *Ilk* gene in HFSCs and to perform lineage-tracing experiments *ILK flox/flox* mice were crossed with *Lgr5-EGFP-Ires-Cre<sup>ERT2</sup>* mice additionally carrying a LacZ Cre reporter (*Rosa26R-LacZ*; (Soriano, 1999)). These mice were described previously (Jaks et al., 2008). Lgr5-specific ILK-knockout mice (from here on ILK-Lgr5) were compared to control littermates (controls).

*Lgr5-EGFP-Ires-Cre<sup>ERT2</sup>* mice express Cre recombinase fused to a mutated hormone-binding domain of the estrogen receptor (ERT) under the Leucine-rich repeat-containing G-protein coupled receptor 5 (Lgr5) promoter. Lgr5 is specifically expressed in HFSCs, restricting the expression of Cre<sup>ERT</sup> to this compartment. Cre<sup>ERT</sup> is constitutively expressed in Lgr5-expressing cells but it is inactive. The Cre can be activated by administration of a synthetic estrogen receptor ligand such as tamoxifen. Tamoxifen binds to the fused receptor and Cre<sup>ERT</sup> translocates from the cytoplasm into the nucleus where it mediates the excision of loxP sites. Cre<sup>ERT2</sup> is an improved Cre<sup>ERT</sup> recombinase system where Cre is fused to a human estrogen receptor ligand-binding domain. It has a decreased background activity and shows increased sensitivity due to enhanced tamoxifen binding specificity.

In order to activate Cre, ILK-Lgr5 mice were injected with 100 µl of 10 mg/ml tamoxifen (Sigma, T5648) into the intraperitoneal cavity from P17 for 5 consecutive

## Materials and methods

days at 24-h intervals. 10 mg tamoxifen was dissolved in 50  $\mu$ l 100 % ethanol at 55 °C and supplemented with corn oil (Sigma, C8267) to a final volume of 1 ml. The mixture was further incubated at 55 °C, with 800 rpm rotation for at least 45 min before injection.

### 3.2.2 Two-stage carcinogenesis experiment

Two-stage carcinogenesis experiments were carried out by Sara A. Wickström in the animal facility of the Max-Planck Institute for Biochemistry in Martinsried, Germany. 8-week old mice were shaved on the back followed by the topical treatment of with 100 nmol 7,12-dimethylbenz[a]anthracene (DMBA; Sigma) in 100  $\mu$ l of acetone 2 days after shaving. The treatment was repeated one more time two days after the first application. 2 weeks post DMBA treatment 10 nmol 12-*O*-tetradecanoylphorbol-13-acetate (TPA; Sigma) in 200  $\mu$ l of acetone was applied twice-weekly for 18 weeks. The experiment was terminated after 18 weeks of TPA treatment due to skin health condition of ILK-K5 mice. All mice were euthanized at the end of the experiment. Tumor size and numbers of tumors were recorded weekly after the start of TPA treatment (week 0). Skin biopsies and tumors were analyzed biochemically and by histology.

### 3.2.3 BrdU and EdU injections

The *in vivo* proliferation experiment on ILK-K5 mice was carried out by injecting the thymidine homolog 5-bromo-2'-deoxyuridine BrdU. For analyses of short-term proliferation 100 mg/ml BrdU (Sigma) was injected intraperitoneally 1 h prior to sacrifice. BrdU incorporation was analyzed by immunofluorescence staining with antibodies against BrdU (see 3.4.6). To mark label-retaining cells (LRCs) in ILK-K5

mice, 50 mg/kg thymidine homolog 5-ethynyl-2'-deoxyuridine EdU (Invitrogen) was injected intraperitoneally four times at 12-h intervals from P10 to P11. The EdU was subsequently chased for 10 days. At P21, mice were sacrificed and skin tissues were dissected and prepared for cryo/paraffin embedding as described in section 3.3.2.1 and 3.3.2.2. EdU incorporation was analyzed as described in section 3.4.7.

### **3.3 Histological analyses**

#### **3.3.1 Equipment and materials**

Light microscope: Leica DMI3000B

Microtome: NM 340E, Thermo Scientific

Water bath: Leica H1210

Cryostat: Microm HM 560, Thermo Scientific

Antigen Retriever: Retriever 2100, electron microscopy sciences

Embedding machine: Leica EG 1160

Tissue processor: STP 120, Thermo Scientific

Embedding cassettes: EBK, Hartenstein, Germany

Filter paper for embedding: Medite 46-6200-00

Cryomold intermediate; 4566, Tissue-Tek, Sakura

Mounting media:

Entellan, Merck 1.07961.0100

Aquatex, Merck 1.08562.0050

#### **3.3.2 Histological methods**

The most critical concern aspect of histochemical techniques is tissue preservation to maintain morphology, but on the other hand to allow histochemical procedures such

## Materials and methods

as antibody penetration and antigen preservation. Therefore, fixation and tissue embedding have to be carried out with care. Paraformaldehyde or glutaraldehyde fix the tissue by reacting with basic amino acid residues thereby crosslinking neighboring proteins. Methanol, ethanol or acetone fix the tissue by denaturing wherein the solubility of proteins gets reduced due to the disruption of tertiary protein structures. Aldehydes preserve the tissue much better than alcoholic fixatives.

Embedding of fixed tissue into paraffin wax helps to maintain tissue architecture and enables cutting of thin sections (see 3.3.2.1). For unfixed tissues, cryopreservation and tissue embedding into cryo-resisting matrix is used and enables sectioning at temperatures below -10 °C.

### **3.3.2.1 Preparation of paraffin sections**

Mice were sacrificed at indicated time points and tissue samples were taken. The samples were then wrapped in filter paper in order to avoid tissue deformation during tissue processing. The isolated samples in filter paper were placed into embedding cassettes and transferred into freshly prepared, ice-cold paraformaldehyde (4 % PFA in phosphate buffered saline (PBS)) and incubated 1-2 h on ice for fixation.

Subsequently, the fixed samples were transferred to 70 % ethanol and incubated at 4 °C overnight. For dehydration and paraffin processing, samples were placed into an automated tissue-processing machine (for detailed program see below). Embedding into paraffin was done using the embedding machine. Paraffin blocks were stored at room temperature (RT) until cutting. Prior to cutting, paraffin blocks were cooled to -20 °C and 6-8 µm sections were cut using the microtome. To ensure tissue straightening, sections were floated on water at 45 °C for at least 5 min. Test sections were inspected under the microscope and adjustments were done to obtain the best

quality and orientation of sections. Slides were dried over night at 37 °C and stored at RT.

***Tissue processor program:***

<i>70 % ethanol</i>	<i>1,5 h</i>
<i>80 % ethanol</i>	<i>1,5 h</i>
<i>96 % ethanol</i>	<i>1,5 h</i>
<i>100 % ethanol</i>	<i>1 h</i>
<i>100 % ethanol</i>	<i>1 h</i>
<i>Xylol</i>	<i>1,5 h</i>
<i>Xylol</i>	<i>1,5 h</i>
<i>Paraffin</i>	<i>2 h</i>
<i>Paraffin</i>	<i>2 h</i>
<i>Paraffin</i>	<i>2 h</i>

***10 x PBS***

<i>80 g</i>	<i>NaCl</i>
<i>2.0 g</i>	<i>KCl</i>
<i>14.4 g</i>	<i>Na<sub>2</sub>HPO<sub>4</sub> x 2 H<sub>2</sub>O</i>
<i>2.0 g</i>	<i>KH<sub>2</sub>PO<sub>4</sub></i>

*filled up with H<sub>2</sub>O to 1000 ml, after diluting to 1x PBS pH becomes 7.4*

***4 % paraformaldehyde /PBS***

*4 g Paraformaldehyde was dissolved in 100 ml 1x PBS at 60 °C while stirring.*

*Solution was cooled down to 4 °C before use.*

### **3.3.2.2 Preparation of cryosections**

Tissue samples were placed into cryomolds containing OCT Tissue Tek directly after dissection and subsequently allowed to solidify on dry ice. Frozen blocks were stored at -80 °C, and 6-8 µm thick sections were cut at -20 °C using the cryostat. Sections were air-dried and finally stored at -80 °C.

### **3.3.2.3 Hematoxylin and eosin staining**

This method is a standard histological method that allows detection of several distinct tissue structures. The principle is based on the application of hemalum, an oxidation product of haematoxylin. Hemalum colors nuclei in blue. Eosin serves as a counterstain and colors eosinophilic structures, mainly structures that are basic, in different shades of red.

For hematoxylin and eosin staining, paraffin sections were deparaffinized (2 x 5 min Xylol) followed by rehydration (100 % isopropanol, 95 %, 75 %, 50 % ethanol, and distilled water; 5 min each). Sections were stained for 50 s with Hematoxylin and blued in tap water. Sections were counterstained for 10 sec with Eosin and subsequently washed in water. Sections were then dehydrated (50 %, 75 %, 95 % ethanol, isopropanol 2 min each), washed 2 x 2 min in Xylol, and finally mounted in Entellan.

*Hematoxylin: Shandon Gill3 Hematoxylin*

*Eosin: Shandon Eosin Y, Aqueous*

### 3.3.2.4 $\beta$ -galactosidase staining

The lacZ reporter gene was used to visualize Cre activity in skin tissue. LacZ encodes for  $\beta$ -galactosidase that can be detected by a chromogenic substrate 5-Bromo-4-Chloro-3-indolyl- $\beta$ -D-galactopyranoside (X-Gal) that becomes hydroxylated by  $\beta$ -galactosidase to produce a blue precipitate.

Tissue samples were fixed in 0,2 % glutaraldehyde/PBS for 1 h on ice. After rinsing 3 x 10 min with PBS, the tissue was permeabilized with wash solution for 1 h at RT.

Samples were then incubated with freshly prepared staining solution at 37 °C overnight. Subsequently, samples were washed 3 x 10 min with PBS and post-fixed with 4 % PFA in PBS for 1 h at RT. Samples were stored in 70 % ethanol until processing for paraffin embedding (see 3.3.2.1). 8-10  $\mu$ m-thick sections were subsequently cut using the microtome. Sections were deparaffinized (see 3.3.2.3) and counterstained with nuclear fast red for 1 min. After this, the sections were dehydrated and mounted in Entellan.

*Glutaraldehyde 25 % Serva 23115*

*Nuclear fast red (Roth N069.1)*

#### ***Wash solution***

*0.02 % Nonidet P-40*

*2 mM MgCl<sub>2</sub>*

*in 1x PBS*

#### ***Staining solution***

*5 mM Kaliumferrocyanide (K<sub>4</sub>Fe(CN)<sub>6</sub>)*

## Materials and methods

5 mM            *K-ferricyanide* ( $K_3Fe(CN)_6$ )

1 mg/ml        *X-Gal* (prepared from a 100 mg/ml stock in DMF; biomol 02249.1)

*in wash solution*

### 3.3.2.5 Alkaline phosphatase staining

Alkaline phosphatases are dephosphorylating enzymes that are active in a basic environment. Alkaline phosphatase staining was used to visualize its endogenous activity within the DP of the HF using the NBT/BCIP reporter system. BCIP (5-Bromo-4-chloro-3-indolyl phosphate) becomes hydrolyzed by alkaline phosphatase and the resultant product is oxidized by NBT (Nitro blue tetrazolium chloride) resulting in the formation of a blue precipitate.

Cryosections were air-dried, fixed with acetone for 10 min at -20 °C, and washed for 5 min in PBS. Staining solution was applied and the reaction was monitored under the microscope in real time. The reaction was terminated by placing the slides into water. After that, sections were counterstained with nuclear fast red for 10 min, washed with water and mounted in Aquatex.

#### *Staining solution*

2 %            *NBT/BCIP stock solution* (Roche, 11681451001)

*in*            *0.1 M Tris-HCl, pH 9.5; 0.1 M NaCl*

### 3.4 Immunological Methods

#### 3.4.1 Materials

##### 3.4.1.1 Primary antibodies

Name	Company	Cat. No.	IF	Fixation/TRS	WB
$\beta$ -Catenin	Santa Cruz	sc-7199	1:300	PFA/pH6	1:5000
BrdU	BD	347580	1:50	pH6	
CD3	Serotec	MCA-1477	1:100	pH9	
CD34	M. Koch	KR66	1:1000	PFA/pH6	
F4/80	Dianova	BM8	1:200	pH6	
$\gamma$ H2AX	Cell Signaling	9718	1:250	pH9	
ILK	BD	611802	1:500		
Keratin 14	Progen	GP-CK14	1:100	PFA/pH6, pH9	
Keratin 14	Covance	PRB-155P	1:1000	PFA/pH6, pH9	
Keratin 15	Thermo	MS-1068-po	1:2000	PFA/pH6, pH9	
Ki67	DAKO	M7249	1:100	IHC pH6	
Lef1	Cell Signaling	2230	1:100	PFA	
LN 332	Aumailley	R14	1:10000	PFA	
LN $\alpha$ 5	Sorokin	405	1:10000	PFA	
p53	Leica	DM5	1:100	pH6	
Paxillin	BD	610051	1:300	PFA/MeOH	
Phalloidin	Sigma		1:600	PFA	
Ras	BD	610001			1:2500
p-Cadherin	Invitrogen		1:200		
p-Smad 1/5/8	Cell Signaling	9511			1:1000
p-Smad 2	Cell Signaling	3101	1:100	IHC 1:100	1:1000
Smad 2	Cell Signaling	3103			1:1000

### 3.4.1.2 Secondary antibodies

Name	Company	Cat. No.	Conjugate	Appl.	dilution
$\alpha$ -IgG guineapig	Invitrogen	98228	A488	IF	1:500
$\alpha$ -IgG rabbit	Invitrogen	A11011	A568	IF	1:500
$\alpha$ -IgG rabbit	Invitrogen	A11008	A488	IF	1:500
$\alpha$ -IgG mouse	Invitrogen	A11001	A488	IF	1:500
$\alpha$ -IgG1 mouse	Invitrogen	A21121	A488	IF	1:500
$\alpha$ -IgG2a mouse	Invitrogen	A21131	A488	IF	1:500
$\alpha$ -IgG2a mouse	Invitrogen	A21134	A568	IF	1:500
$\alpha$ -IgG mouse	BioRad	170-6516	HRP	WB	1:10 000
$\alpha$ -IgG rabbit	BioRad	170-6515	HRP	WB	1:10 000
$\alpha$ -IgG rabbit	Thermo	31820	Biotin	IHC	1:300

### 3.4.2 Immunofluorescence staining of paraffin sections

Immunofluorescence staining was carried out on paraffin sections using the protocol described below. The antigen retrieval method was specifically chosen for each antibody. The antigen retrieval method used for a particular antibody is described in the table for primary antibodies.

Paraffin sections were deparaffinized and rehydrated as described. Subsequently antigen retrieval was performed. During antigen retrieval protein cross-links that were formed during formalin fixation are released and hidden antigen sites are uncovered. Hot antigen retrieval was carried out using target retrieval solution (TRS) with pH 6 or pH 9 in a pressure cooker, where samples are cooked in high pressure for 20 min. followed by 1 h of cooling. Sections were then blocked with 5 % normal goat serum (NGS), 3 % bovine serum albumin (BSA) in PBS for 1 h at RT. Primary antibodies diluted in Antibody Diluent was applied overnight at 4 °C. After that, samples were washed 3 times for 5 min in PBS. Sections were incubated with fluorescent-labeled secondary antibodies diluted in PBS for 1 h in the dark. The nuclei were counterstained with 1 mg/ml 4',6-Diamidino-2'-phenylindole dihydrochloride (Dapi; 1:1000). After 3 x 5 min washes in PBS, samples were mounted in elvanol and dried at RT in the dark.

<i>Antibody Diluent</i>	<i>Dako S3022</i>
<i>Target Retrieval Solution, pH6 (10x)</i>	<i>Dako S1699</i>
<i>Target Retrieval Solution, pH9 (10x)</i>	<i>Dako S2367</i>
<i>R-Buffer A (10 x; pH6)</i>	<i>EMS 62706-10</i>
<i>Dapi</i>	<i>Roche 10236276001</i>

### ***Elvanol***

2.4 g            *Mowiol-Dabco (Roth)*

7.5 ml           *87 % glycerol*

11.7 ml          *distilled water*

-> *stir for 2 h at RT, then add*

4.8 ml           *Tris-HCl, pH 8,5*

-> *stir at 53 °C until dissolved, then add*

0.02 g           *Dabco (Roth)*

*aliquot and store at -20 °C*

### **3.4.3 Immunofluorescence staining of cryosections**

Cryosections were air-dried for 20 min. Sections were fixed with the indicated fixative (see table for primary antibodies). Fixation was carried out as follows:

For acetone and methanol fixation slides were covered with ice-cold dried acetone/methanol and incubated at -20 °C for 10 min. Acetone/methanol was then removed and slides were rehydrated with PBS.

For PFA fixation sections were covered with freshly prepared, cold 4 % PFA in PBS and incubated for 10 min at RT. The fixative was then removed and slides were

## Materials and methods

washed with PBS. The tissue was subsequently permeabilized by treatment with 0,2 % Triton-X-100 in PBS for 10 min at RT.

After fixation, unspecific antibody binding was blocked with 5 % GNS, 3 % BSA in PBS for 1 h at RT. The primary antibody was applied overnight at 4 °C in 1 % BSA in PBS (0,1 % Triton-X-100 was supplemented for proteins with anticipated nuclear localization). The next day, slides were washed 3 times for 5 min with PBS. The fluorescent-labeled secondary antibody was applied for 1 h at RT in the dark. The nuclei were counterstained with 1 mg/ml Dapi (1:1000). After 3 washes for 5 min each with PBS, samples were mounted in elvanol and dried at RT in the dark.

### **3.4.4 Immunofluorescence staining of adherent cells**

Cells grown on coverslips were fixed with 4 % PFA in PBS for 10 min at RT. The staining procedure was carried out in a 24-well plate. Cells were washed once with PBS and then permeabilized with 0,2 % Triton-X-100 in PBS for 10 min at RT. After 2 washes for 5 min with PBS cells were blocked with 5 % BSA in PBS for 1 h at RT. The primary antibody was applied over night at 4 °C in blocking solution. The next day, cells were washed 3 times for 5 min with PBS followed by secondary antibody treatment for 1 h at RT in PBS in the dark. Cells were washed 3 times for 5 min with PBS and coverslips were mounted on an objective slide using elvanol. Samples were air dried in the dark.

### **3.4.5 Immunohistochemistry**

The stainings were carried out utilizing the Avidin-Biotin-Peroxidase Complex (ABC) principle. A biotinylated secondary antibody bridges the primary antibody to an avidin-containing enhancer complex. Avidin (or streptavidin) binds strongly to up

to four biotin molecules. Streptavidin is coupled to horseradish peroxidase (HRP) that is used for a chromogenic end reaction. Thereby the ABC system serves as a signal amplification bridge for the primary antibody.

Paraffin sections were deparaffinized and rehydrated, followed by antigen retrieval as described above. Subsequently, slides are washed with PBS for 5 min. To reduce background, sections were incubated with unconjugated avidin for 10 min, followed by incubation with unconjugated biotin for 10 min and finally with peroxidase blocking solution for 10 min. After 3 washes with PBS for 5 min each, sections were blocked with 5 % GNS, 3 % BSA in PBS for 1 h. The primary antibody was applied in Antibody Diluent over night at 4 °C. The next day, sections were washed 3 times for 5 min with PBS. A secondary biotinylated antibody was applied in Antibody Diluent for 30 min at RT. After 3 washes for 5 min each with PBS, tertiary labeling was performed by incubation with HRP-coupled streptavidin for 30 min at RT. Samples were washed 3 times for 5 min in PBS and the signal was developed using 3,3'-diaminobenzidine (DAB) as a substrate. DAB reacts with the coupled peroxidase resulting in a product of intense brown color. The staining reaction was followed under the microscope and samples were placed in distilled water to stop the reaction. Sections were counterstained with Hematoxylin (1:10 dilution) for 30 sec. Finally, sections were dehydrated, incubated twice for 2 min in Xylol, and mounted in Entellan.

<i>Avidin-Biotin-Block</i>	<i>Dako X0590</i>
<i>Peroxidase-Blocking solution</i>	<i>Dako S2023</i>
<i>Streptavidin/HRP</i>	<i>Dako P0397</i>

### 3.4.6 BrdU staining

5-bromo-2'-deoxyuridine (BrdU) incorporation is used to measure cell proliferation. DNA replication is required for cell division. BrdU is a thymidine homolog that can be added to cells or tissues where it is then incorporated into newly synthesized DNA. The incorporated BrdU can be visualized with specific antibodies. The detection of BrdU was carried out on paraffin sections using the protocol for immunofluorescence stainings on paraffin sections described above.

### 3.4.7 EdU staining

5-ethynyl-2'-deoxyuridine (EdU) is a thymidine homolog like BrdU but its detection does not require an antibody. As BrdU, EdU is incorporated into DNA during DNA synthesis. The basis for the detection of EdU is the click reaction. Herein an alkyne (EdU) reacts with an azide in a copper (I)-catalyzed reaction. The product is a stable triazole ring that is linked to a fluorophore.

EdU staining was carried out on paraffin sections. Paraffin section were deparaffinized and rehydrated. Samples were incubated in staining solution for 30 min at RT. After 3 washes for 5 min in PBS, antigen retrieval was performed as described above.

#### *EdU staining solution:*

<i>100 mM</i>	<i>Tris, pH 8,5</i>
<i>1 mM</i>	<i>CuSO<sub>4</sub></i>
<i>10 μM</i>	<i>488-Azide (Invitrogen A10266)</i>
<i>100 mM</i>	<i>ascorbic acid</i>

### **3.4.8 TUNEL staining**

Apoptosis is associated with DNA degradation where double-stranded or single-stranded DNA breaks are exposed. The TUNEL (Terminal deoxynucleotidyl transferase dUTP nick end labeling) assay is a method for the detection of fragmented DNA by labeling free 3`-ends of nucleic acids. Terminal deoxynucleotidyl-transferase (TdT) catalyzes the transfer of fluorescent-labeled dUTP toward the free DNA end, enabling the visualization of apoptotic cells. TUNEL staining was carried out on paraffin sections according to the manufactures instructions.

*DeadEnd Fluorometric TUNEL System Kit, Promega G3250*

## **3.5 Cell culture methods**

### **3.5.1 Equipment and materials**

Centrifuge: Heraeus Multifuge X1R, Thermo Scientific

5 ml, 10 ml, 25 ml Pipettes: Cellstar, Greiner bio-one

Light microscope: Axiovert 40C, Zeiss

24-well and 6-well plates: Cellstar, Greiner bio-one

10 cm dishes: Cellstar, Greiner bio-one, 100 x 20 mm, 664160

Sterile filters: Acrodisc syringe filters, 0,2 µm, PALL

Sterile filter bottles: Nalgene Rapid-flow, 1564020

Cell strainers: BD Falcon, 70 µm (352350), 40 µm (352340)

Cryo tube vials: Nunc, 368032

P/S: Penicillin, Streptomycin (10.000 U/ml) Gibco, 15140-122

Trypsin 10 x: Gibco 15090-046

Serum: Fetal bovine serum (FBS) secure, Gibco 10099-141

### **3.5.2 Cell culture of immortalized mouse fibroblasts**

Primary kidney fibroblasts were isolated from 3-week-old ILK f/f mice, and immortalized with SV40 virus. Single cell clones from ILK f/f fibroblasts were subsequently obtained, from which the ILK gene was deleted by adenoviral expression of Cre-recombinase to generate ILK <sup>-/-</sup> cells. The cells were established at and received from the Max-Planck Institute for Biochemistry (Martinsried, Germany). These fibroblasts were maintained on 10-cm dishes in fibroblast growth medium in a humidified atmosphere at 37 °C and 5 % CO<sub>2</sub>. To obtain a single cell suspension, cells were washed once with PBS and incubated with 2 x Trypsin/EDTA in PBS for 3-5 min at 37 °C. Detached cells were resuspended in growth medium, centrifuged at 900 rpm for 3 min and plated. For cell storage, cells were resuspended in freezing medium after centrifugation and frozen down in cryovials using isopropanol freezing containers. Cells were stored at -80 °C for up to one month, for long-term storage they were placed in liquid nitrogen tanks at -196 °C. For thawing, cells were placed in a water bath at 37 °C, subsequently mixed with prewarmed growth medium and centrifuged for 3 min at 900 rpm. The cell pellet was resuspended in growth medium and cells were plated.

#### ***Fibroblast growth medium***

*DMEM (with Glutamax, Gibco 61965-026) supplemented with 1 % P/S solution and 10 % FBS*

#### ***Freezing medium***

*Fibroblast growth medium supplemented with 10 % DMSO*

### 3.5.3 Gel contraction assay

$2 \times 10^6$  fibroblasts were suspended in 800  $\mu$ l of 5 x Hank's Balanced Salt solution (Sigma), 50% fetal calf serum and mixed with 3 ml of 4mg/ml acid-extracted rat tail type I collagen, avoiding air bubble formation. 500  $\mu$ l of the suspension was loaded into wells of a 24-well plate and allowed to polymerize at 37°C for 30 min. 500  $\mu$ l fibroblast medium was subsequently applied on top of the gel. After 3 days of culture gel contraction was determined by measuring gel diameter.

### 3.5.4 Isolation of primary keratinocytes

Primary keratinocytes were isolated from mouse skin in telogen phase (P21-P23 or 8-9 weeks old). The mouse was sacrificed and shaved. Subsequently, the mouse was incubated in 70 % ethanol for 1 min, rinsed in distilled water and incubated in PBS for 1 min. Tail and limbs were removed and the skin was isolated. The subcutaneous fat was removed by scraping with a round surgical blade (No 22). The skin was then incubated in 2x antibiotic/antimycotic in PBS dermis side up for 5 min at RT. The skin was cut into smaller pieces and transferred epidermal side up in 0,8 % trypsin in PBS for 50 min at 37 °C. Skin pieces were subsequently transferred to a new dish containing keratinocyte growth medium (KGM), the epidermis was separated from the dermis using small forceps, and finally minced into small pieces. The epidermis suspension was subsequently transferred into a 50 ml falcon tube and mechanically disrupted by passing through a 25 ml pipette 8-10 times. The suspension was filtered through a 70  $\mu$ m cell strainer and centrifuged at 900 rpm for 5 min. The supernatant was removed and the cells were resuspended and plated on dishes precoated with coating medium. Cells were incubated at 37 °C, 5 % CO<sub>2</sub> and medium was changed the day after isolation.

## Materials and methods

*Antibiotic Antimycotic Solution (100×), Sigma A5955*

*Trypsin powder Gibco 27250-018*

### ***Keratinocyte Growth Medium (KGM):***

<b><i>Final concentration of reagent</i></b>	<b><i>Stock concentration</i></b>	<b><i>Add vol</i></b>
<i>MEM (Spinners modified, Sigma M8167)</i>		<i>500ml</i>
<i>5 ug/ml Insulin (Sigma I5500)</i>	<i>5mg/ml 4mM HCL</i>	<i>0.5ml</i>
<i>10 ng/ml EGF (Sigma)</i>	<i>200ug/ml PBS</i>	<i>25µl</i>
<i>10 ug/ml Transferrin (Sigma T8158)</i>	<i>5mg/ml PBS</i>	<i>1ml</i>
<i>10 uM Phosphoethanolamine (Sigma P0503)</i>	<i>10mMPBS</i>	<i>0.5ml</i>
<i>10 uM Ethanolamine (Sigma E0135)</i>	<i>10mM PBS</i>	<i>0.5ml</i>
<i>0.36 ug/ml Hydrocortisone (Calbiochem 386698)</i>	<i>5mg/ml Ethanol</i>	<i>36µl</i>
<i>1x Glutamine (Gibco 25030)</i>	<i>100x</i>	<i>5ml</i>
<i>1x Pen/Strep (Gibco 15140-122)</i>	<i>100x</i>	<i>5ml</i>
<i>8 % Chelated FBS</i>		<i>40ml</i>
<i>45 µM CaCl<sub>2</sub></i>	<i>100mM</i>	<i>225µl</i>

All reagents were combined and sterile filtered.

### ***Chelated FBS:***

*Add 500g Chelex (Biorad #142-2832) to 1l 1M Tris (121.1g Tris-base, adjust pH to 7.4 with ~66ml 37% HCl).*

*Stir over night at 4 °C*

*Filter through folded filter (Schleicher&Schuell 314856).*

*Add the chelex resin to 1250 ml FBS and stir at 4 °C for overnight.*

*To remove chelex, filter again through folded filter, sterile filter and aliquot and store at -20 °C.*

***Coating medium:***

*25 ml MEM (Sigma M8167)*

*0.5 ml Hepes pH 7.3(1 M stock)*

*0.25 ml Collagen I (Millipore, 08-115)*

*0.25 ml Fibronectin (1 mg/ml Stock, Millipore FC010)*

*11.25 µl CaCl<sub>2</sub> (100 mM stock)*

**3.5.5 Cell substrate adhesion assay**

Primary mouse keratinocytes were isolated as described above (see 3.5.4). 6-well plates were coated with defined matrix substrates over night at 4 °C. Recombinant proteins were diluted in sterile PBS. Unspecific binding was blocked with heat-inactivated 2 % BSA (heated for 1h at 70 °C) in PBS for 1h at RT, after which freshly isolated keratinocytes were suspended in KGM and allowed to adhere for 6 h before extraction of RNA or protein.

To generate a wild type ECM platform, wild type keratinocytes were isolated (see 3.5.4) and plated on coated 6-wells or coated activated coverslips (see 3.5.6).

Keratinocytes were cultured in KGM for 4-6 days to allow the deposition of ECM. After that, cells were removed by adding pre-warmed extraction buffer (1 ml for 6-well, 0.2 ml for coverslip in 24-well plate) for 30-45 s under visual control using a microscope. To stop the reaction, a 5-fold excess of PBS was added, after which the attached matrix was washed 5 times with PBS and blocked with heat-inactivated 2%

## Materials and methods

BSA in PBS for 1h at RT. Freshly isolated keratinocytes were subsequently plated in KGM and allowed to adhere for 12 h before harvesting.

*Collagen I/ Fibronectin: 25 µg/ml / 10 µg/ml*

*Human recombinant laminin-511 (Biolamina LN511): 10 µg/ml*

*Human recombinant laminin-332 (Biolamina LN332): 1 µg/ml*

### **3.5.6 Coverslip activation**

10-mm round coverslips were used for culturing of cells within a 24-well plate. Coverslips were activated to ensure better cell adhesion on glass substrate. To this end, coverslips were soaked in 0,1 N NaOH and air-dried. 50 % 3-aminopropyltrimethoxysilane (Sigma) was spread on the coverslip and incubated for 5 min. Coverslips were subsequently soaked in distilled water, placed into a 24-well plate and washed with distilled water for 3 times. 0.5 % glutaraldehyde in PBS was added and coverslips were incubated for 30 min. After 3 washes for 5 min with distilled water coverslips were air-dried. For sterilization, coverslips were treated with UV for 30 min before use.

## **3.6 Biochemical Methods**

### **3.6.1 Equipment and materials**

Electrophoresis chambers: Mini-Protean, BioRad

Membrane transfer: Trans-Blot Turbo transfer system, BioRad; Power Pac Basic, BioRad

Spectrophotometer: TECAN infinite M200

Developing machine: Curix 60, Agfa

### 3.6.2 Preparation of cell extracts from adherent cells

Cells were washed once with ice-cold PBS and subsequently incubated with lysis buffer (150 µl/well for a 6-well plate or 200 µl for a 6-cm dish) for 10 min on ice. Subsequently, cells were scraped and lysates were placed into eppendorf tubes, incubated for a further 10 min on ice and centrifuged for 10 min at 15000 x g at 4 °C. The supernatant was transferred into a fresh tube and protein concentration was measured using the BCA assay (see 3.6.4). The appropriate amount of 4 x Laemmli sample buffer was added and lysates were denatured by incubation for 5 min at 95 °C. Lysates were then either directly subjected to SDS-PAGE or stored at -20 °C. In the latter case lysates were heated at 95 °C for 1 min after thawing before subjecting to SDS-PAGE.

#### *Lysis Buffer*

150 mM      NaCl

50 mM      Tris-HCl, pH 7,4

1 mM      EDTA pH 8,0

0.5 %      Triton-X-100

+ 1 tablet of protease inhibitor and 1 tablet of phosphatase inhibitor per 10 ml lysis buffer

*Protease Inhibitor*                      cOmplete Mini EDTA-free, Roche 04693159001

*Phosphatase inhibitor*                  PhosSTOP, Roche 04906845001

#### *4 x Laemmli sample buffer*

125 mM      Tris-HCl, pH 6,8

4 %      SDS

## Materials and methods

50 %            *glycerol*

0.2 %           *bromphenol blue*

5%                *beta-mercaptoethanol, added fresh before use*

### **3.6.3 Preparation of ECM extracts from mouse skin**

Monika Pesch and Monique Aumailley from the University of Cologne, Germany, carried out the ECM extraction as well as the corresponding immunoblot in Figure 4.5.1.2.

After skin isolation, the subcutaneous fat was removed and the skin piece was cut into small pieces of  $\sim 2 \text{ cm}^2$ . The tissue was homogenized using mortar and pestle in liquid nitrogen. All subsequent steps were performed at 4 °C with solutions containing protease and phosphatase inhibitors. The tissue was suspended in Tris buffered saline (TBS) and centrifuged for 5 min at 15000xg. The pellet was washed with TBS with 0,1% Tween-20, resuspended in EDTA buffer over night with shaking. After this, the samples were centrifuged (5 min, 15000 x g) and the pellet was resuspended in 1 x Laemmli sample buffer containing 5 M urea. The samples were subsequently allowed to rotate over night at RT. After centrifugation (5 min, 15000 x g) the supernatant was subjected to SDS-PAGE (see 3.6.5) and subsequent western blotting (see 3.6.6).

*HALT Protease Inhibitor cocktail Thermo Scientific 78430*

*PhosStop Roche 04906845001*

#### ***EDTA buffer***

*1x TBS with 20 mM EDTA pH 8.0*

### **3.6.4 Determination of protein concentration**

The BCA protein assay was used to determine protein concentration. The principle of the assay is based on the Biuret test. Proteins in an alkaline environment, mediated by sodium hydroxide, reduce  $\text{Cu}^{2+}$  to  $\text{Cu}^+$  leading to complex formation with bicinchoninic acid resulting in a bluish color change that can be measured by absorbance at 562 nm. The assay was performed according to the manufacturers instructions. The absorbance was measured using a spectrophotometer.

*Pierce BCA Protein Assay Kit, 23227*

### **3.6.5 One-dimensional SDS-polyacrylamide-gel electrophoresis**

SDS-polyacrylamide-gel electrophoresis (SDS-PAGE) is a method used for separation of proteins, where denatured proteins are subjected to a one-dimensional electric field within a denaturing gel and thereby separated according to their molecular weight. To enable concentration of the loaded protein sample before passing the separation gel, the samples are first run through a differentially buffered stacking gel that is cast on top of the separation gel. SDS-PAGE was carried out in a Minigel format (7.3 mm x 8.3 mm x 1.5 mm) using the MiniProtean System (BioRad) and subsequently used for western blotting (see 3.6.6).

Polyacrylamide gels were casted as described below. After polymerization of the polyacrylamide gel, the electrophoresis module was assembled and protein samples were loaded onto the stacking gel. The electrophoresis module was filled with SDS running buffer and electrophoresis was performed at 100 V at RT.

## Materials and methods

### **10x SDS Running buffer**

30.3 g      *Tris base*

144.2 g      *glycine*

50 ml      20 % SDS

*filled to a final volume of 1000 ml with distilled water*

### **Stacking gel**

2.75 ml      *distilled water*

3.5 ml      *0,5 M Tris-HCl, 0,4 % SDS, pH 6,8*

0.8 ml      *acrylamide*

93.8  $\mu$ l      *10 % APS*

9.8  $\mu$ l      *TEMED*

### **Separating gel**

	<b>7,5 %</b>	<b>10 %</b>	<b>12 %</b>
<i>distilled water</i>	<i>3,5 ml</i>	<i>2 ml</i>	<i>0,9 ml</i>
<i>acrylamide</i>	<i>4 ml</i>	<i>5,4 ml</i>	<i>6,5 ml</i>
<i>1.5 M Tris-HCl, 0.4 % SDS, pH 8.8</i>	<i>8,4 ml</i>	<i>8,4 ml</i>	<i>8,4 ml</i>
<i>10 % APS</i>	<i>135 <math>\mu</math>l</i>	<i>135 <math>\mu</math>l</i>	<i>135 <math>\mu</math>l</i>
<i>TEMED</i>	<i>13,5 <math>\mu</math>l</i>	<i>13,5 <math>\mu</math>l</i>	<i>13,5 <math>\mu</math>l</i>

*N,N,N',N'-Tetramethylethylenediamine (TEMED), Roth 2367.1*

*Acrylamide: Rotiphorese Gel30, Roth 3029.1*

### 3.6.6 Western blotting and immunodetection

Western blotting is a method to detect specific proteins from a protein mixture.

Proteins separated by SDS-PAGE are transferred onto a Polyvinylidene fluoride (PVDF) membrane. The proteins bind to the membrane, after which specific antibodies can be applied to detect specific proteins.

After SDS-PAGE the stacking gel was removed and the separating gel was placed in blotting buffer. The PVDF membrane was activated by incubating in methanol for at least 10 min, followed by washing in blotting buffer for at least 10 min. The SDS-PAGE gel and the PDVF membrane were assembled into a sandwich and transferred onto the Trans-Blot machine. Proteins were transferred at 20 V, 0.3 A for 90 min at RT. After transfer, the sandwich was disassembled, the membrane stained with Ponceau S solution for 30-60 s, and rinsed with water to detect protein bands and to confirm successful transfer. Membranes were subsequently washed with TBS-T and blocked for 1 h at RT with blocking buffer (5 % skimmed milk in TBS-T). Incubation with primary antibodies (see Table) was carried out at 4 °C overnight with shaking. The next day, membranes were washed 3 times for 5 min in TBS-T and incubated with the secondary antibody conjugated with HRP in 5 % skimmed milk in TBS-T for 30 min at RT. After 3 washes of 10 min with TBS-T and once for 10 min with TBS, bound HRP was detected using chemiluminescence exposed on X-ray film.

*Ponceau S Sigma P7170*

*Chemiluminescence Kit Immobilion Western, Millipore WBKLS0500*

*Immobilion-P transfer membrane, Millipore IPVH00010*

*CL-XPosure Film, Thermo Scientific 34089*

## Materials and methods

### ***10x Blotting buffer***

30.3 g        *Tris base*

144.1 g        *glycine*

*filled to a final volume of 1000 ml with distilled water.*

*1x blotting buffer was diluted from 10x blotting buffer and 20 % methanol were added. The buffer was stored at 4 °C.*

### ***10x TBS***

60.5 g        *Tris base*

87.6 g        *NaCl*

*filled to a final volume of 1000 ml distilled water and pH adjusted to 7,5*

### ***TBS-T***

*10x TBS was diluted to 1x TBS and 0.1 % Tween20 was added*

## **3.7 Molecular biology methods**

### **3.7.1 Equipment and materials**

Eppendorf Thermomixer compact

Centrifuge: 5417R, Rotor HL118, Eppendorf

Agarose gel chambers: PerfectBlue Gelsystem, Peqlab

Geldoc station: U:Genius, Syngene

PCR machine: Thermocycler Professional trio, Biometra, analytic Jena

qPCR machine: StepOne Plus Real-Time PCR System, Applied Biosystems

Flow cytometer: BD Biosystems FACS Canto II with BD FACS Diva Software 6.1.3

FlowJo software 7.6

### 3.7.2 Extraction of mouse tail DNA

For mouse genotyping, DNA was isolated from small tail biopsies. The tissue was digested in 250  $\mu$ l DNA lysis buffer overnight at 55 °C with shaking at 800 rpm. After this, 250  $\mu$ l isopropanol was added and mixed by inverting the tube several times, followed by centrifugation for 10 min at 15000 x g. The supernatant was removed and the pellet was washed with 200  $\mu$ l 70 % ethanol followed by centrifugation for 5 min at 15000 x g. The pellet was air-dried for 10 min, 100  $\mu$ l Tris-EDTA (TE) buffer was added and samples were incubated 2 hours at 55 °C to dissolve the pellet.

#### *DNA lysis buffer*

<i>0.1 M</i>	<i>Tris-HCl, pH 8.5</i>
<i>5 mM</i>	<i>EDTA, pH 8.0</i>
<i>0.2 %</i>	<i>SDS</i>
<i>0.2 M</i>	<i>NaCl</i>
<i>100 <math>\mu</math>g/ml</i>	<i>Proteinase K (Roche 03115828001)</i>

#### *TE Buffer*

<i>10 mM</i>	<i>Tris-HCl, pH 8.0</i>
<i>1 mM</i>	<i>EDTA, pH 8.0</i>

### 3.7.3 Extraction of mouse epidermis

Mouse epidermis was extracted using ammonium thiocyanate that induces a split within the lamina lucida zone of the BM and therefore allows the separation of epidermis from dermis without further damage to the tissue. After isolation of the skin as described earlier, the skin piece was floated epidermis side up on ammonium

## Materials and methods

thiocyanate solution for 30-45 min on ice. Subsequently, the skin was washed with PBS and the epidermis was carefully removed using forceps. Epidermis was either snap frozen in liquid nitrogen and stored at -80 °C or directly processed for protein or RNA isolation. To this end, the epidermis was mixed with lysis buffer or RNA extraction buffer for protein or RNA isolation, respectively. The tissue was subjected to homogenization in Lysing Matrix tubes using a MP FastPrep tissue disrupter at a speed of 6.0 and 4 intervals of 30 sec of milling. The samples were allowed to cool down for 5 min on ice before centrifugation at 15000 x g for 10 min at 4 °C. The supernatant was used for either protein quantification (see 3.6.4) or RNA isolation (see 3.7.7).

### *Ammonium thiocyanate solution*

0.1 M  $Na_2HPO_4$

0.1 M  $KH_2PO_4$

*mixed to obtain a 0.1 M NaKHPO<sub>4</sub> buffer, and adjusted to pH 6.8*

*380 mg NH<sub>4</sub>SCN was dissolved in 10 ml NaKHPO<sub>4</sub> buffer, prepared fresh before use*

### **3.7.4 Magnetic-activated cell separation**

For magnetic-activated cell separation (MACS), cells in single-cell suspension are magnetically labeled using magnetic microbead-conjugated antibodies. The labeled cells are then applied to column coupled to a magnet that enables the separation of positively labeled cells from un-labeled cell populations.

Primary mouse keratinocytes were isolated as described above (see 3.5.4).  $10^7$  cells were then resuspended in 100  $\mu$ l MACS buffer and transferred into a 2 ml eppendorf tube. FITC-conjugated CD49f ( $\alpha$ 6-integrin) was added to the cell suspension (1:50),

mixed and incubated for 20 min on ice, protected from light. Cells were washed in 1.5 ml MACS buffer and centrifuged for 10 min at 4 °C at 600 x g. The supernatant was removed and cells were resuspended in 90 µl MACS buffer. 10 µl of anti-FITC MicroBeads were added, mixed and incubated for 15 min on ice, protected from light. Cells were washed and centrifuged as before, the supernatant was removed and the cells were resuspended in 500 µl MACS buffer. The column was attached to a magnet and primed by rinsing with 500 µl MACS buffer. Cells were passed through a 30 µm filter and placed onto the column. The flow-through was the α6-integrin-negative population. After 3 washes with 500 µl MACS buffer the column was removed from the magnet and the magnetic labeled α 6 integrin positive population was eluted with 1 ml of MACS buffer. The cells were pelleted and subjected to RNA isolation (see 3.7.7).

*FITC-conjugated primary antibody α6 integrin (CD49f; BD, 555735)*

*Anti-FITC MicroBeads Miltenyi Biotech, 130-048-701*

*MS Columns Miltenyi Biotech, 130-042-201*

*Pre-Separation Filters, 30 µm (Miltenyi, 130-041-407)*

### **MACS Buffer**

2 %            *FBS*

2 mM            *EDTA, pH 8.0*

*in PBS, sterile filtered*

### **3.7.5 Polymerase chain reaction**

Polymerase chain reaction (PCR) is a technique for DNA amplification. In the presence of a DNA template strand, oligonucleotides (forward and reverse primers)

## Materials and methods

bind to the template at specific complementary sites and the DNA polymerase (Taq polymerase) synthesizes a new DNA strand using dNTPs. To amplify a specific DNA fragment, several (30-35) cycles of the following 3 steps are performed: the DNA template strand is first denatured at 95 °C, primers are subsequently allowed anneal to the template (55-68 °C depending on the primers) and the DNA is synthesized at 72 °C. Custom designed oligonucleotides were synthesized by Eurofins MWG Operon (Ebersberg, Germany). Oligonucleotides used for genotyping and the corresponding PCR product fragment sizes are listed below.

### ***Genotyping PCR reaction***

2  $\mu$ l            10x Dreamtaq PCR buffer (Fermentas)

0.4  $\mu$ l            dNTP (10 mM) (Fermentas)

1  $\mu$ l                forward primer (10 pmol)

1  $\mu$ l                reverse primer (10 pmol)

0.2  $\mu$ l            Dream Taq Polymerase (Fermentas)

1  $\mu$ l                isolated tail DNA

*final volume adjusted to 20  $\mu$ l with distilled water*

### ***PCR programs***

The following PCR reactions were performed for 35 cycles (step 5-7), as a touch down PCR from 68 - 60 °C (ILK) and 60 - 53 °C (Cre) in 9 cycles by sequential reduction of the annealing temperature (-1 °C/cycle; step 2-4):

***ILK PCR***

<i>Step</i>	<i>temp (°C)</i>	<i>time (sec)</i>
1	95	60
2	95	30
3	68	30
4	72	30
5	95	30
6	60	30
7	72	30
8	72	300
9	16	∞

***Cre PCR***

<i>Step</i>	<i>temp (°C)</i>	<i>time (sec)</i>
1	95	60
2	95	30
3	68	30
4	72	45
5	95	30
6	60	30
7	72	45
8	72	300
9	16	∞

The following PCRs were performed for 36 cycles (step 2-4) for rTA PCR and for 35 cycles (step 2-4) for LacZ PCR:

***rTA PCR***

<i>Step</i>	<i>temp (°C)</i>	<i>time (sec)</i>
1	95	60
2	95	30
3	60	30
4	72	20
5	72	300
6	16	∞

***LacZ PCR***

<i>Step</i>	<i>temp (°C)</i>	<i>time (sec)</i>
1	95	90
2	95	20
3	60	45
4	72	60
5	72	120
6	16	∞

Name	Sequence 5`-3	Product size
ILK fw	GTCTTGCAAACCCGTCTCTGCG	fw and rev: 340 bp floxed allele 290 bp wild type allele Fw and KO: 1000 bp wild type allele 250 bp KO allele
ILK rev	CAGAGGTGTCAGTGCTGGGATG	
ILK KO	CCCTTCACATCCCATAACCAACTC	
Cre fw	AACATGCTTCATCGTCGG	350 bp for transgene
Cre rev	TTCCGATCATCAGCTACACC	
rTA fw	CGCTGTGGGGCATTCTTTACTTTAG	450 bp for transgene
rTA rev	CATGTCCAGATCGAAATCGTC	
LacZ 1	AAAGTCGCTCTGAGTTGTTAT	550 bp wild type allele 250 bp transgene allele
LacZ 2	GCGAAGAGTTTGTCTCAACC	
LacZ 3	GGAGCGGGAGAAATGGATATG	

### 3.7.6 Agarose gel electrophoresis

Agarose gel electrophoresis is a standard method to separate DNA fragments according to their size. The method was used to identify amplified PCR products. The gel was prepared by dissolving 1,5 % w/v agarose in 1xTAE buffer by boiling in a microwave. For 100 ml of melted agarose, 4 µl of ethidium bromide was added. Ethidium bromide is a DNA intercalating reagent that emits fluorescence when exposed to UV light. The melted agarose was poured into a casting mold and allowed to set at RT. The gel was subsequently placed into a gel electrophoresis chamber and the chamber was filled with 1xTAE buffer. The DNA was mixed with 6 x loading buffer and loaded on the gel. Electrophoresis was carried out at 100-130 V at RT and

DNA bands were detected under UV light at 366 nm. The DNA fragment size was determined by comparison to a DNA ladder of known size.

*DNA ladder: Gene Ruler DNA ladder mix, Thermo Scientific SM0331*

***TAE buffer (50 x)***

*2 M Tris base*

*50 mM EDTA*

*57.1 ml glacial acetic acid*

*adjusted to a final volume of 1 l with distilled water*

***6x DNA loading buffer***

*7.5 ml glycerol*

*3.0 ml 0,5 M EDTA, pH 8,0*

*0.0625 g bromphenol blue*

*14.5 ml distilled water*

**3.7.7 RNA isolation**

Cells or tissue extracts were lysed in RNA lysis buffer and homogenized by passing them through a 20 G needle 5 times.

The RNeasy Plus Mini Kit (Qiagen) was used for RNA isolation following the manufacturer's instructions. In brief, genomic DNA was removed by passing the RNA lysate through a gDNA eliminator column (Qiagen). Ethanol was added to precipitate the RNA that is subsequently trapped in a spin column. After washing, the

## Materials and methods

RNA is subsequently eluted in distilled water. RNA was either used directly for cDNA synthesis (see below) or stored at -80 °C.

*RNeasy Plus Mini Kit, Qiagen 74134*

### 3.7.8 Quantitative real-time polymerase chain reaction

Quantitative real-time polymerase chain reaction (qRT-PCR) is a PCR-based method that allows the detection and visualization of the amplified DNA product using fluorescent dyes in real time. This method was used to quantitatively measure gene expression at the RNA level. The isolated RNA was first reverse-transcribed to cDNA, and then using target gene-specific primers and SYBR-green fluorescent reagent the amount of cDNA amplification was quantified. Analysis was done manually using the comparative cyclic threshold method (see below). For a complete list of primers used in this study see Appendix A.

*cDNA synthesis (Applied Biosystems High Capacity cDNA Reverse Transcriptase Kit (4368814))*

<i>2 µl</i>	<i>10x RT Buffer</i>
<i>2 µl</i>	<i>10x random primer</i>
<i>0.8 µl</i>	<i>25x dNTPs (100 mM)</i>
<i>1 µl</i>	<i>reverse transcriptase</i>
<i>0.5 - 1 µg</i>	<i>RNA</i>

*final volume adjusted to 20 µl with RNase-free water*

***Thermocycler program***

25 °C      10 min

37 °C      2 h

85 °C      5 min

4 °C      ∞

*cDNA was stored for 2 days at 4 °C or at -20 °C for long-term storage****qPCR Mix****Measurements were always performed in triplicates**Single reaction:*

10 µl      2x SYBR Green (DyNAmo Color Flash, Thermo Scientific F-416)

0.5 µl      forward primer (10 µM)

0.5 µl      reverse primer (10 µM)

8 µl      distilled water

1 µl      cDNA (diluted 1:5)

**3.7.8.1 Analysis of qRT-PCR**

qRT-PCR analysis was carried out according to the relative quantification method with primer efficiency correction.

Efficiency (E) was calculated from the slopes of a cDNA dilution (1:2, 1:5, 1:10) calibration curve according to the equation:  $E = 10^{(-1/\text{slope})}$

The calculation of the ratio was made according to the equation:

$$\text{Ratio} = ((E_{\text{target}})^{\Delta C_{\text{t}}_{\text{target}}(\text{control-sample})}) / ((E_{\text{reference}})^{\Delta C_{\text{t}}_{\text{reference}}(\text{control-sample})})$$

where  $\Delta C_{\text{t}}$  = crossing point difference of cyclic threshold

### 3.7.9 Flow cytometry

Flow cytometry and Fluorescence-activated cell sorting (FACS) are methods for specific cell type identification and quantification from a mixed cell suspension. Cells can be identified by their size, granularity, by expression of genetically engineered fluorescent proteins (such as Enhanced Green Fluorescent Protein; EGFP) or by differential expression of cell surface markers that can be detected by fluorescent-labeled antibodies. Cells in suspension are passed through a stream of fluid where lasers of different wavelengths can excite the fluorescent labels. An electronic detection system reads these signals and displays them as events of passed cells. For this study, flow cytometry was used to quantify the number of HFSCs and Lgr5-EGFP-expressing cells.

Primary mouse keratinocytes were isolated as described above (see 3.5.4). Keratinocytes were resuspended in 5 ml FACS buffer and passed through a 40  $\mu$ m cell strainer. Cells were counted and the appropriate number of cells was transferred to eppendorf tubes for antibody staining. Cells were centrifuged at 300 rcf for 8 min at 4 °C, resuspended in 100  $\mu$ l FACS buffer, and incubated with antibodies (see below) for 30 min on ice. Cells were washed with 1 ml FACS buffer, centrifuged as before, resuspended in 500  $\mu$ l FACS buffer containing 7-aminoactinomycin D (7-AAD) and subjected to flow cytometry. Before the first measurement, flow cytometer settings and compensation settings were calibrated and antibody dilutions were titrated.

Flow cytometry analysis of processed samples was carried out using FlowJo software. Here, cells were gated according to their size (FSC-A/SSC-A), cell doublets were excluded (FSC-W/FSC-A) and live cells were discriminated by 7-AAD (FSC-A/PerC-CP-Cy7). From the live cell population, cells were gated for their expression of

$\alpha$ 6-integrin (FITC/Pacific blue) and CD34 (APC-A), or for the expression of EGFP (FITC).

*FACS buffer: 5 % FCS in 1 x PBS*

*Antibodies:*

*CD49f-FITC (BD 555735; 1:500)*

*CD49f-Pacific Blue (eBioscience; 1:300)*

*CD34 (eBioscience clone RAM34; 1:100)*

*7-AAD (eBiosciences, 1:100)*

### 3.8 Microscopy

#### 3.8.1 Light microscopy

Light microscopy was carried out for histological analysis using Leica DM4000 and 10x or 20x objectives.

#### 3.8.2 Laser scanning confocal microscopy

Fluorescence images were collected by laser scanning confocal microscopy. All images were recorded sequentially and averaged at least from two frames. Fluorescent images were quantified using ImageJ (NIH, version 1.47h).

*Confocal microscope Leica TSC SP-5X with Leica software LAS software version 4*

Objectives used:

Objective type	Magnification/Aperture	Immersion	Article number
HC PL APO	20x/0.70	IMM/CORR	11506191
HCX PL APO	40x/1.25-0.75	OIL	11506253

HCX PL APO CS	63x/1.30	GLYC 21°C	11506194
HCX PL APO CS	100/1.46	OIL	11506274

### 3.8.3 Traction force microscopy

Traction force microscopy (TFM) was carried out to visualize and measure cellular traction forces. The method is a combination of cell microscopy and computational analysis. The principle behind TFM is that fluorescent microbeads embedded within an elastic substrate can be tracked. Deformation of the substrate caused by cellular traction forces leads to the displacement of the beads. Cellular traction forces can then be computed based on the elastic modulus of the substrate and the displacement of the beads.

Glass-bottomed imaging  $\mu$ -dishes (Ibidi) were activated as described for glass coverslips (see 3.5.6). Polyacrylamide gels (7.5 % acrylamide/0.25 % bis-acrylamide) containing 0.2  $\mu$ m-diameter fluorescent beads (1:125) were cast on the glass surface resulting in a gel with a Young`s modulus of 50 kPa. The gel was allowed to polymerize for 5 min at RT after which unpolymerized acrylamide was removed by 3 washes with PBS. The gel was submerged with 10 mM Sulfo-SANPAH (Sigma) in 50 mM HEPES, pH 8.5 and exposed to UV light at 254 nm for 30 min to activate the crosslinker. After 3 washes with 50 mM HEPES in the dark, the FN (5  $\mu$ g/ml in 50 mM HEPES) was crosslinked to the gels over night at 4 °C. Subsequently, coating medium was removed and the gels were washed for 3 times with PBS. The gel was covered with PBS and sterilized by exposure to UV light for 30 min. Gels were kept submerged in PBS protected from light until cells were plated.

The elasticity of the gel was determined manually as described previously (Pelham and Wang, 1997). Polyacrylamide gels of a defined size were deformed with a

defined force (F). The Young`s modulus (Y) was calculated according to the equation:  $Y=(F/A)/(\Delta l/l)$

l= length of gel

$\Delta l$ = change in length

A= cross-sectional area of gel

Fibroblasts were trypsinized (see 3.5.2) and plated in low density ( $5 \times 10^3$  cells per dish) onto the gel. Cells allowed to adhere and spread for 6 h prior to imaging.

Imaging was performed with a 63x oil objective at 37 °C and 5 % CO<sub>2</sub>. Live images were captured with an Axio Observer (Zeiss) microscope, a CSU10 spinning-disc confocal scanhead (Yokogawa), and a Cascade II EMCCD camera (Photometrics).

Acquisition was controlled by Metamorph software. Differential interference contrast (DIC) images were taken to measure cell size. Beads were simultaneously imaged with a 488 nm laser. To quantify the total traction force a single cell exerts on a substrate, bead displacement was quantified while cells were detaching from a substrate. For this, cells were imaged for 20 min at 1 min/frame rate in DMEM containing 0,05 % trypsin.

Displacement vectors were calculated using Particle Imaging Velocimetry (PIV).

Subsequent Fourier transform traction cytometry (FTTC) with regularization ( $7 \times 10^9$ ) was performed to calculate traction forces using the ImageJ Plug-In (Tseng et al., 2011). The sum of all force magnitudes was multiplied with the cell size to achieve total traction force per cell.

*Microbeads Fluoresbrite Plain YG 0.2  $\mu$ m Polysciences 17151-10*

### **3.9 Statistical Analysis**

Statistical analyses were performed using GraphPad Prism software (GraphPad, version 5.0). Statistical significances were determined by the Mann-Whitney U-test, ANOVA with Dunn's post hoc test, Student's t-test, or Chi-square test. The test used for each experiment and the number of biological replicates is indicated in the corresponding figure legend. When a test for normally distributed data was used, normal distribution was confirmed with the Kolmogorov–Smirnov test ( $\alpha = 0.05$ ).

## 4 Results

### 4.1 ILK promotes force generation and matrix assembly

ILK is an essential adaptor protein that links the actin cytoskeleton to  $\beta 1$ - and  $\beta 3$  integrins at cell-ECM contact sites (Wickström et al., 2010). The ECM-actin linkage is essential for force generation. On the other hand, force generation is critical for essential processes such as cell shape regulation and ECM remodeling (Daley and Yamada, 2013; Stanchi et al., 2009). Therefore it was of great interest to examine the role of ILK in these processes.

#### 4.1.1 ILK-deficient fibroblasts show a disorganized actin cytoskeleton and altered FA structures

FBs are specialized adhesions essential for FN fibrillogenesis. Interestingly, FB maturation is a force-dependent process (Pankov et al., 2000). To investigate the impact of ILK on cellular force generation and matrix assembly *in vitro*, the formation and maturation of integrin-actin adhesion complexes was first examined. For this, fibroblasts lacking ILK (ILK  $-/-$ ) and control fibroblasts (ILK *f/f*) were subjected to immunofluorescence analysis with antibodies against paxillin, a marker of mature FAs and FBs, and phalloidin to detect F-actin.

ILK *f/f* fibroblasts displayed a spread and elongated morphology with long, thick actin stress fibers (Figure 4.1.1). Immature FCs and mature FAs were present at the edges of the cell. Thin, elongated FBs were present in the cell center. Both FAs and FBs were directly linked to the actin cytoskeleton. ILK-deficient fibroblasts, however, showed a less spread and rounded morphology and lacked cytoplasmic actin stress fibers (Figure 4.1.1). Instead, large, cortical actin bundles were present. Large, paxillin-containing FAs were present at cell edges, but they were poorly associated

## Results

with the F-actin bundles. Strikingly, small FCs and FBs were completely absent.

These data indicate that ILK is required for FA maturation in fibroblasts.

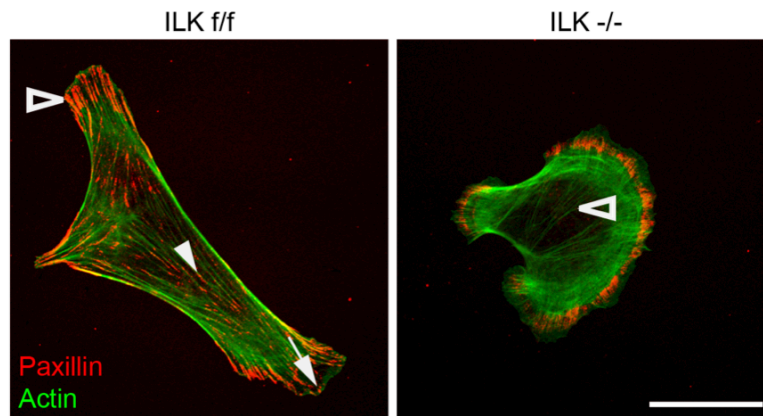


**Figure 4.1.1.** Immunofluorescence analysis of *ILK f/f* and *ILK -/-* fibroblasts stained for Paxillin (red) and phalloidin (green). *ILK f/f* fibroblasts contain FCs (arrow), mature FAs (empty arrowhead), and FBs (arrowhead), which are linked to the actin cytoskeleton. *ILK-deficient* fibroblasts lack FCs as well as FBs (empty arrowhead) and display a disorganized actin cytoskeleton.

### 4.1.2 ILK is required for force generation

FA maturation is a force-dependent process that is driven by myosin activity (Vicente-Manzanares and Horwitz, 2011). On the other hand FA maturation is required to generate and transduce force to the cellular substrate in order to remodel the ECM. To investigate whether ILK is required for force generation, TFM was carried out. TFM can be used to measure adhesive forces that a single cell exerts on its underlying substrate (Tseng et al., 2011). The analysis revealed that the total traction force generated by *ILK f/f* fibroblasts was  $128 \pm 15$  nN, whereas *ILK -/-* fibroblasts generated traction forces of  $44.3 \pm 9.2$  nN (Figure 4.1.2). This indicates that ILK is essential for cellular force generation.

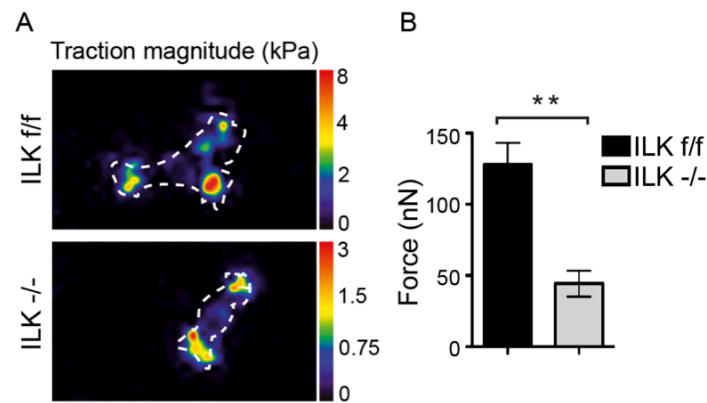


**Figure 4.1.2.** *A. Heat-scale map of traction stress magnitudes. The color code indicates local traction in kilopascals (kPa). Cell outlines are indicated by dotted lines. B. Quantification of total cellular traction forces. ILK -/- cells generate less traction forces than wild type cells. Data are presented as mean  $\pm$  SEM,  $n=56/22$ ,  $**p=0.0011$ , Student's *t*-test.*

### 4.1.3 ILK is required for matrix assembly and remodeling

To analyze whether ILK is required for force-dependent ECM assembly, fibroblasts were cultured *in vitro* and their ability to deposit FN matrices was analyzed. The analyses were performed in the context of a study in which the stability and turnover of ILK was investigated (Radovanac et al., 2013). Heat shock protein 90 (Hsp90) was found to bind and stabilize ILK thereby facilitating its interaction with  $\alpha$ -parvin. Therefore, the effect of an Hsp90 inhibitor 17AAG (Gorska et al., 2012) on FN fibrillogenesis was additionally assessed in this experiment (Figure 4.1.3.1).

Immunofluorescence analysis showed that ILK f/f fibroblasts had deposited a FN-rich matrix with distinct fibrillar network architecture within 24 h after plating (Figure 4.1.3.1A). Inhibition of Hsp90 by treatment with 17AAG led to a significant reduction of FN fibrillogenesis (Figure 4.1.3.1A, B). FN deposition was also detected in ILK -/- fibroblasts cultures but it was strongly reduced and the formation of FN fibrils was absent. Treatment with 17AAG had no additive effect (Figure 4.1.3.1A, B). Western

## Results

blot analyses of cell lysates revealed no difference in FN protein expression between ILK-deficient and wild type fibroblasts. Furthermore, inhibition of Hsp90 by 17AAG had no impact on FN expression in either ILK f/f or ILK -/- fibroblasts. (Figure 4.1.3.1C). Together the data show that ILK is not required for FN expression but is critical for force-dependent FN matrix assembly.

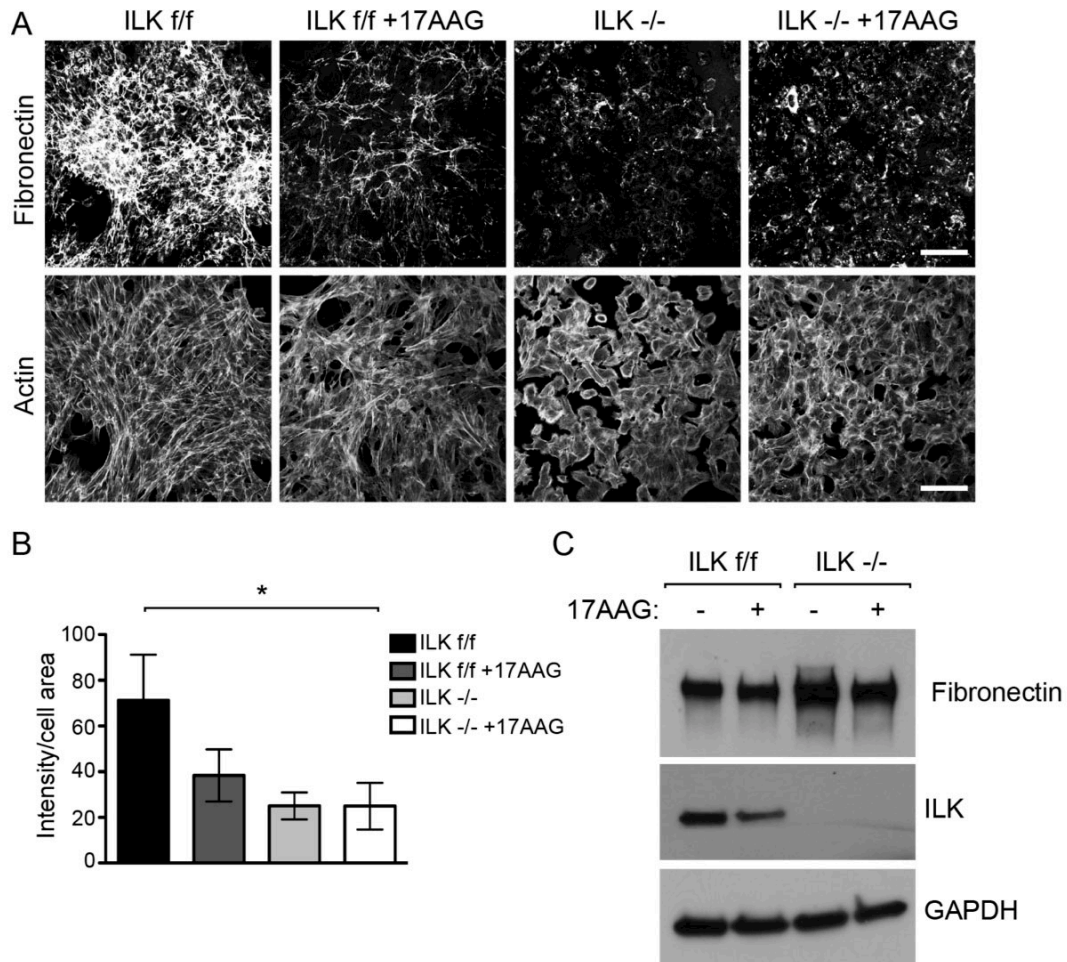


**Figure 4.1.3.1. A.** Immunofluorescence staining of the FN matrix and the actin cytoskeleton (phalloidin) to visualize cell area. Decreased FN matrix deposition is seen in ILK -/- cells compared to ILK f/f cells as well as in ILK f/f cells treated with 17AAG. Scale bar 100  $\mu$ m. **B.** Quantification of the integrated intensity of the FN staining normalized to total cell surface area. Data are presented as mean  $\pm$  SEM, n=4. **C.** Western blot analysis of FN protein expression in ILK f/f and ILK -/- fibroblasts shows no difference in FN protein levels. GAPDH was used as loading

*control. Treatment with the HSP90 inhibitor 17AAG for 24 h does not affect FN protein levels.*

To test whether the impaired adhesion maturation and local force generation in ILK-deficient fibroblasts impacts ECM remodeling in a more physiological setting, 3D collagen gel contraction assays were performed. This assay can be used to measure the ability of cells to migrate, generate forces and to remodel the collagen network. Wild type fibroblasts that were embedded into a 3D collagen matrix exerted forces on their substrate and caused significant gel contraction (Figure 4.1.3.2). Fibroblasts lacking ILK were completely unable to contract the gel (Figure 4.1.3.2).

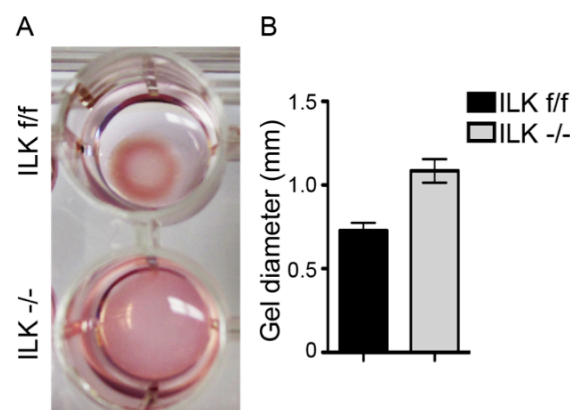


**Figure 4.1.3.2.** *A. Gel contraction assay with ILK f/f and ILK -/- fibroblasts. ILK-deficient fibroblasts are unable to contract the gel. B. Quantification of gel contraction. Data are presented as mean  $\pm$  SEM, n=3.*

## 4.2 ILK is required for the maintenance of HFSCs

The results so far indicated that ILK is required for adhesion maturation, cellular force generation and ECM assembly. To investigate the role of these processes *in vivo*, a mouse model with an epidermis-specific deletion of ILK was used (ILK f/f - Keratin-5 Cre; from here on ILK-K5). This model was chosen as it is known that the interaction with SCs and their niche is essential for tissue homeostasis (Scadden,

## Results

2006). However, the functional importance of ECM remodeling within the SC niche has not been assessed. SCs in the skin, and especially in the HF, are well characterized, making the epidermis a particularly suitable model organ for these studies.

### 4.2.1 Epidermal deletion of ILK causes progressive loss of HFSCs

The most obvious phenotype of ILK-K5 mice is their progressive hair loss. At the time of birth, ILK-K5 mice are indistinguishable from their heterozygous littermates but from week 3 onwards ILK-K5 mice start losing their hair, resulting in nearly complete alopecia around 6-8 weeks of age (Figure 4.2.1.1).

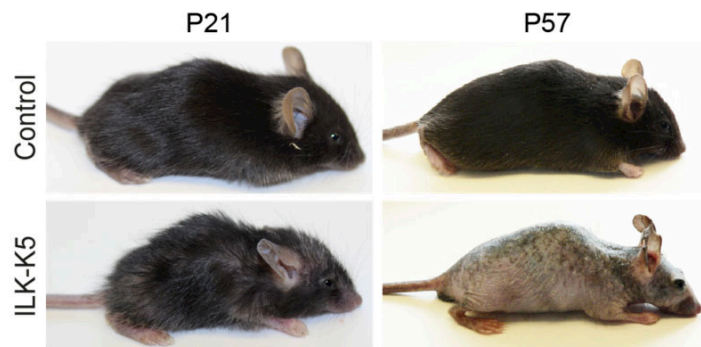


**Figure 4.2.1.1.** *ILK-K5 mice display partial alopecia at P21 and progressively loose their hair resulting in complete alopecia at P57.*

The bulge HFSC niche of the cycling part of the HF is established around P21, when HF morphogenesis is completed. The onset of alopecia in ILK-K5 at the time of bulge establishment suggested a role of ILK in regulation of HFSCs. Bulge HFSCs can be identified on the basis of the expression of two cell surface markers, CD34 and  $\alpha 6$  integrin. FACS analysis of epidermis at P21, the first telogen phase after HF morphogenesis, using these two markers revealed a 50 % decrease in bulge HFSC numbers in ILK-K5 mice (Figure 4.2.1.2A, B). Immunofluorescence staining for CD34 further showed that a CD34-positive compartment was not present in all HFs of

ILK-K5 mice. HFs positive for CD34 showed a reduction in the size of the bulge compartment (Figure 4.2.1.2C, D). In order to exclude that the reduction in bulge SCs at P21 was due to a reduction in the number of HFs in ILK-K5, HF density was assessed. The analysis revealed no difference in the HF density between control and ILK-K5 at P21 (Figure 4.2.1.2E).

At P57, when HFs of control mice had entered the second telogen phase, the majority of HFs was destroyed in ILK-K5 mice. The remaining HFs did not show CD34 staining (Figure 4.2.1.2F). In addition, no CD34-positive bulge SCs were detected by FACS analysis of the epidermis (Figure 4.2.1.2A, B). These data indicated that the progressive hair loss was associated with a loss of bulge SCs in ILK-K5 and that the reduction of SCs occurred prior to the loss of HFs.

# Results

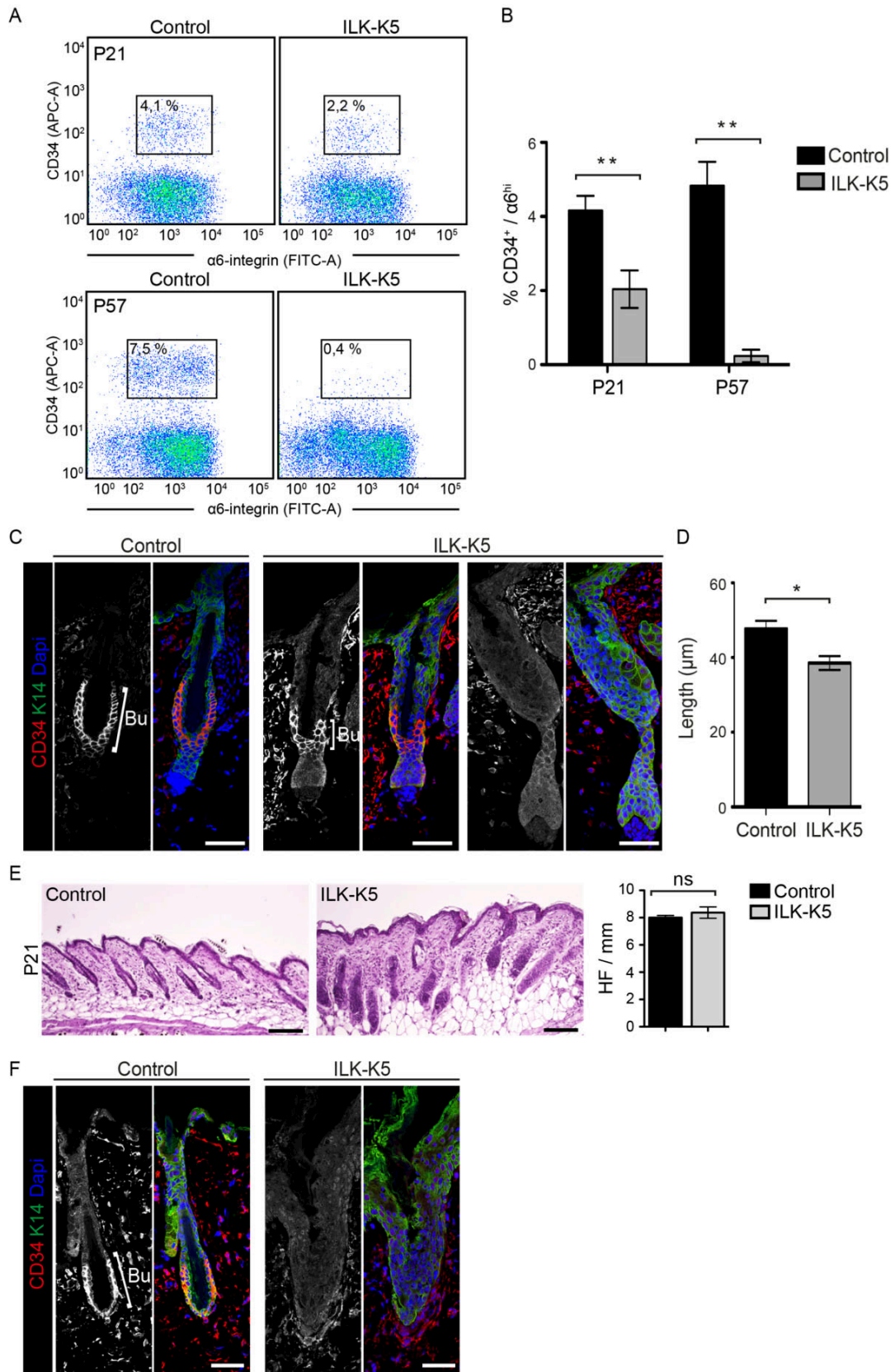


**Figure 4.2.1.2. A.** Representative plots of FACS analyses with antibodies against CD34 and  $\alpha 6$ -integrin from P21 and P57 epidermis. **B.** ILK-K5 mice show reduced amounts of CD34<sup>+</sup>/ $\alpha 6$ <sup>+</sup> HFSCs. FACS analyses of CD34<sup>+</sup>/ $\alpha 6$ -integrin<sup>hi</sup> bulge SCs shows progressive reduction of these cells in ILK-K5 skin from P21 to P57 (mean  $\pm$  SEM; n=8; \*\*p=0.0042 for P21; n=5; \*\*p=0.0079 for P57; Mann-Whitney). **C.** Immunofluorescence staining for the bulge SC marker CD34 (red) and EPC marker K14 (green) from P21 skin. CD34 staining within the bulge (Bu) is decreased in P21 and absent in P57 ILK-K5 HF. Scale bars 30  $\mu$ m. **D.** Quantification of bulge length from CD34 stainings at P21. Only HF where CD34 staining was clearly present were analyzed (mean  $\pm$  SEM; n=3; \*p=0.05, Mann-Whitney). **E.** Hematoxylin/eosin staining of P21 skin (scale bars 100  $\mu$ m). No difference in HF density between control and ILK-K5 mice is observed (mean  $\pm$  SEM; n=3; ns=not significant, p=0.70, Mann-Whitney). **F.** Immunofluorescence staining for the CD34 (red) and K14 (green) from P57 skin. CD34 staining is absent in ILK-K5 HF. Scale bars 30  $\mu$ m.

To investigate whether HFSC lineage identity is established in ILK-K5 by P21, qRT-PCR analysis of transcription factors that have been shown to be essential to the establishment of bulge SC identity (Schepeler et al., 2014) was performed from  $\alpha 6$ -integrin<sup>+</sup> sorted EPCs (Figure 4.2.1.3). No difference in *Sox9*, *Nfatc1* or *Lhx2* expression was detected between control and ILK-K5 cells, indicating that HF lineage identity was not affected per se.

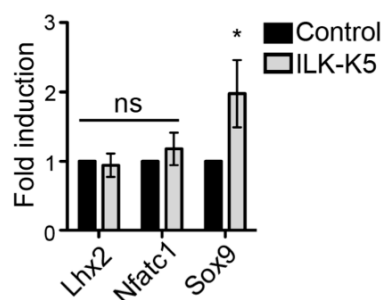


**Figure 4.2.1.3.** RT-qPCR analysis of key transcription factors required to establish bulge SC fate. No significant difference is observed in expression of *Lhx2* or *Nfatc1*. *Sox9* expression is slightly increased (mean  $\pm$  SEM; n=4; ns=not significant, p>0.2817; \*p=0.0211, Mann Whitney).

## Results

Upon activation, a subset of HFSCs transform into HG cells, divide and generate a pool of TACs (Greco et al., 2009; Hsu et al., 2014). TACs lack expression of CD34, but maintain the expression of the progenitor marker Keratin-15 (K15) and initiate expression of P-Cadherin, a specific marker for these cells (Li et al., 2003; Muller-Rover et al., 1999). To determine whether TACs were present in ILK-K5 HF, immunofluorescence analysis for P-Cadherin was carried out. In control HF, P-Cadherin staining was restricted to the HG, whereas in ILK-K5 HF the staining significantly extended upwards (Figure 4.2.1.4). Interestingly, this pool partly overlapped with K15 at the putative bulge. These results indicated that the pool of actively cycling TACs might be increased in ILK-deficient HF and that these cells might be replacing the quiescent bulge HFSCs.

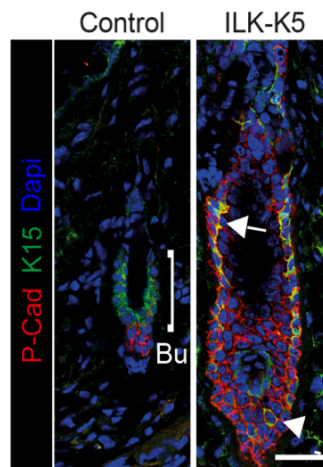


**Figure 4.2.1.4.** Immunofluorescence analysis of the bulge (Bu) marker K15 (green) and the TAC marker P-Cadherin (P-Cad; red) in P21 HF shows expansion of both markers and mixing of the K15 and P-Cad-positive compartments (arrows). Scale bars 30  $\mu$ m.

To assess whether the HFSC were indeed activated, a short pulse BrdU labeling assay was performed to identify proliferating cells. After a 1-h BrdU pulse, a significant, 3-fold increase of BrdU-positive cells were observed in ILK-K5 HF compared to

controls (Figure 4.2.1.5A), indicating that proliferation was increased in ILK-deficient HFJs.

Bulge SCs have been shown to be quiescent, and this manifests in their ability to retain incorporated EdU or BrdU for a long period of time. Hence, these cells are also termed label retaining cells (LRCs) (Cotsarelis et al., 1990). To test whether the increased proliferative activity in ILK-K5 HFJs was accompanied with a reduction in quiescent LRCs, an EdU-label retaining assay was performed. Control and ILK-K5 mice were pulsed with EdU at P10 for a period of 48 hours at 12-hour intervals and label-retention was analyzed in telogen at P21. A significant decrease in LRC numbers was observed in ILK-K5 compared to controls (Figure 4.2.1.5B). Together, these data indicate that deletion of ILK leads to a progressive depletion of quiescent bulge HFJs. This is accompanied by an increased pool of activated TACs and increased proliferation within the HFJs.

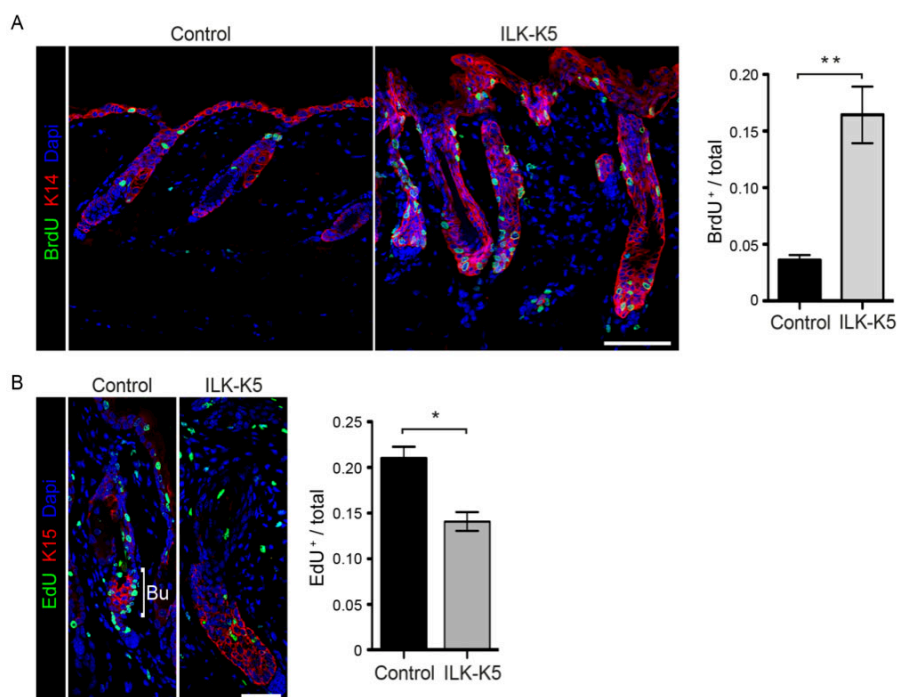


**Figure 4.2.1.5. A.** Detection of BrdU-positive cells within HFJs of P21 mice after a 1 h BrdU pulse shows increased numbers of BrdU-positive cells in ILK-K5 HFJs. Scale bars 50  $\mu$ m. Values in quantification represent mean  $\pm$  SEM of BrdU-positive cells

## Results

*per total HF cells (n=3; \*\*p=0.0036, Mann-Whitney). B. Analysis of EdU-positive LRCs within HFs of P21 mice after 10 d of EdU chase. Immunostaining shows decreased presence of LRCs in ILK-K5 bulge (Bu) SCs. Scale bars 30  $\mu$ m. Values in quantification represent mean  $\pm$  SEM of EdU-positive cells per total cells in HFs (n=4; \*p=0.05, Mann-Whitney).*

### **4.3 Loss of HFSCs in ILK-deficient epidermis occurs**

#### **independently from morphogenesis**

We next asked whether the progressive loss of HFSCs was secondary to impairment of HF morphogenesis in ILK-K5 mice, or whether ILK is also required to maintain a stable pool of HFSCs in adult mice. To this end an inducible, epidermis-specific ILK knockout mouse was generated (ILK-iK14). In this system Cre expression is induced by doxycycline. After 8 months of doxycycline feeding the mice began showing patches of spontaneous alopecia (Figure 4.3A).

The deletion of ILK at this time point was confirmed by immunofluorescence staining of ILK-iK14 skin, which showed absence of ILK staining within the IFE and HFs in the areas affected by hair loss (Figure 4.3B). Histological analyses of HFs showed the typical thin and short architecture of telogen HFs in controls (Figure 4.3C). In contrast, the HFs in ILK-iK14 mice were thicker with a wider infundibulum and thickened ORS (Figure 4.3C), resembling HFs of ILK-K5 mice. FACS analysis further revealed a reduction in CD34-positive bulge SCs (Figure 4.3D). These data indicate that ILK plays an essential role in the maintenance of quiescent HFSCs independently from morphogenesis. Due to the inefficiency of the knockout and the long time period required to achieve the phenotype, these mice were not used for further analyses.

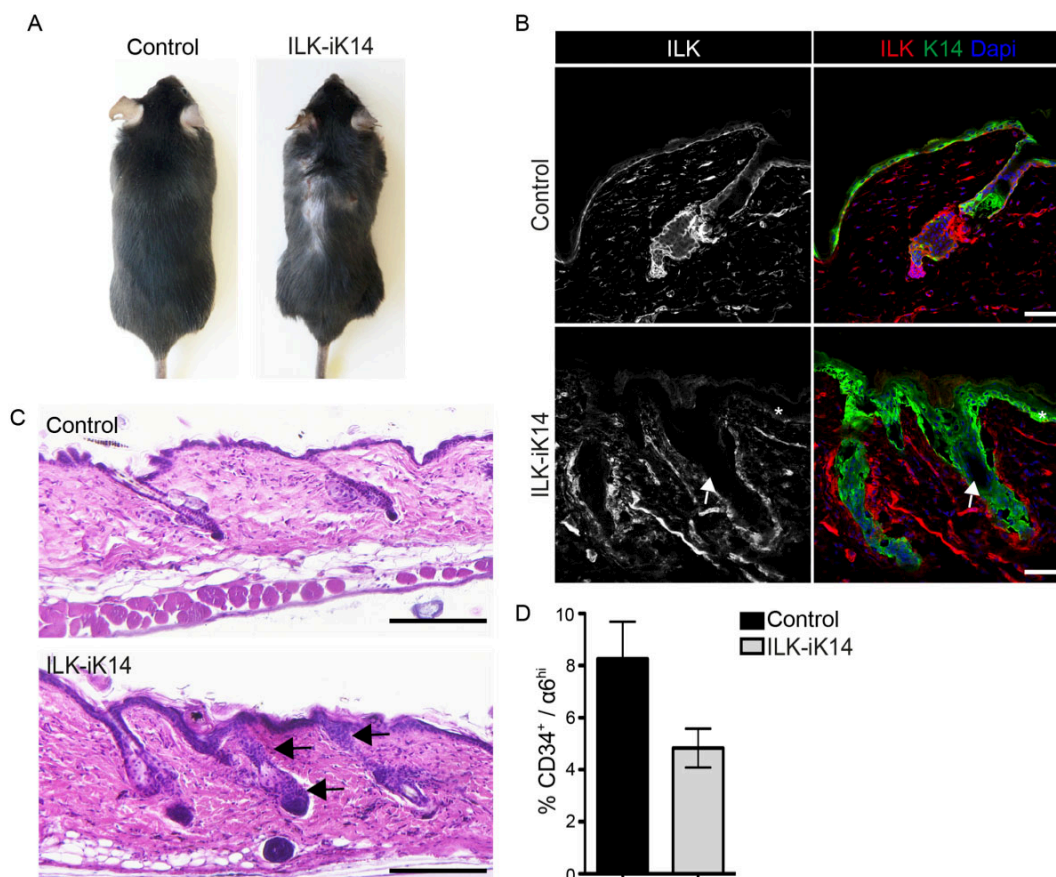


**Figure 4.3.** *A. Macroscopic phenotype of ILK-iK14 mice after 8 months of doxycycline feeding reveals hair loss and blister-induced wounding. B. Immunofluorescence staining for ILK (red) and K14 (green). ILK staining is not detected within the IFE (asterisk) or HF (arrows) of ILK-iK14 mice. Scale bars 50  $\mu$ m. C. Hematoxylin and eosin staining shows telogen HF morphology in control skin, whereas HF in ILK-iK14 are enlarged with a thickened infundibulum and ORS (arrows). Scale bar 200  $\mu$ m. D. FACS analysis of CD34<sup>+</sup>/α6<sup>hi</sup> integrin<sup>hi</sup> bulge SCs shows reduction of these cells in ILK-iK14 skin (mean  $\pm$  SEM; n=3).*

#### 4.4 ILK-deficiency leads to loss of bulge SCs through enhanced differentiation

The data so far indicated that deletion of ILK leads to loss of SCs quiescence and progressive exhaustion of the bulge SC pool. To investigate the fate of these cells *in vivo*, we performed lineage tracing experiments. To this end ILK f/f mice were crossed with an Lgr5-promoter-driven inducible Cre line that contains an IRES-EGFP

## Results

as well as a LacZ Cre reporter. This model allowed us to: 1) Delete ILK specifically in Lgr5-expressing cells that are a subpopulation of CD34-expressing bulge HFSC. 2) Quantify Lgr5-expressing HFSC after ILK deletion using the EGFP marker. 3) Trace the fate of ILK-deficient HFSCs using the LacZ reporter.

Daily administration of tamoxifen in ILK-Lgr5 mice from P17 until P21 resulted in Lgr5-Cre activation that was confirmed by the expression of LacZ (Figure 4.4.1). Analyses of mice at P22, one day after the last tamoxifen injection, revealed Lgr5-expressing cells marked by  $\beta$ -galactosidase label within the telogen HF bulge and in the HG, as expected. Control mice and ILK-deficient mice showed comparable numbers of labeled HFs as well as similar localization of  $\beta$ -galactosidase-positive cells (Figure 4.4.1).

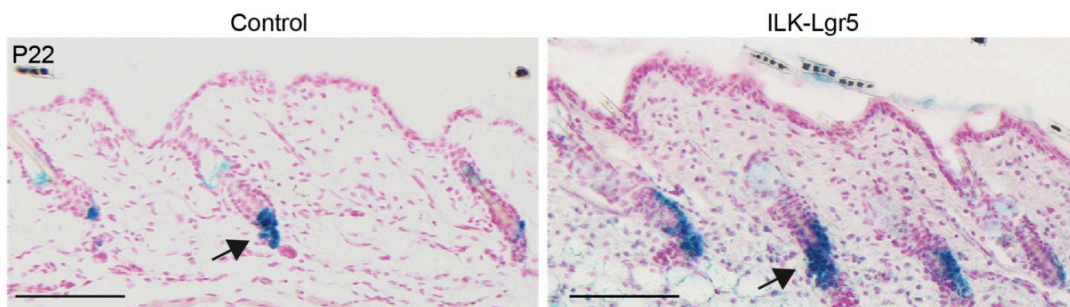


**Figure 4.4.1.** Lineage-tracing analysis of  $\beta$ -galactosidase-positive Lgr5<sup>+</sup> SC progeny of control and ILK-Lgr5 mice in P22 skin, directly after 5 consecutive days of tamoxifen application.  $\beta$ -galactosidase-positive Lgr5 progeny are seen in the bulge and secondary germ regions of HFs (arrows) both in controls and ILK-Lgr5 mice. Scale bars 100  $\mu$ m.

Upon activation of Lgr5-positive SCs during the first post-morphogenesis anagen phase at P30,  $\beta$ -galactosidase-positive Lgr5 progeny were found in the permanent part of the HF, the isthmus and the bulge, as well as in the non-permanent part within the ORS and in the matrix of control HFs (Figure 4.4.2A, B). ILK-Lgr5 HFs, however, showed less  $\beta$ -galactosidase label within the isthmus, but comparable labeling within bulge and ORS, when compared to controls (Figure 4.4.2A, B). More strikingly, ILK-Lgr5 mice showed a significant increase in the presence of  $\beta$ -galactosidase-positive matrix cells (Figure 4.4.2A, B).

The expression of Lgr5 is restricted to the bulge, HG, and ORS, whereas the matrix cells no longer express Lgr5 (Jaks et al., 2008). We therefore used the Lgr5-promoter driven EGFP to further quantify the differentiation of these cells. FACS analysis of EGFP-positive Lgr5-expressing SCs revealed a significant reduction in the number of EGFP-positive cells in ILK-Lgr5 mice (Figure 4.4.2C). Immunofluorescence analysis showed efficient deletion of ILK at this point (Figure 4.4.2D).

## Results

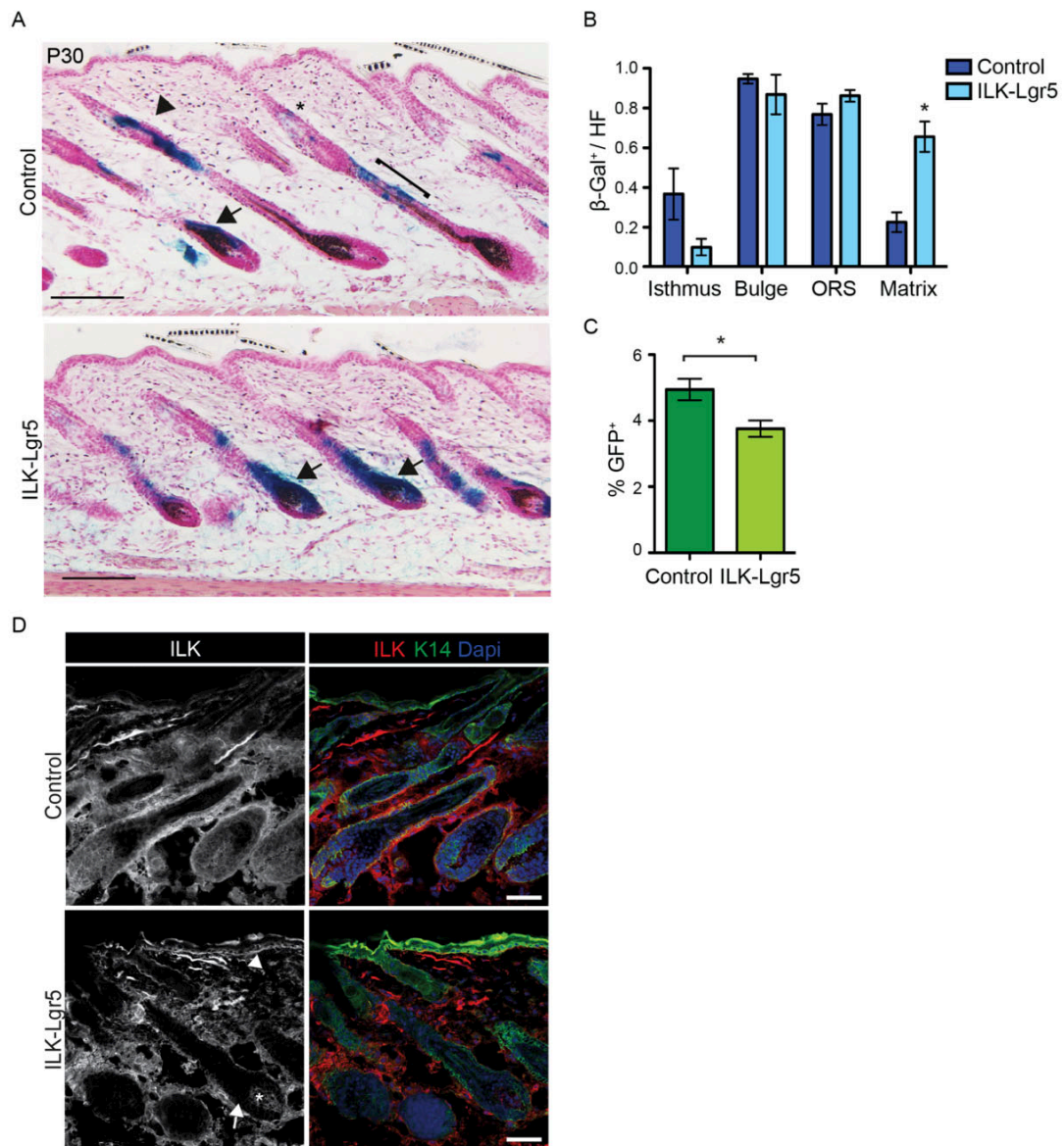


**Figure 4.4.2.** *A.*  $\beta$ -galactosidase staining of P30 skin shows *Lgr5* progeny in the isthmus (asterisk), bulge (arrowhead), ORS (bracket) and matrix (arrow) compartments in HF's of control mice, whereas ILK-*Lgr5* mice show strongest staining in the matrix cells (arrows). Scale bars 100  $\mu$ m. *B.* Quantification of the distribution of  $\beta$ -galactosidase-positive cells within P30 HF's (mean  $\pm$  SEM; n=4; \**p*=0.0159, Mann-Whitney). *C.* FACS analysis of EGFP<sup>+</sup> *Lgr5*-Cre expressing cells shows a reduction in this cell population in P30 ILK-*Lgr5* mice (mean  $\pm$  SEM; n=7; \**p*=0.0013, Student's *t*-test). *D.* Immunofluorescence staining for ILK (red) and K14 (green) at P30. ILK staining is not detected in HF's of ILK-*Lgr5* mice (arrows), whereas the IFE (arrowhead) and DP (asterisk) show comparable staining to control mice. Scale bars 50  $\mu$ m.

After anagen and subsequent catagen, a population of Lgr5-expressing cells returns to the bulge and re-establishes its quiescence (Jaks et al., 2008). To determine whether this process is perturbed in the absence of ILK, we traced the fate of these cells through 2 full rounds of anagen and analyzed the skin at P85. At this stage the overall number of HF s that contained  $\beta$ -galactosidase labeled cells was significantly reduced in ILK-Lgr5 mice (Figure 4.4.3A, B). In addition, FACS analysis revealed a further reduction of EGFP-positive cells in these mice (Figure 4.4.3 C, D). This indicated that the ILK-deficient Lgr5-expressing cells were unable to return to the bulge and were progressively lost from HF s during cycling. Taken together, these results indicate that deletion of ILK in Lgr5-positive bulge SCs leads to their enhanced activation and differentiation into hair matrix cells. This results in the progressive loss of the HFSC pool.

## Results

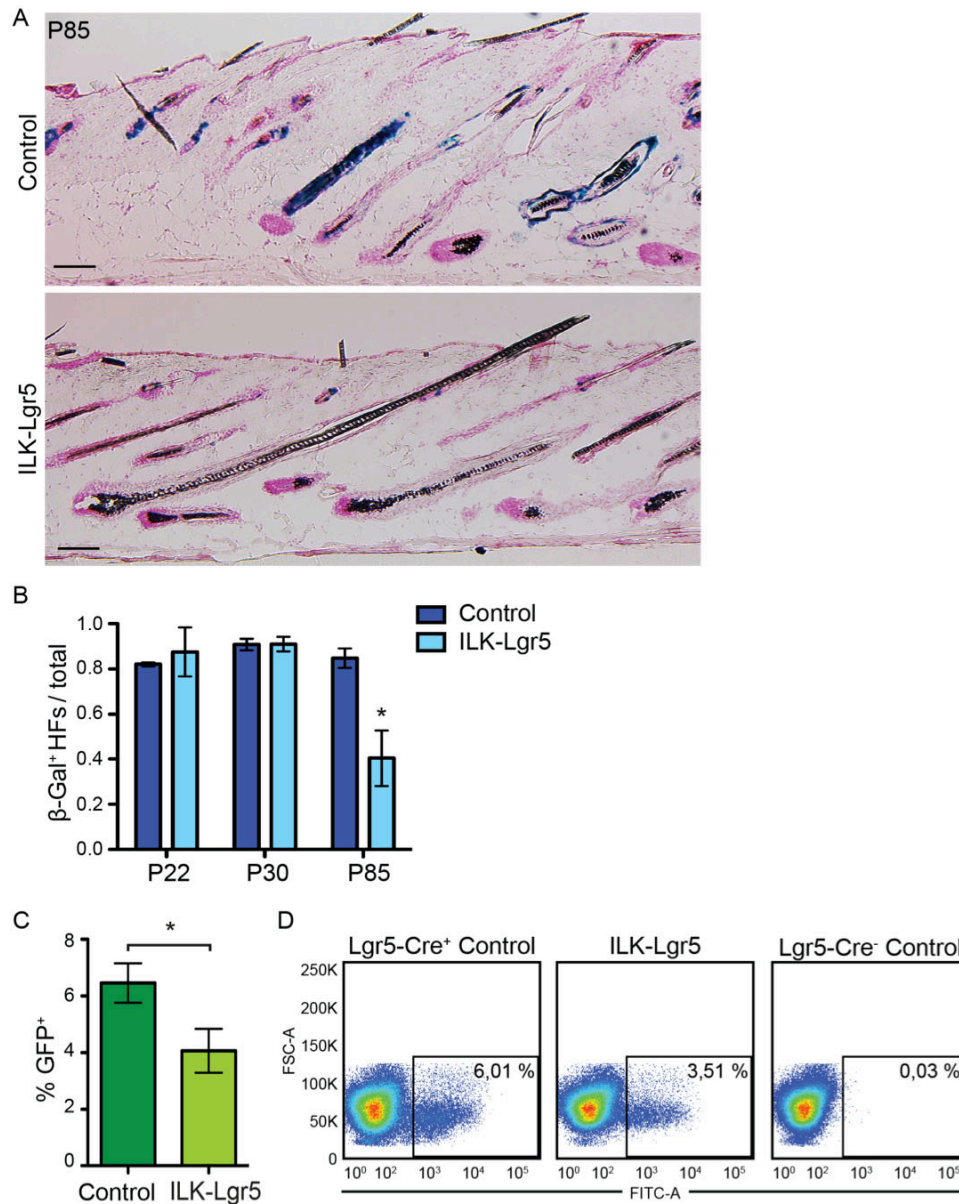


**Figure 4.4.3.** *A. Lineage-tracing of Lgr5 progeny at P85 from control and ILK-Lgr5 mice shows positive cells throughout HF of controls, whereas ILK-deleted mice show strongly reduced staining. Scale bars 100 μm. B. Quantification of the distribution of β-galactosidase staining within P22, P30, and P85 HF. ILK-Lgr5 mice show reduced β-galactosidase staining at P85 (mean ± SEM; n=4; \*p= 0.0286, Mann-Whitney). C. FACS analysis of GFP<sup>+</sup> Lgr5-expressing cells shows a reduction in this cell population in P85 ILK-Lgr5 mice (mean ± SEM; n=4; \*p=0.0381, Mann-Whitney). D. Representative FACS plots for quantification of Lgr5-EGFP cells. ILK-Lgr5 mice show reduced amounts of EGFP-positive cells.*

## **4.5 ILK is required to establish and maintain the bulge SC niche**

Our previous analysis of ILK-deficient fibroblasts had shown that ILK is crucial for ECM deposition and remodeling. In addition it was reported that ILK is essential for BM maintenance at the dermo-epidermal junction within the IFE (Lorenz et al., 2007). As the BM represents an integral part of the HFSC niche, it raised the question whether changes in the BM microenvironment could regulate SC activation. We focused our analyses on LN-332 and LN-511, the two major BM components, as they have been shown to influence HF growth and cycling (Sugawara et al., 2007; Tateishi et al., 2010).

### **4.5.1 ILK-deficiency leads to alterations in LN-332 and LN-511 deposition**

First, the composition of the HF BM was analyzed in more detail.

Immunofluorescence staining for LN-332 and LN-511 in P21 telogen HFs and skin showed an inverse gradient of these two LNs within the IFE and HFs in control mice (Figure 4.5.1.1). LN-332 staining was more intense in the IFE compared to the HFs (Figure 4.5.1.1A), whereas LN-511 staining was weaker in the IFE than around the HF (Figure 4.5.1.1B). Within the HF LN-511 was most intense at the distal end of the HF surrounding the HG as well as at the isthmus region (Figure 4.5.1.1B). However, the bulge region showed only weak staining for LN-511 (Figure 4.5.1.1B). In ILK-K5 skin, staining for LN-332 and LN-511 was observed in the BM of the IFE and HFs (Figure 4.5.1.1). In line with previous observations (Lorenz et al., 2007), LN-332 and LN-511 staining showed fragmentation within the IFE of ILK-K5 mice. The BM around HFs seemed more intact than that of the IFE. LN-332 staining of ILK-K5 HFs revealed reduced deposition around the HG compared to controls (Figure 4.5.1.1A).

## Results

In addition, LN-511 expression was strongly increased around the putative bulge marked by K15 staining, as well as surrounding the HG (Figure 4.5.1.1B).

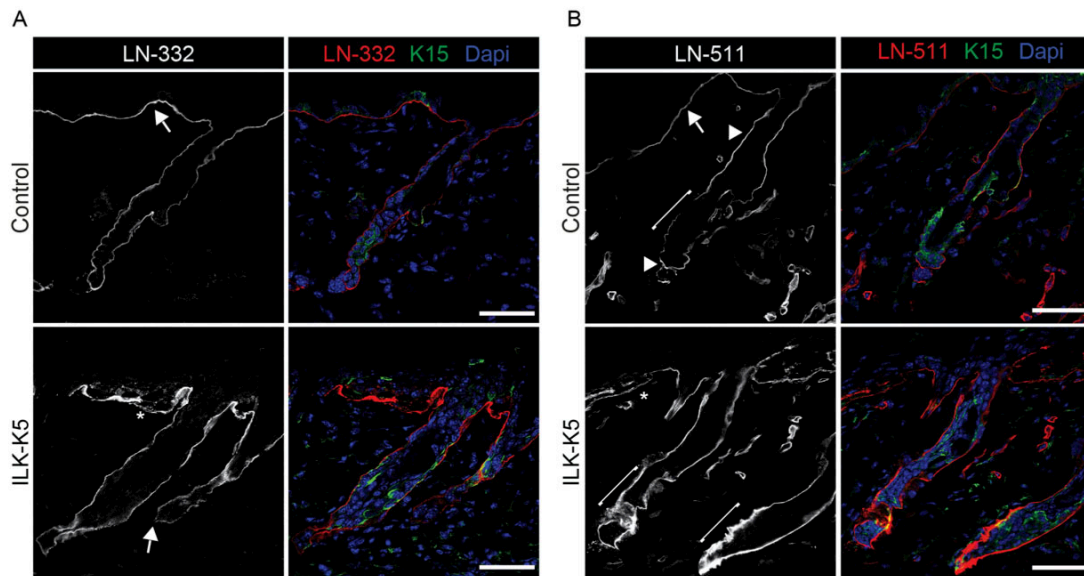


**Figure 4.5.1.1. A.** Immunofluorescence staining for LN-332 (red) and K15 (green) from P21 skin. LN-332 staining shows higher intensity beneath IFE (arrow) than around HFs in control skin. Fragmentation of LN-332 staining in the IFE (asterisk) and tips of HFs (arrow) is seen in ILK-K5 skin. Scale bars 50  $\mu$ m. **B.**

Immunofluorescence staining for LN-511 (red) and K15 (green) from P21 skin. LN-511 staining shows highest intensity at the isthmus region and around the HG (arrowheads). Only faint staining is observed beneath the IFE (arrow) and around the bulge (bracket) in control skin. Fragmentation of LN-511-staining in the IFE (asterisk) and high intensity around bulge and HG (brackets) is observed in ILK-K5 skin. Scale bars 50  $\mu$ m.

These alterations in LN-332 and LN-511 were further analyzed by western blotting. Protein extracts of skin ECM showed increased levels of LN- $\gamma$ 1, representing LN-511, and decreased levels of LN- $\gamma$ 2, representing LN-332 in ILK-K5 skin (Figure 4.5.1.2), demonstrating that the LN-332/LN-511 ratio is dramatically altered in the absence of ILK. Taken together these results show that LN-332 and LN-511 are deposited in inverse gradients along the IFE and HFs. IFE contains high levels of LN-

332 and low levels of LN-511, whereas the HF and in particular the HG contains high levels of LN-511 and low levels of LN-332. This gradient is severely disrupted in ILK-deficient skin, resulting in a reduction in LN-332/LN-511 ratio.

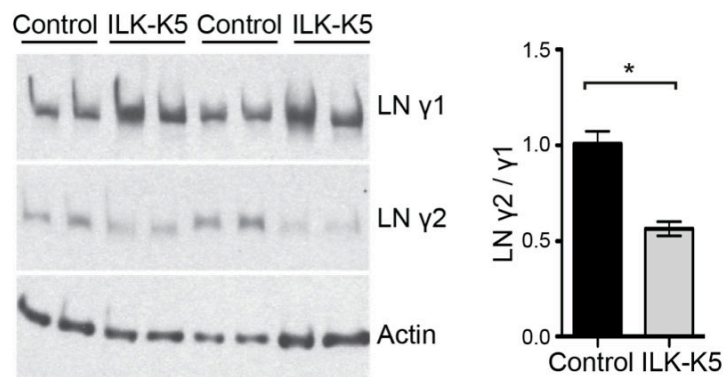


**Figure 4.5.1.2.** Western blot analysis of LN  $\gamma$ 1 and LN  $\gamma$ 2 chains from skin extracts. Actin is used as loading control. ILK-K5 skin shows increased levels of  $\gamma$ 1 and decreased levels of  $\gamma$ 2, resulting in a decreased  $\gamma$ 2 to  $\gamma$ 1 ratio (mean  $\pm$  SEM;  $n=4$ ;  $*p=0.0286$ , Mann-Whitney).

We next asked whether ILK would not only be required to establish but also to maintain the HFSC BM niche. As we observed loss of HFSCs also when ILK was deleted in adult mice, we predicted that the BM defects should also be present in this model. To assess this, we analyzed LN-332 and LN-511 distribution in ILK-iK14 mice. Here, control HFs were in telogen and LN-332 and LN-511 showed an inverse gradient with high LN-332 expression in the IFE and highest LN-511 in the HG (Figure 4.5.1.3), as already observed earlier in the K5-Cre control mice at P21. Immunofluorescence analysis of both LN-332 and LN-511 in ILK-iK14 skin revealed fragmentation of the staining beneath the IFE. In addition, ILK-iK14 HFs showed weaker staining for LN-332 in the distal end of HFs compared to controls. Furthermore, LN-511 staining of ILK-iK14 HFs showed increased intensity around

## Results

the bulge and HG (Figure 4.5.1.3). These data demonstrate that ILK is important for the establishment and maintenance of the architecture of the HFSC niche.

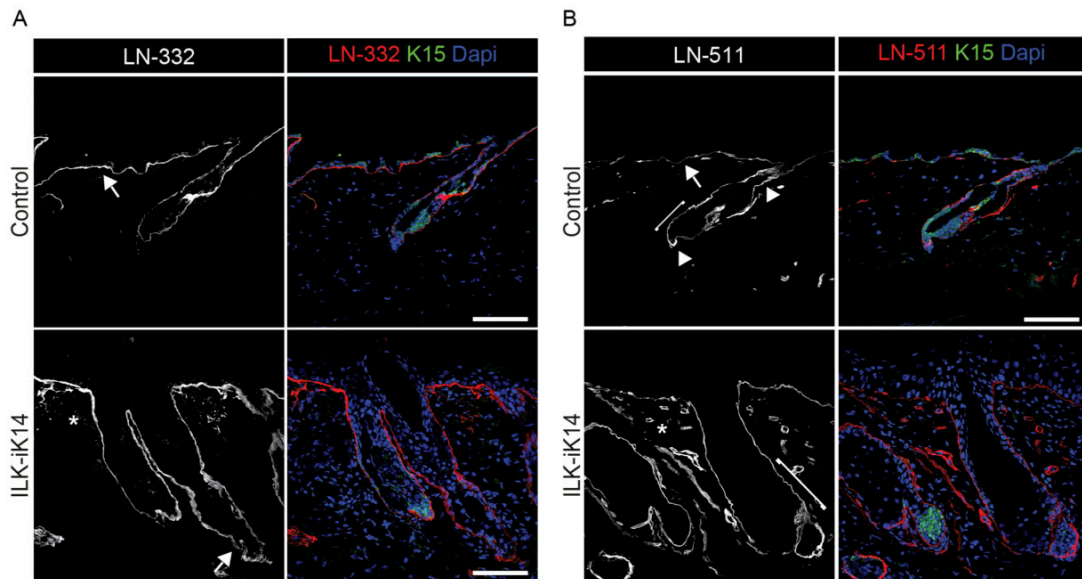


**Figure 4.5.1.3. A.** Immunofluorescence staining for LN-332 (red) and K15 (green). LN-332 staining shows higher intensity beneath the IFE (arrow) than around HF's in control skin. Fragmentation of LN-332 staining in the IFE (asterisk) and tips of HF's (arrow) is observed in ILK-iK14 skin. Scale bars 50 μm. **B.** Immunofluorescence staining for LN-511 (red) and K15 (green). LN-511 staining shows highest intensity at the isthmus region and around HG (arrowheads). Only faint staining is observed beneath the IFE (arrow) and around bulge (bracket) in control skin. Fragmentation of LN-511 staining in the IFE (asterisk) and high intensity around bulge and HG (brackets) is seen in ILK-iK14 skin. Scale bars 50μm.

### 4.5.2 ILK-deficiency leads to alterations in the epithelial-mesenchymal crosstalk

As we had observed alterations in the BM niche of the HF, we sought to characterize the HFSC niche in more detail. A second important component of this niche is the DP. It contains highly specialized mesenchymal cells that respond to epidermal Wnt signals by secreting growth factors and inhibitors essential for the regulation of SC activation and quiescence (Driskell et al., 2011; Millar, 2002). The physical contact of

the DP with the HF is crucial for this crosstalk. Mesenchymal cells within the DP are marked by the expression of endogenous alkaline phosphatase (AP). Analyses of AP-stained control HFs at P21 showed a distinct cluster of AP-positive cells in close contact with the distal tip of the HF. ILK-K5 HFs showed severe alterations in the distribution of AP-positive cells (Figure 4.5.2A). The DPs were enlarged and surrounded the entire lower part of the HF. These defects in DP architecture were also observed in ILK-iK14 HFs (Figure 4.5.2B). ILK-iK14 control telogen HFs showed a DP attached at the distal tip whereas ILK-iK14 HFs, like ILK-K5 HFs, showed an enlarged sheet of AP-positive DP cells at the distal tip of the HF (Figure 4.5.2B). This indicated that ILK plays an important role in the crosstalk between the HFSC and the DP and that impairment is independent of HF morphogenesis.

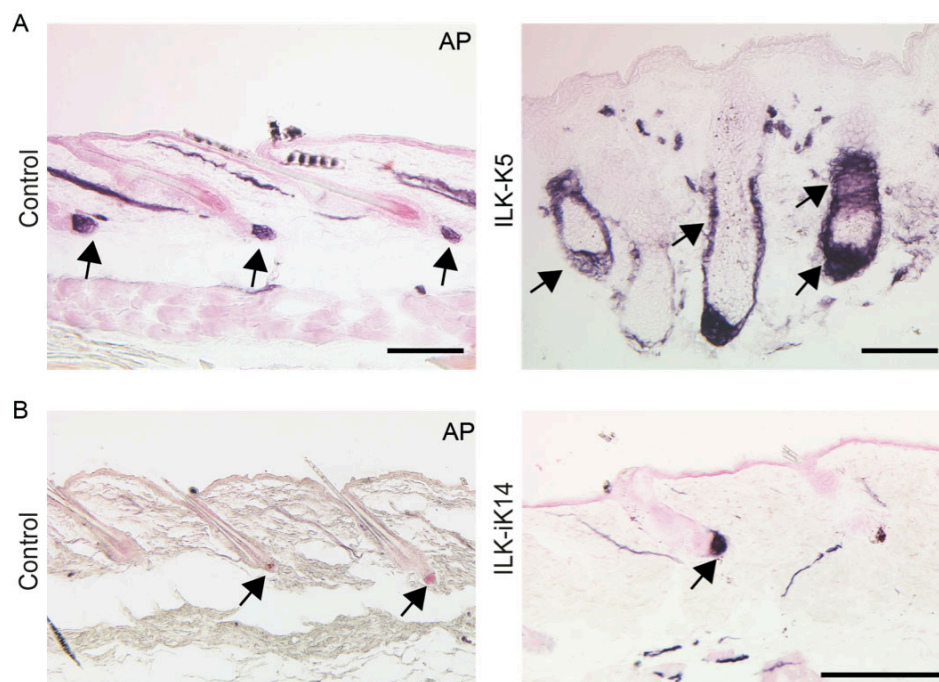


**Figure 4.5.2.** *A. Alkaline phosphatase (AP) staining to detect DP cells in P21 skin. In control skin the DP is found attached to the base of each HF (arrows; left panel). In ILK-K5 skin AP-positive cell population is increased and encapsulates the entire base of the HF (arrows; right panel) Scale bars 200  $\mu$ m. B. AP staining to detect DP cells in ILK-iK14 skin after 8 months of doxycycline administration. In control skin the DP*

## Results

is attached to the base of telogen HFs (arrows; left panel), whereas the DP is enlarged and surrounds the hair bulb in ILK-iK14 HFs (arrows; right panel). Scale bars 200  $\mu\text{m}$ .

### 4.5.3 No alterations in the immune cells within the HF microenvironment

A third important component of the HF niche are the inflammatory cells.

Inflammation and the infiltration of immune cells have been shown to cause alopecia in human and mice. To exclude the possibility that the presence of immune cells would induce HFSC activation, the presence of T cells and macrophages was assessed by immunofluorescence and the levels of pro-inflammatory cytokines within the epidermis were analyzed by qRT-PCR. Immunofluorescence staining for the T cell marker CD3 and quantification of CD3-positive cells showed no major differences in T cell infiltrates between control and ILK-K5 skin at P14 or at P21 (Figure 4.5.3A, B). Immunofluorescence staining for the macrophage marker F4/80 revealed no differences between control and ILK-K5 skin at the same time points (Figure 4.5.3C, D). RNA isolated from epidermal splits of P21 mice was analyzed for the expression of the pro-inflammatory cytokines *TNF- $\alpha$* , *IL-6* and *IL-1 $\beta$* . No significant differences were detected between in the levels of pro-inflammatory cytokines between control and ILK-K5 epidermis (Figure 4.5.3E). The findings indicate that inflammation is unlikely to trigger for HFSC activation in ILK-K5 epidermis.

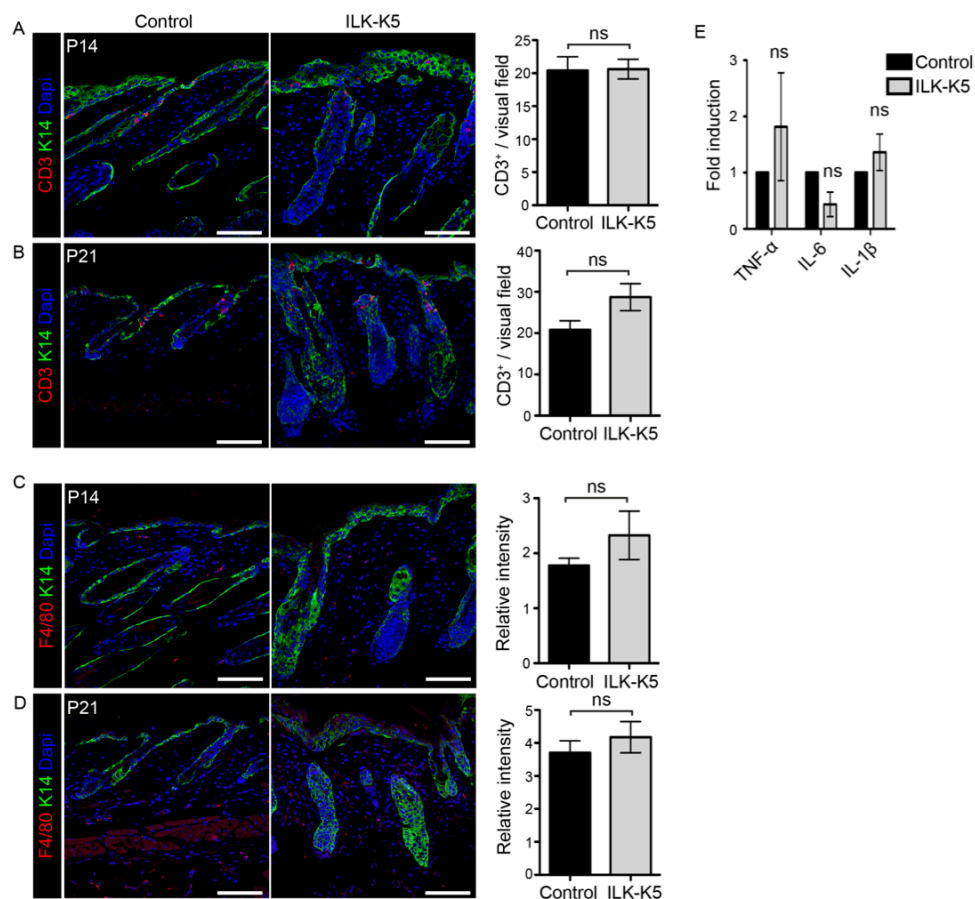


**Figure 4.5.3.** *A, B.* Immunofluorescence staining for CD3 as a marker for T-cells (red) in P14 (*A*) and P21 (*B*) control and ILK-K5 skin shows no significant difference in the amount of T-cells in the tissue. Scale bars 50  $\mu$ m. *C, D.* Immunofluorescence staining for F4/80 as a marker for macrophages (red) in P14 (*C*) and P21 (*D*) control and ILK-K5 skin shows no significant difference in the amount of macrophages in the tissue. Scale bars 50  $\mu$ m. *E.* RT-qPCR analysis of pro-inflammatory cytokines shows no major changes in TNF- $\alpha$ , IL-6 and IL-1 $\beta$  expression in P21 ILK-K5 epidermis. Values in all quantifications represent mean  $\pm$  SEM;  $n=3$ ; ns=not significant,  $p>0.06$ , Mann-Whitney.

#### 4.6 SC fate-determining pathways are altered upon ILK-deficiency

Quiescence during the telogen phase at P21 is enforced by low Wnt and Tgf- $\beta$  pathway activities and high BMP pathway activity (Blanpain and Fuchs, 2006). To identify the molecular mechanism that underlies the aberrant activation and differentiation of HFSCs in ILK-deficient mice, we next investigated the activation status of these key SC-regulatory pathways. To this end,  $\alpha$ 6-integrin-positive EPCs were sorted by MACS and analyzed by qRT-PCR. The gene expression signature of ILK-K5 EPCs at P21 was characterized by high expression levels of Wnt pathway target genes *Lef1*, *CD44*, *Dkk3*, *Tcf3*, and *Lgr5*, as well as Tgf- $\beta$  pathway target genes *Pai1* and *Tgf $\beta$ 1*. In contrast, BMP pathway target genes *Id2*, *Grem1*, and *Bambi* were downregulated. Collectively the pattern of target gene expression reflected a signature of activated SCs when compared to controls (Figure 4.6.1).

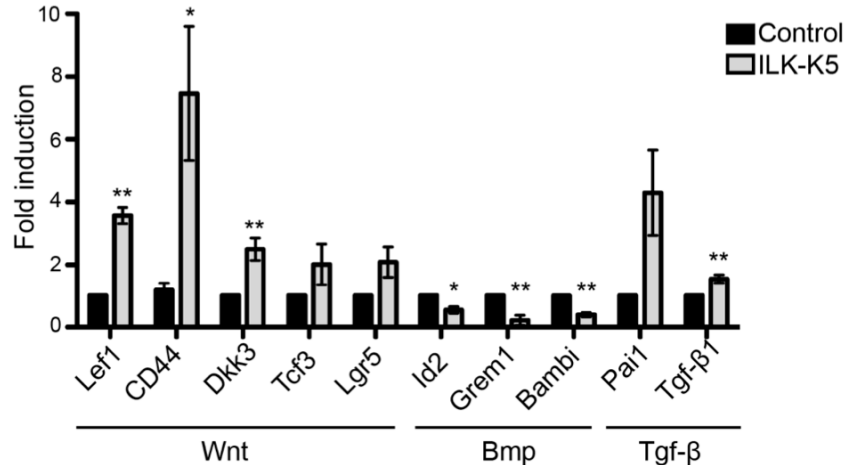


**Figure 4.6.1.** RT-qPCR analysis of target gene expression of key SC regulatory pathways shows upregulation of Wnt and Tgf- $\beta$  pathway target genes and downregulation of BMP pathway target genes in sorted EPCs from P21 ILK-K5 skin (mean  $\pm$  SEM; n=5; \*\*p=0.0075, \*p<0.0211, Mann-Whitney).

Immunohistochemical staining for phosphorylated (p) Smad2 as readout for Tgf- $\beta$  signaling revealed a significant increase in number of pSmad2-positive nuclei in the HFs of ILK-K5 skin compared to controls (Figure 4.6.2A), confirming the increased Tgf- $\beta$  pathway activity in the absence of ILK. Immunofluorescence analysis for  $\beta$ -catenin showed an increased number of cells with nuclear  $\beta$ -catenin cells within the HG of P21 ILK-K5 HFs (Figure 4.6.2B), indicative for increased Wnt activation. Enhanced Wnt pathway activity was further confirmed by analyzing the downstream target Lef1. While Lef1-positive cells were only detectable in the DP of P21 control mice, Lef1-positive cells were also found in the HG expanding into the K15-positive compartment in ILK-K5 skin (Figure 4.6.2C). Protein extracts from P21 ILK-K5 epidermis showed increased levels of pSmad2 and decreased levels of pSmad1/5/8 indicative for upregulated Tgf- $\beta$  and downregulated BMP pathway activity, respectively (Figure 4.6.2D). Overall, these data showed that loss of ILK caused an increase in Tgf- $\beta$  and Wnt/  $\beta$ -catenin signaling activities and a concomitant decrease in BMP activity, a molecular signature typically found in activated SC.

## Results

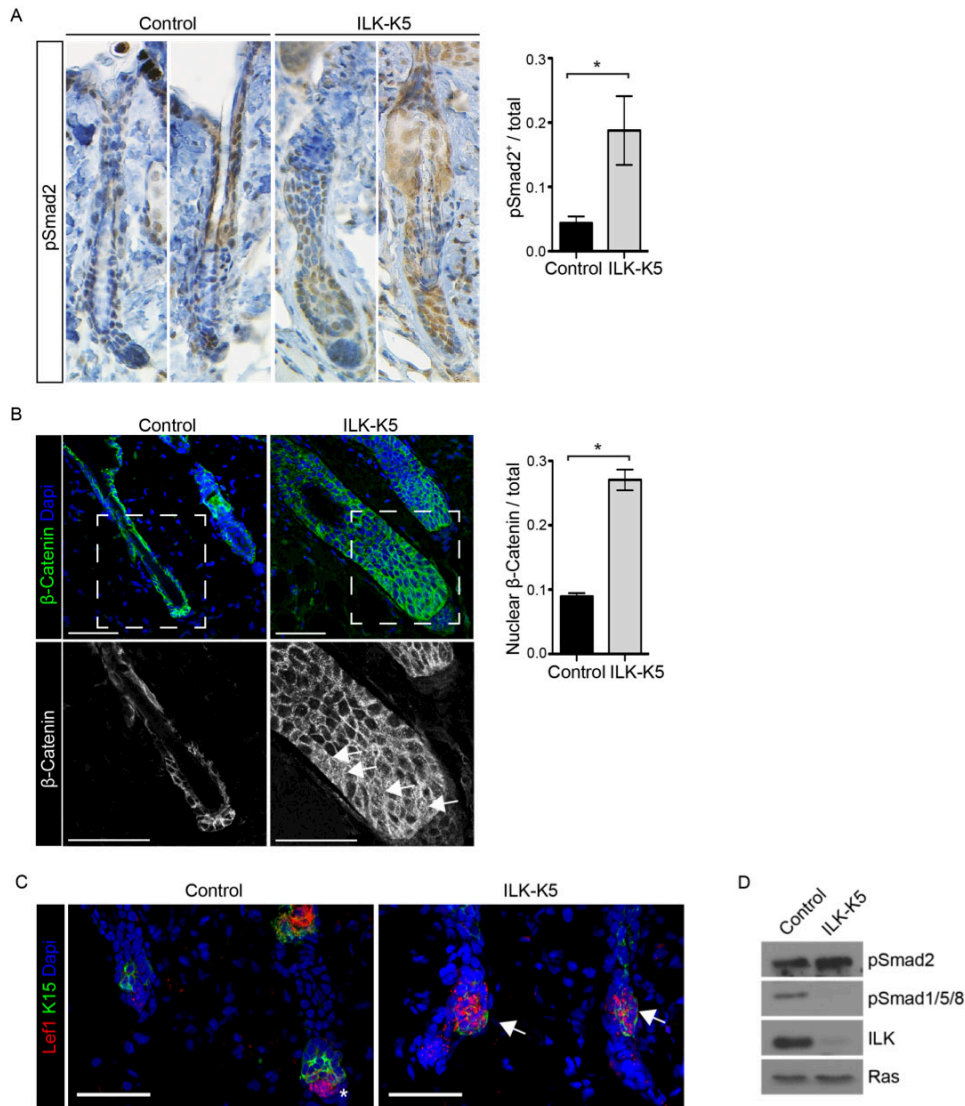
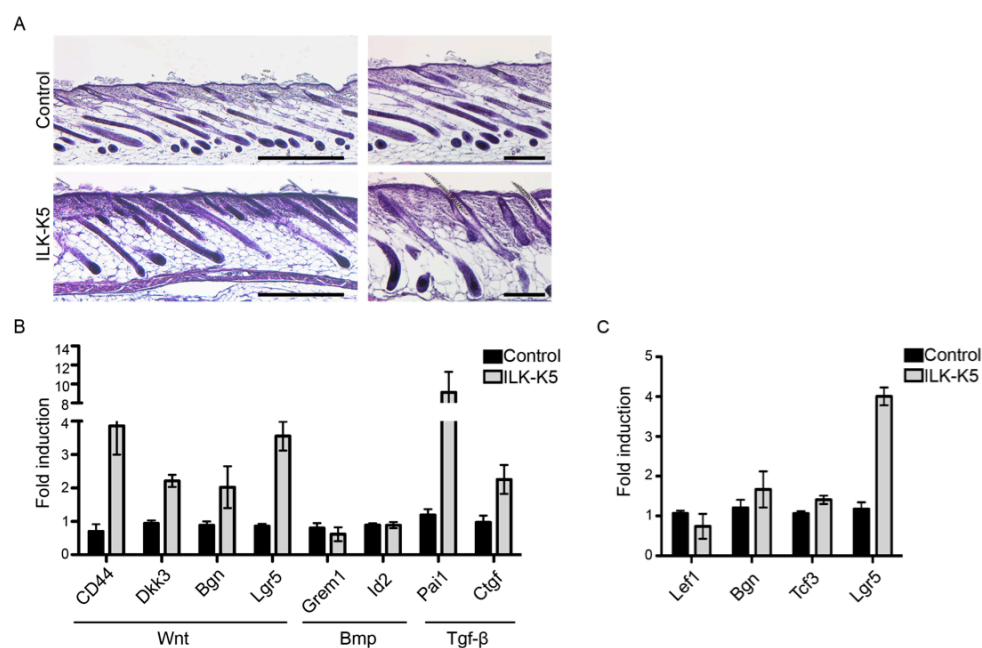


**Figure 4.6.2.** **A.** Immunohistochemical staining for pSmad2 (brown) from P21 HF<sup>s</sup> shows increased Smad2 phosphorylation in ILK-K5 HF<sup>s</sup>. Right panel shows quantification of pSmad2 staining (mean  $\pm$  SEM;  $n=5$ ;  $*p=0.0297$ , Student's *t*-test). **B.** Immunofluorescence staining for  $\beta$ -Catenin (green) from P21 HF<sup>s</sup>. Lower panel represents blow up of area marked with white rectangle. Increased nuclear localization of  $\beta$ -Catenin is observed in ILK-K5 HF<sup>s</sup> (arrows). Scale bars 50  $\mu$ m. Right panel shows quantification of nuclear  $\beta$ -Catenin staining (mean  $\pm$  SEM;  $n=3$ ;  $*p=0.05$ , Mann-Whitney). **C.** Lef-1 staining (red) from P21 control and ILK-K5 skin. Controls show staining only in the DP (asterisk) whereas also K15-positive (green) cells show staining for Lef1 in ILK-K5 HF<sup>s</sup>. Scale bar 50  $\mu$ m. **D.** Western blot analysis from P21 epidermal lysates shows increased phosphorylation of Smad2 and decreased phosphorylation of Smad1/5/8 in ILK-K5 epidermis.

To address whether the increase in SC-activating pathways in ILK-K5 skin was due to the fact that the HFs were not entering the telogen phase and remained in an anagen-like state, earlier time points were subsequently analyzed. At P14, during anagen phase of HF morphogenesis, both control and most ILK-K5 HFs are elongated and reach into the deep fat layer of the skin (Figure 4.6.3A). At this time point, Wnt and Tgf- $\beta$  target genes were already upregulated in ILK-K5 mice (Figure 4.6.3B), indicating that the differences observed in SC fate regulating pathways at P21 could not be attributed to the difference in HF cycling. However, BMP pathway target genes were not altered in ILK-K5 skin at this time point (Figure 4.6.3B), indicating that changes in BMP pathway activity were secondary to the difference in HF cycle stage. No major differences in Wnt target gene expression were found at P7 (early anagen of morphogenesis), with the exception of *Lgr5* that was slightly upregulated (Figure 4.6.3C). Taken together, these results show that ILK-deficiency leads to sustained activation of Wnt and Tgf- $\beta$  pathways in late anagen, leading to the inability of HFs to enter the quiescent telogen phase.



## Results

**Figure 4.6.3. A.** Hematoxylin and eosin staining of P14 skin. Both control and ILK-K5 HF<sup>s</sup> display anagen morphology. Scale bars 500  $\mu\text{m}$  (left panel); 100  $\mu\text{m}$  (right panel). **B.** RT-qPCR analysis of target gene expression from P14 control and ILK-K5 EPCs shows upregulation of Wnt and Tgf- $\beta$  pathway target genes, but no change in BMP pathway target genes (mean  $\pm$  SEM;  $n=3$ ). **C.** RT-qPCR analysis of Wnt target gene expression from P7 EPCs. Only *Lgr5* expression is found upregulated at this point (mean  $\pm$  SEM;  $n=4$ ;  $p>0.0765$ , Mann-Whitney).

### 4.7 LN-332 and LN-511 regulate SC fate determining pathways

As we had observed changes in the SC niche as well as in key SC regulatory pathways, we next addressed the question whether the changes in the niche could directly impact the activity of these pathways and thereby SC activation.

#### 4.7.1 LN-332 regulates Wnt and LN-511 regulates Tgf- $\beta$ signaling

To test whether the observed changes in altered LN-332 and LN-511 deposition might be involved in the deregulation of SC fate pathways, wild type EPCs were isolated and plated onto human recombinant LN-332 or LN-511, respectively, and allowed to adhere for 6 h before analysis. A mixture of type I collagen (Col1) and FN was used as a control substrate to exclude effects from altered adhesion or integrin usage.

Adhesion to LN-332 and LN-511 as well as to Col1 and FN is mediated  $\beta$ 1 integrins. Adhesion of EPCs on LN-511 led to an increase in Smad2 phosphorylation as well as to significant upregulation of Tgf- $\beta$  target gene (*p21*, *Pai1*, *Tgf $\beta$ 1*) expression (Figure 4.7.1A, B). In contrast,  $\beta$ -catenin stabilization and expression of Wnt/  $\beta$ -catenin target genes (*Axin2*, *Lef1*, *Dkk3*) were unaffected (Figure 4.7.1A, B). Adhesion of EPCs on LN-332 showed the opposite.  $\beta$ -catenin was destabilized as indicated by decreased protein levels and Wnt/  $\beta$ -catenin pathway target genes (*Axin2*, *Lef1*, *Dkk3*, *Sfrp1*) were downregulated (Figure 4.7.1C, D). In contrast, Smad2 phosphorylation and Tgf-

$\beta$  pathway target gene expression (*Pai1*, *Tgf $\beta$ 1*) were not changed (Figure 4.7.1C, D).

Collectively, these findings demonstrate that LN-511 promotes the activation of the

Tgf- $\beta$  pathway, whereas LN-332 suppresses Wnt/  $\beta$ -catenin pathway activity.

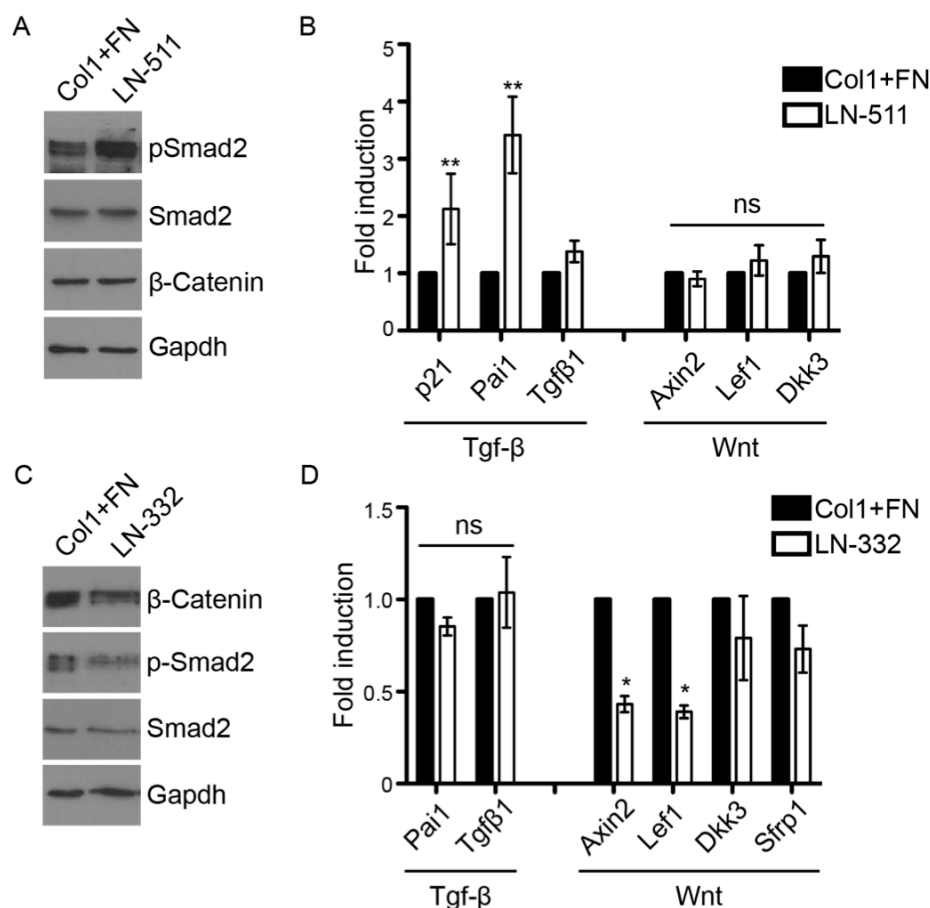


**Figure 4.7.1.** **A.** Western blot analysis of freshly isolated EPCs plated on LN-511 or a mixture of Col1 and FN as control. Cells adhering on LN-511 for 6 h show increased Smad2 phosphorylation, whereas  $\beta$ -Catenin is unchanged. Gapdh was used as loading control. **B.** RT-qPCR analysis of Wnt/ $\beta$ -Catenin and Tgf- $\beta$  pathway target gene expression shows selective upregulation of Tgf- $\beta$  pathway target genes in cells adhering to LN-511 (mean  $\pm$  SEM; n=5; \*\*p=0.0075, Mann-Whitney). **C.** Western blot analysis of freshly isolated EPCs plated on LN-332 or Col1+FN as control. Cells adhering on LN-332 for 6 h show decreased  $\beta$ -Catenin levels, whereas Smad2 phosphorylation is unchanged. Gapdh was used as loading control. **D.** RT-qPCR analysis of Wnt and Tgf- $\beta$  pathway target gene expression shows selective

## Results

*downregulation of Wnt/ $\beta$ -Catenin pathway target genes in cells adhering to LN-332 (mean  $\pm$  SEM; n=4; \*p=0.0211, Mann-Whitney).*

### **4.7.2 A wild type matrix rescues the altered signaling activity in ILK-deficient keratinocytes**

Our results so far indicated that ILK regulates the LN-332/LN511 ratio within the HF BM as well as SC activation. In addition, we observed that LN-332 and LN-511 are capable of regulating key SC fate determining pathways. Therefore we next addressed whether the changes in Wnt and Tgf- $\beta$  signaling in ILK-K5 EPCs arise from alterations in the LN-332/LN-511 ratio. To this end, *in vitro* rescue experiments were performed where the ECM of ILK-deficient EPCs was substituted by that deposited by wild type EPCs. A mixture of Col1 and FN was used as a control substrate. First, the different matrices were characterized by immunofluorescence. In contrast to control cells that assembled a LN-332 matrix, ILK-deficient EPCs deposited patchy aggregates of LN-332 when plated onto the Col1+FN control substrate (Figure 4.7.2.1A). Interestingly ILK-deficient cells were found to displace themselves from the LN-332 aggregates (Figure 4.7.2.1A). When wild type EPCs were allowed to deposit ECM for 4-5 days after which the cells were removed leaving an intact matrix, the deposited preassembled ECM showed abundant LN-332 staining. ILK-deficient EPCs adhered and spread on this matrix (Figure 4.7.2.1A). Control EPCs plated onto Col1+FN did not deposit detectable amounts of LN-511. In contrast, ILK-deficient EPCs deposited low amounts LN-511 and adhered on it (Figure 4.7.2.1B). In agreement with the limited deposition of LN-511 by control cells, the preassembled wild type ECM also contained very little LN-511 (Figure 4.7.2.1B). ILK-K5 EPCs that adhered on the preassembled ECM showed reduced deposition of LN-511 (Figure 4.7.2.1B).

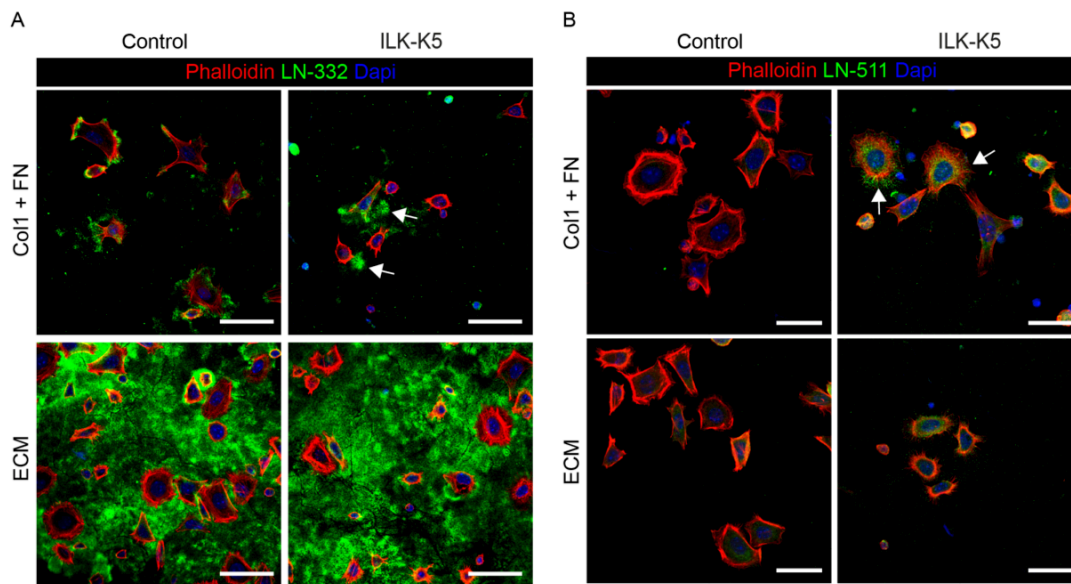


**Figure 4.7.2.1. A.** Freshly isolated EPCs were allowed to adhere on Col1+FN (upper panel) or preassembled ECM (lower panel), after which they were analyzed by immunofluorescence. Control cells deposit a LN-332 matrix (in green), whereas EPCs from ILK-K5 skin deposit LN-332 aggregates and the cells displace themselves from the aggregates (arrows). The preassembled ECM contains large amounts of LN-332 that supports adhesion in both control and ILK-K5 EPCs (lower panels). Phalloidin (red) was used to counterstain adhering cells. Scale bars 35  $\mu\text{m}$ . **B.** EPCs were allowed to adhere on Col1+FN (upper panel) or preassembled ECM (lower panel), after which they were analyzed by immunofluorescence. Control cells do not deposit detectable amounts of LN-511 (in green), whereas EPCs from ILK-K5 skin deposit and adhere on LN-511 (arrows). The preassembled ECM contains very low levels of LN-511 (lower panels). Phalloidin (red) was used to counterstain adhering cells. Scale bars 25  $\mu\text{m}$ .

Next, we assessed the activities of Tgf- $\beta$  and Wnt/ $\beta$ -Catenin pathways on the different substrates. qRT-PCR analyses of control and ILK-deficient EPCs plated on Col1+FN substrate revealed that ILK-K5 EPCs maintained their molecular signature characterized by high Tgf- $\beta$  (*Pai1*, *Tgf $\beta$ 1*) and high Wnt (*Axin2*, *Lef1*, *Dkk3*, *Tcf3*) target gene expression in vitro (Figure 4.7.2.2). Adhesion of control EPCs onto the preassembled ECM did not significantly alter their gene expression pattern. In

## Results

contrast, adhesion of ILK-deficient EPCs to the preassembled ECM restored both the Tgf- $\beta$  and Wnt pathway target gene expression to resemble that of control cells (Figure 4.7.2.2). These data indicate that the ratio of LN-332 and LN-511 regulates Tgf- $\beta$  and Wnt/ $\beta$ -Catenin pathway activities and that restoring the altered ECM microenvironment of ILK-deficient cells also rescues the aberrant signaling activities of Tgf- $\beta$  and Wnt/ $\beta$ -Catenin pathways in these cells.

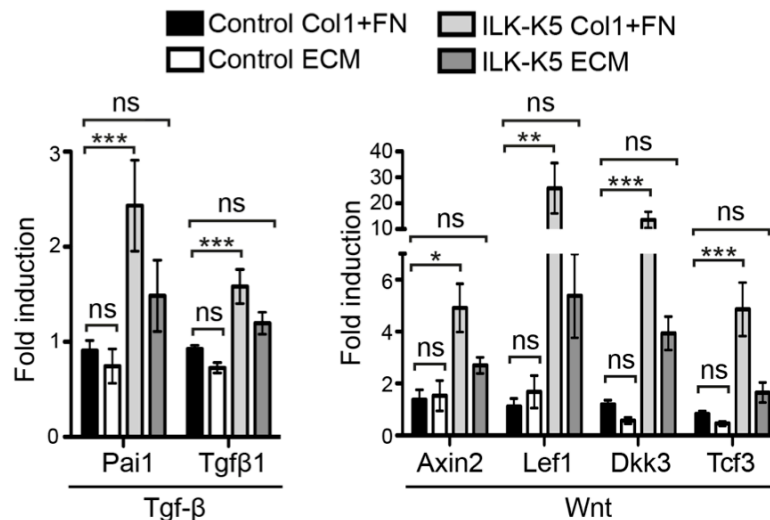


**Figure 4.7.2.2.** RT-qPCR analyses show that adhesion of EPCs from ILK-K5 skin on preassembled wild type ECM restores Wnt and Tgf- $\beta$  pathway target gene expression to the level of control cells (mean  $\pm$  SEM;  $n=7$ ; \*\*\* $p<0.0001$ , \*\* $p<0.0045$ , \* $p=0.0062$ , ns=not significant, ANOVA and Dunnet's).

## 4.8 Aberrant SC activation causes replication stress and predisposes to skin carcinogenesis

Loss of quiescence and sustained SC activation leads to SC exhaustion and can lead to the formation of tumor-initiating cells (Beck and Blanpain, 2013). The balance of SC quiescence and activation has been described to act as a tumor-suppressing mechanism in hematopoietic cells (Bakker and Passegue, 2013). It has been proposed that SC quiescence acts as a protective mechanism that minimizes replication stress

and thereby prevents accumulation of DNA damage in SCs (Bakker and Passegue, 2013). We hypothesized that due to its SC-activating effect deletion of ILK might cause enhanced replication stress and DNA damage and even predispose the epidermis to carcinogenesis.

To test this hypothesis we first analyzed DNA damage in P21 skin by immunofluorescence staining using the DNA damage marker histone 2A member X (H2A.X). H2A.X becomes phosphorylated at serine 139 ( $\gamma$ H2AX) upon DNA damage caused by either DNA double strand breaks or replication fork collapse (Lukas et al., 2011). The latter state is characterized by a pan-nuclear staining of  $\gamma$ H2AX (Murga et al., 2009). These analyses revealed that  $\gamma$ H2AX-positive nuclei were rarely present in controls but significantly more abundant in ILK-K5 HFs, with mainly pan-nuclear staining observed (Figure 4.8.1A). Immunofluorescence staining for the tumor suppressor protein p53 provided further evidence for increased DNA damage. Upon DNA damage p53 becomes N-terminally phosphorylated and subsequently stabilized within the nucleus where it activates target gene expression (Elias et al., 2014). At P21, there was a significant increase in number of p53-positive cells within the HFs of ILK-K5 as compared to controls (Figure 4.8.1B). Collectively these data show that deletion of ILK leads to increased replicative stress and DNA damage.

## Results

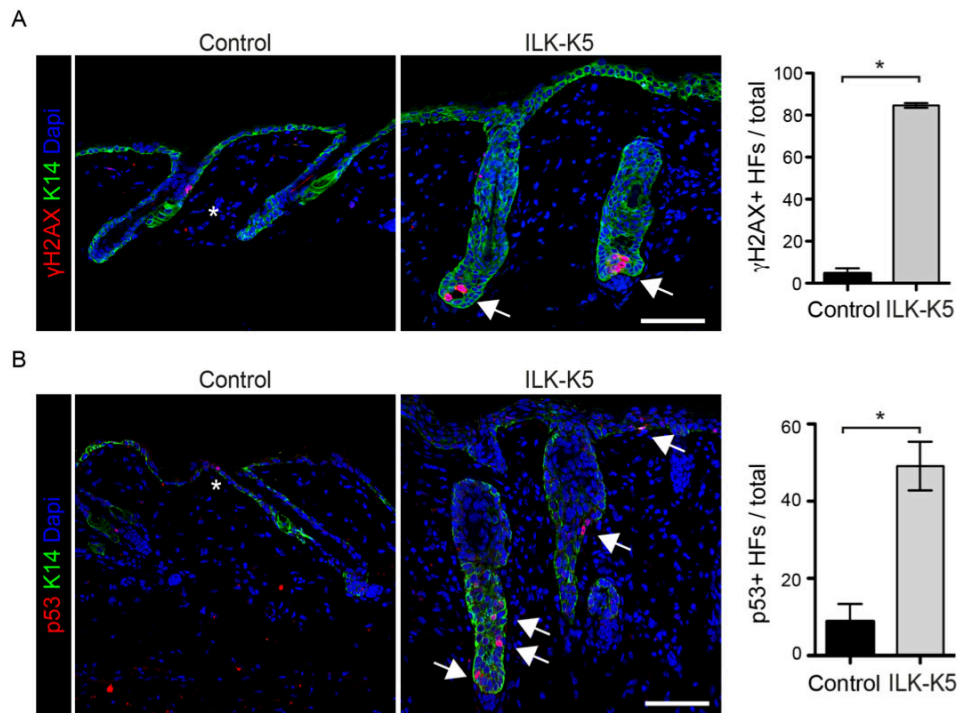


**Figure 4.8.1. A.** Immunofluorescence staining for  $\gamma$ H2AX (red) and K14 (green) from P21 skin. Control mice rarely show  $\gamma$ H2AX-positive cells (asterisk), whereas ILK-K5 HF show clusters of cells with pan-nuclear  $\gamma$ H2AX within HF (arrows). Scale bars 50  $\mu$ m. Right panel shows quantification of HF containing more than two  $\gamma$ H2AX-positive cells (mean  $\pm$  SEM;  $n=3$ ;  $*p=0.0383$ , Mann-Whitney). **B.** Staining for p53 (red) and K14 (green) from P21 skin. In contrast to control mice that show only solitary p53 positive cells (asterisk), ILK-K5 mice frequently show p53-positive cells within HF and IFE (arrows). Scale bars 50  $\mu$ m. Right panel shows quantification of HF containing more than two p53-positive cells (mean  $\pm$  SEM;  $n=4$ ;  $*p=0.0286$ , Mann-Whitney).

In addition to regulating HFSC activation, Wnt/ $\beta$ -catenin signaling has been shown to maintain the homeostatic balance between proliferation and differentiation within the IFE. Increased Wnt activity in the IFE leads to hyperproliferation that is also observed in the ILK-K5 IFE (Choi et al., 2013; Lorenz et al., 2007). We therefore assessed Wnt target gene expression at later stages (P57), when HF were almost completely depleted in ILK-K5 mice, and found Wnt target genes to be upregulated (Figure

4.8.2A). Immunofluorescence analysis for  $\gamma$ H2AX was performed at P57 to determine if the upregulation of Wnt activity was accompanied by increased replication stress in ILK-deficient epidermis. Very few  $\gamma$ H2AX-positive nuclei were detectable within the IFE of control mice, whereas significant numbers of  $\gamma$ H2AX-positive nuclei with pan-nuclear staining were identified in ILK-K5 skin (Figure 4.8.2B). These data suggest that replication stress persists in 8-week old mice and that cells with DNA damage accumulate in the epidermis of ILK-K5 mice.

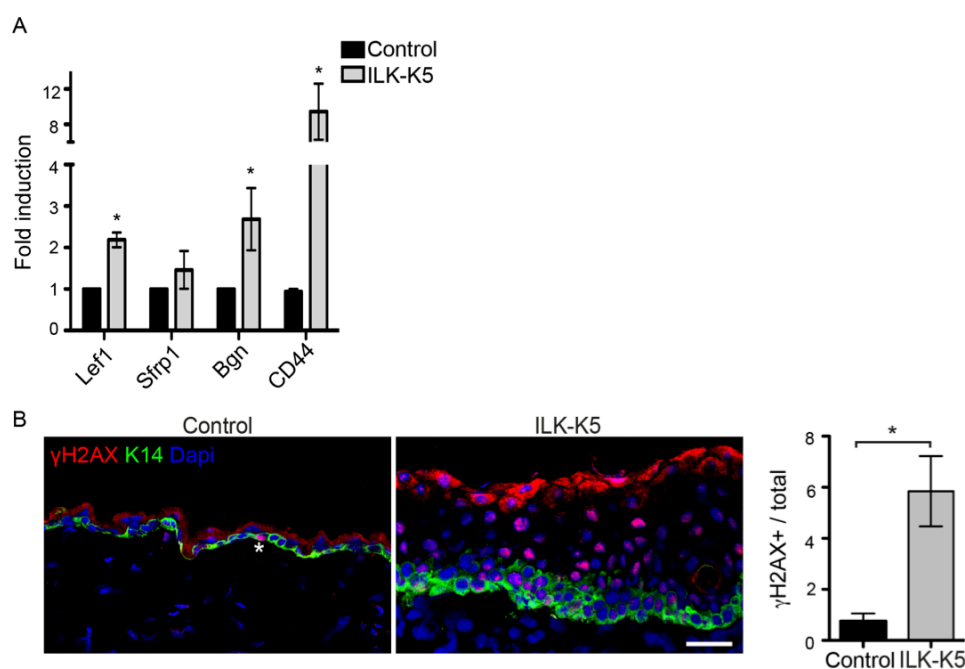


**Figure 4.8.2.** **A.** RT-qPCR analysis of Wnt pathway target gene expression shows upregulation of Wnt target gene expression in EPCs from P57 ILK-K5 skin (mean  $\pm$  SEM;  $n=4$ ;  $*p=0.0211$ , Mann-Whitney). **B.** Staining for  $\gamma$ H2AX (red) and K14 (green) from P57 skin. Control mice show only solitary  $\gamma$ H2AX-positive cells (asterisk) within the IFE, whereas ILK-K5 IFE shows abundant pan-nuclear  $\gamma$ H2AX staining (asterix). Scale bars 50  $\mu$ m. Right panel shows quantification of  $\gamma$ H2AX-positive cells within the IFE (mean  $\pm$  SEM;  $n=4$ ;  $*p=0.0286$ , Mann-Whitney).

## Results

Hyperproliferation can be caused by inflammation. To assess whether inflammation was associated with the hyperproliferation of ILK-K5 IFE at this stage, the immune cell infiltrate of T cells and macrophages was assessed at P57, as described previously for P21 skin. Immunofluorescence staining for the T cell marker CD3 and macrophage marker F4/80 revealed no differences in the immune cell infiltrate between ILK-K5 and control skin at P57 (Figure 4.8.3). These findings suggested that the transient inflammation caused by HF destruction (Lorenz et al., 2007) was resolved at this time point.

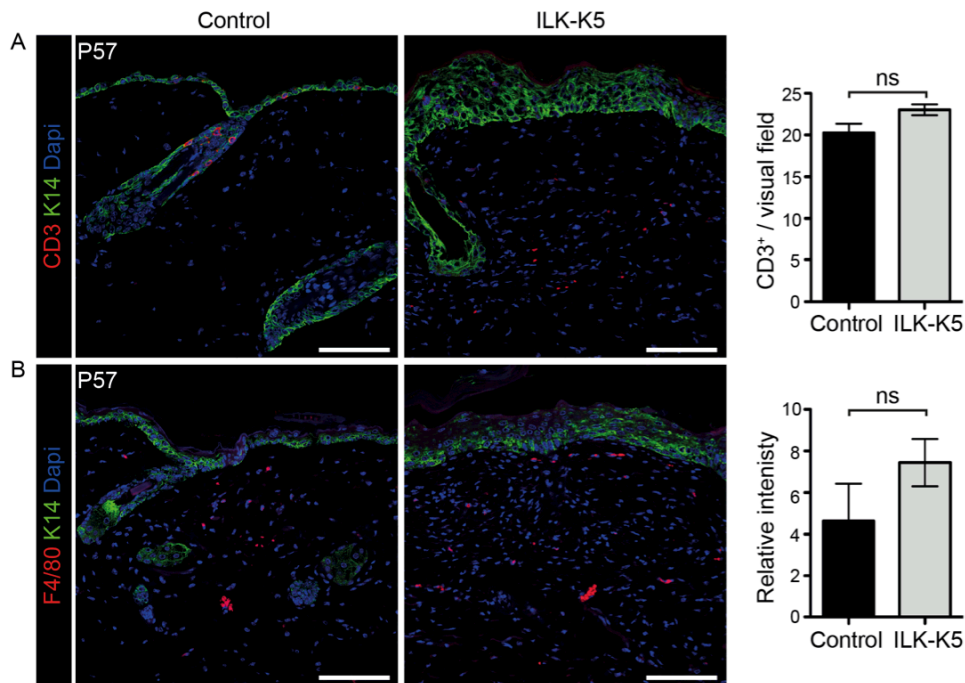


**Figure 4.8.3.** **A.** Immunofluorescence staining for CD3 (red) in P57 control and ILK-K5 skin shows no significant difference in the amount of T-cells in the tissue. Scale bars 50  $\mu$ m. Values in quantification represent mean  $\pm$  SEM;  $n=3$ ; ns=not significant,  $p=0.20$ , Mann-Whitney. **B.** Immunofluorescence staining for F4/80 (red) in P57 control and ILK-K5 skin shows no significant difference in the amount of macrophages in the tissue. Scale bars 50  $\mu$ m. Values in quantification represent mean  $\pm$  SEM;  $n=3$ ; ns=not significant,  $p=0.20$ , Mann-Whitney.

Next, to examine whether the accumulation of DNA damage would predispose ILK-K5 to skin carcinogenesis, mice were subjected to a two-stage carcinogenesis experiment (Abel et al., 2009). Tumor initiation was performed by topical application of 7,12-dimethylbenz[a]-anthracene (DMBA) on shaved skin of 8-week old mice. The treatment was performed twice within 1 week, followed by a two-week break. After this, tumor formation was promoted by twice-weekly application of 12-*O*-tetradecanoylphorbol-13-acetate (TPA). After 18 weeks of TPA treatment all ILK-K5 mice had developed papillomas, whereas only 50 % of control mice had tumors (Figure 4.8.4A). Due to the deteriorating skin health condition of the ILK-K5 mice, most likely due to the irritating effect of the vehicle acetone, the experiment was then terminated. Quantitative analyses of tumor formation showed that ILK-K5 mice displayed a significant increase in papilloma incidence and in the number of papillomas per affected mouse (Figure 4.8.4A, B). No obvious differences in papilloma morphology were observed (Figure 4.8.4C). In addition, analyses of tumor size revealed no differences between control and ILK-K5 tumors (Figure 4.8.4D). Proliferation and apoptosis within the papillomas was further examined. As assessed by TUNEL staining there was no difference in the rate of apoptosis between control and ILK-K5 papillomas (Figure 4.8.4E). Furthermore, no significant change in proliferation was observed (Figure 4.8.4F). This indicated that ILK increases the incidence of tumor formation, but does not impact the behavior of the tumor cells themselves.

Taken together, these data show that ILK-deficiency causes upregulation of the Wnt signaling pathway and hyperproliferation within the IFE. These changes are accompanied with increased replication stress that promotes the accumulation of DNA damage, thereby predisposing the skin for carcinogenesis.

## Results

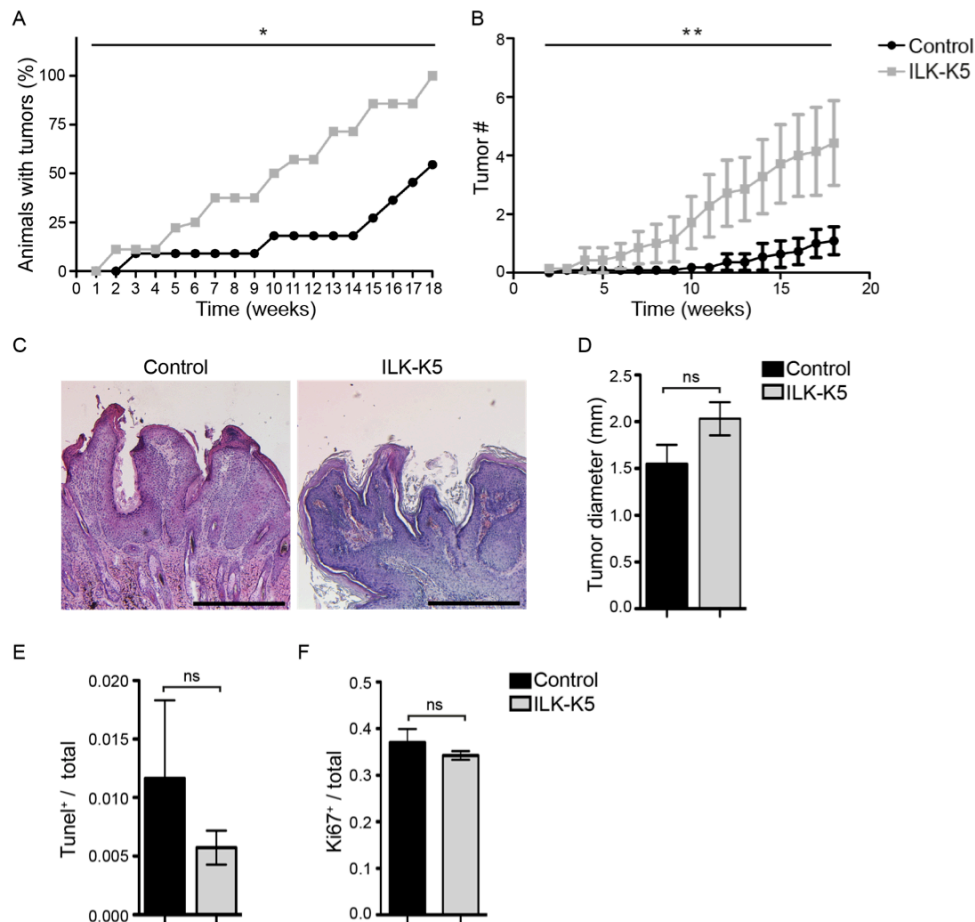


**Figure 4.8.4.** **A.** Tumor incidence of control and ILK-K5 mice treated twice with DMBA followed by 18 weeks of biweekly TPA treatment. ILK-K5 mice show increased tumor incidence ( $n=11/11$ ;  $*p=0.0209$ , Chi-square). **B.** Tumor multiplicity in affected control and ILK-K5 mice. ILK-K5 mice show increased tumor multiplicity (mean  $\pm$  SEM;  $n=11/11$ ;  $**p<0.01$ , Two-way ANOVA). **C.** Hematoxylin and eosin stainings of papillomas from control and ILK-K5 mice show comparable histology. Scale bars 500  $\mu$ m. **D.** Quantification of tumor diameter shows no significant difference in tumor sizes from control and ILK-K5 mice (mean  $\pm$  SEM;  $n=11/31$ ; ns=not significant,  $p=0.1386$ , Student's *t*-test). **E.** Quantification of apoptosis within tumors using TUNEL assay shows no significant difference in tumor cell apoptosis in control and ILK-K5 mice (mean  $\pm$  SEM;  $n=3$ ;  $p=0.344$ , Mann-Whitney). **F.** Quantification of proliferation within tumors using Ki67 staining shows no significant difference in tumor cell proliferation in control and ILK-K5 mice (mean  $\pm$  SEM;  $n=3$ ;  $p=0.344$ , Mann-Whitney).

## 5 Discussion

ILK is a central adaptor protein that links  $\beta 1$  and  $\beta 3$  integrins to the actin cytoskeleton and thereby regulates integrin-dependent actin remodeling. Therefore, multiple processes dependent on actin regulation such as adhesion, spreading, migration, proliferation and differentiation rely on the function of ILK. Reciprocally, actin rearrangement causes deformation within the cell and generation of cellular tension, which is directly coupled to changes in integrin-dependent adhesions and leads to the remodeling of the local ECM environment. The relevance for ILK in this crosstalk has already been shown in a large variety of functional *in vitro* and *in vivo* studies (Lange et al., 2009; Larsen et al., 2006; Wickström et al., 2010). However, it is still unclear how ILK regulates ECM and BM remodeling and how the BM, as part of the SC niche, regulates SC fate. The current thesis work shows that ILK is essential for cellular force generation and subsequent FN fibrillogenesis *in vitro*. Using skin as a model tissue, the findings further indicate that ILK is essential for deposition of precise LN-511 and LN-332 gradients within the niche of bulge SCs. This is required to adjust the activities of SC fate-determining signaling pathways Wnt and Tgf- $\beta$  to regulate SC activation and quiescence. ILK-deficiency drives SCs towards an activated phenotype that is more susceptible to replication stress, causing DNA damage and predisposes skin to carcinogenesis.

### 5.1 ILK promotes force generation and matrix assembly

During FA maturation, the connection between integrin ligands and the actin cytoskeleton is strengthened and myosin II-dependent actin stress fibers form, thus enabling cell contraction (Schiller and Fässler, 2013). FBs are specialized FAs that evolve from mature FAs and are bound to FN. Binding of integrins to FN and the

## Discussion

subsequent generation of tension via the actin cytoskeleton induces FN fibril formation (Pankov et al., 2000). We observed large FAs at the cell edges but absence of nascent FCs and FBs in ILK-deficient fibroblasts. This indicates that ILK is required for FA maturation. These observations are in line with previous studies where ILK was also implicated in the maturation of FBs (Stanchi et al., 2009). Here, the authors concluded that ILK together with its actin-binding partner  $\alpha$ -parvin, as part of the IPP complex, mediates the segregation of  $\alpha 5\beta 1$  integrins from FAs, thus allowing the recruitment of tensin and maturation of FBs (Stanchi et al., 2009). FB maturation is a prerequisite for subsequent FN fibrillogenesis. Although the expression of FN in ILK-deficient fibroblasts is unaltered compared to controls, FN fibrillogenesis is absent. Interestingly, it was recently shown that the recruitment of proteins to adhesion sites is dependent on myosin II activity (Schiller and Fässler, 2013). However, ILK recruitment to FA sites is upstream of myosin II activity (Schiller and Fässler, 2013), suggesting that ILK might be involved in myosin II-dependent recruitment of FA-associated proteins. The results of this thesis showing that ILK is required for the generation of traction forces, provides functional evidence for this notion. This inability to generate force probably affects further recruitment of FB-associated proteins and explains the observed failure in force-dependent ECM remodeling in ILK-deficient fibroblasts. Besides driving  $\alpha 5\beta 1$  integrin segregation along the actin cytoskeleton, ILK could additionally be involved in mediating force-dependent conformational changes in  $\alpha 5\beta 1$  integrins, which are required for fibrillogenesis (Clark et al., 2005).

Although  $\alpha 5\beta 1$  integrin is the primary FN receptor (Huveneers et al., 2008), integrin  $\alpha v\beta 3$  (Wennerberg et al., 1996),  $\alpha 4\beta 1$  (Sechler et al., 2000) and  $\alpha I\text{Ib}\beta 3$  (Olorundare et al., 2001) have been shown to be involved in FN fibrillogenesis *in vitro*. Knockout

studies in mice suggest overlapping as well as independent functions for  $\alpha 5$ - and  $\alpha v$ -class integrins in this process and only the double knockout of  $\alpha 5$ - and  $\alpha v$ - integrins in mice results in loss of fibrillogenesis (Yang et al., 1999). It is tempting to speculate that ILK, through its ability to bind both to  $\beta 1$ - and  $\beta 3$ -integrins, might be involved in their differential engagement and thereby tuning the forces required for FN fibrillogenesis.

Additionally, it has been proposed that the assembly state of FN fibers plays an important role in regulating cell behavior by acting as a checkpoint signal for subsequent ECM remodeling (Schwarzbauer and DeSimone, 2011). For instance, only the precise ratio of FN fibril assembly ensures epithelial branching morphogenesis during cleft formation (Sakai et al., 2003a). Furthermore, FN fibrillogenesis regulates fibrillin-1 microfibril assembly (Kinsey et al., 2008) and could thereby impact on growth factor bioavailability. Therefore it is becoming clear that the ECM-remodeling function of ILK is central to its role as an essential regulator of cell and tissue behavior. It will be of great interest to evaluate how force-induced fibril assembly driven by ILK impacts these processes and what is the role of ECM remodeling in the various phenotypes of ILK-deficient mice.

## **5.2 ILK is required for HFSC quiescence and maintenance**

The observation that ILK is required for cellular force generation and subsequent ECM remodeling raised the question of the functional implications of these processes *in vivo*. The adhesion of cells to the BM, a specialized form of ECM, plays an important role in regulating cell fate (Gattazzo et al., 2014). In many organs including the skin, the BM is an inherent part of the adult SC niche. Adult SCs are capable of long-term self-renewal and the generation of differentiating cells. In order to ensure

## Discussion

tissue homeostasis throughout the lifetime of an individual a stable pool of adult SCs needs to be maintained. Therefore, SC activation and quiescence needs to be precisely regulated in a spatial and temporal manner. Perturbations in this regulation can cause SC exhaustion or malignant transformation (Beck and Blanpain, 2013). Deletion of ILK in the ILK-K5 mice led to progressive hair loss, which was associated with the loss of CD34-positive HFSCs. The bulge HFSC niche is formed after HF morphogenesis, around P21 (Cotsarelis et al., 1990). At this time, ILK-K5 HFs contained some CD34-positive HFSCs, although the number was significantly reduced. While the bulge further develops during the next HF cycle and the number of CD34-positive cells increased in controls, ILK-K5 mice completely lost their CD34-positive bulge SCs, indicating that ILK is required for the establishment and maintenance of the bulge SC niche. This is further supported by the observation that the inducible deletion of ILK in adult ILK-iK14 animals also led to a reduction in bulge HFSCs.

Whether loss of HFSCs and alopecia also cause the observed regression of HFs is not entirely clear. Different forms of alopecia are described in humans and in most cases the HFs are destroyed by immune cell infiltrates. However in reversible cases of alopecia the HF remains intact (Sinclair et al., 2003). Interestingly, it has been reported that in human alopecia the arrector pili muscle plays an important role in the decision whether a HF persists or is destroyed (Torkamani et al., 2014). In this respect it is intriguing to note that bulge SCs within their niche create a muscle niche by expressing nephronectin, a specialized ECM protein that serves as an anchoring platform for tendon cell attachment of the arrector pili muscle (Fujiwara et al., 2011). As ILK is important for ECM remodeling, the loss of HFs in ILK-K5 and ILK-iK14 mice might be caused by the impairment of the bulge SC niche architecture. Analysis

of nephronectin deposition and arrector pili anchoring is therefore an interesting future experiment.

Aberrant loss of quiescence and subsequent activation in the long-term leads to SC exhaustion. HFSC fate is regulated by the SC-activating pathways Wnt and Tgf- $\beta$  and the quiescence-promoting BMP pathway. Lorenz and colleagues (Lorenz et al., 2007) showed that Wnt/ $\beta$ -catenin activity was unchanged in 2 week-old mice. Their analyses, using a Wnt reporter mouse model where  $\beta$ -galactosidase expression is controlled by nuclear  $\beta$ -catenin–Lef1, showed that hair shafts from both controls and ILK-K5 contained  $\beta$ -galactosidase label, indicative for an active Wnt pathway. As control and ILK-K5 mice were both in anagen by 2 weeks of age, detection of  $\beta$ -galactosidase label in both genotypes can be expected. They did not analyze the activity of the reporter in telogen. Furthermore, this particular Wnt reporter was shown to be rather insensitive compared to other reporters such as the Axin2 promoter-based Wnt reporter mouse model (Lien et al., 2014), and only very high Wnt activity as in mid-anagen can be detected. Using qRT-PCR analysis, which is a more sensitive method to detect alterations in Wnt target gene expression, we observed that Wnt and Tgf- $\beta$  target genes became gradually upregulated during morphogenetic anagen progression in ILK-deficient EPCs. Consistent with Lorenz et al., no difference was observed in early anagen at P7 whereas no differences became visible at p14. This upregulation became even more striking in the quiescent telogen phase, when Wnt and Tgf- $\beta$  pathways are normally downregulated and the BMP pathway is upregulated.

The overall gene expression signature of ILK-K5 EPCs resembled that of activated SCs, marked by high Wnt and Tgf- $\beta$  and low BMP activity. In line with the upregulation of the pro-proliferative Wnt and Tgf- $\beta$  pathways, an increased

proliferation rate in ILK-K5 was observed. Interestingly, the Wnt target genes that were observed to be highly upregulated are implicated in lineage progression within the HF. *Sox9*, *Tcf3* and *Lgr5* all regulate ORS differentiation (Jaks et al., 2008; Merrill et al., 2001; Vidal et al., 2005), whereas *Lef1* promotes generation of matrix cells (Zhang et al., 2013). These findings provide a molecular mechanism for the enhanced differentiation of ILK-deficient HFSC into matrix cells in the *Lgr5*-Cre model as well as for the observed enlargement of the ORS compartment in ILK-K5 mice (Lorenz et al., 2008 17485490). Besides its pro-proliferative properties, the Wnt/ $\beta$ -catenin pathway is also implicated in the inhibition of apoptosis (Chen et al., 2001). Therefore it is interesting to speculate that the ORS cells could be protected from apoptosis during catagen due to their high Wnt activity. This might explain why ILK-K5 HFs do not enter telogen at P21. It would be interesting to study this by analyzing the apoptosis rates of the ILK-deficient ORS cells in catagen. It would further be interesting to investigate the specific gene expression signature of the various SC populations to directly assess the status of the different HFSC lineages. However, isolating CD34-positive bulge SCs from P21 ILK-K5 mice is challenging because of their low abundance.

### **5.3 ILK-deficiency leads to loss of bulge SCs through enhanced differentiation**

The results of the thesis work suggested that ILK regulates SC activation and its deletion leads to SC exhaustion. However, an inducible deletion of ILK in K15-positive SCs has previously been published, and it showed no phenotype under homeostatic conditions (Nakrieko et al., 2011). The SC-specific deletion of ILK in *Lgr5*-positive HFSCs reported in this thesis also caused no macroscopic phenotype.

However, lineage-tracing analysis of ILK-deleted Lgr5-positive HFSCs revealed that ILK-deficient SCs more frequently differentiated to hair matrix and HG cells compared to controls. As a result, ILK-deficient SCs did not repopulate the bulge and only very few HFs contained ILK-Lgr5 progeny in the next hair cycle. The loss of actively cycling Lgr5-positive cells upon deletion of ILK was confirmed by the loss of EGFP-positive cells that reflects the undifferentiated pool of Lgr5-positive cells. Therefore a SC-specific phenotype was probably not observed in the ILK-K15 mice because the authors analyzed the mice only within the same HF cycle during which ILK-deletion was induced. In addition the deletion efficiency in their model was reported to be 50 %. As heterozygous ILK-K5, ILK-iK14 or ILK-K14 (Nakrieko et al., 2008) mice also show no phenotype, and the ILK-deficient SCs are lost to differentiation whereas the wild type cells persist, it is not surprising that no obvious difference between the ILK-K15 and control mice was detected.

Taken together, the results show that ILK regulates HFSC fate by coordinating the differentiation of HFSCs into ORS and hair matrix. Interestingly, Lgr5 was initially identified as a SC marker of cycling crypt base columnar cells, which represent a cycling SC population attached to the BM in the small intestine of mice (Barker et al., 2007). Until now, Lgr5 has been identified as a marker for a variety of epithelial SC including the ovary (Ng et al., 2014), the olfactory epithelium (Chen et al., 2014) and cochlea (Shi et al., 2013). Therefore it would be interesting to assess whether ILK has similar functions in SC fate regulation in other organs.

#### **5.4 ILK is required to establish and maintain the bulge SC niche**

LN-332 and LN-511 are integral components of the skin BM. Their relevance for skin development and physiology was already demonstrated in mouse knockout studies,

## Discussion

where the absence of LN-332 leads to severe skin blistering and the deletion of LN-511 results in severe HF morphogenesis defects (Bruckner-Tuderman and Has, 2012; Li et al., 2003). Both LNs are regulated during the HF cycle. LN-511 expression is high during anagen and decreases during catagen (Sugawara et al., 2007; Tateishi et al., 2010), whereas LN-332 levels decrease during anagen around the HF and remain stable throughout catagen (Sugawara et al., 2007; Tateishi et al., 2010). The findings of this thesis work show that LN-332 and LN-511 form inverse gradients in telogen HFs. LN-332 is more abundant beneath the IFE, whereas LN-511 shows higher expression around the HF bulb. In ILK-K5 skin this distribution was compromised. In ILK-K5 HFs LN-332 was less abundant around the distal HF whereas LN-511 expression was increased and expanded from the distal HF towards the K15-positive putative bulge compartment. The mechanism by which ILK regulates this inverse gradient is not clear. One possibility is that  $\alpha$ -dystroglycan that binds LN-511 but not LN-332 (Kikkawa et al., 2004) might be able to stabilize LN-511 in the BM. Dystroglycan is an adhesion receptor that also associates with the actin cytoskeleton, but does not require ILK for its function (Higginson and Winder, 2005), and hence could compensate the absence of functional  $\beta$ 1 integrins in ILK-deficient epidermis. Another possibility is that the LN-511 is derived from the DP fibroblasts that show expansion around the HFs of ILK-K5 skin. Interestingly, abnormal fibroblast attachment to a disrupted *lamina densa* of HFs was also observed in  $\alpha$ 3-integrin-deficient skin grafts (Conti et al., 2003), suggesting that fibroblast might also be involved in LN deposition to compensate for the loss of BM integrity around the HF. During telogen, the DP appears as a small cluster of cells attached to the HF tip in controls. However, AP-positive cells formed an enlarged capsule-like structure around the lower part of the ILK-deficient HF, coating the lateral lower surface of the

HF by forming a sheet. The severe abnormalities observed in the DP of ILK-K5 mice and to a lesser extent also in ILK-iK14 mice are secondary to the loss of ILK in the epidermis because ILK is not deleted in the DP that do not express K5 or K14. The enlarged DP in ILK-deficient epidermis could further be induced by increased interaction between DP cells and the increased LN-511-positive BM encompassing the HF.

## 5.5 Functional consequences of the altered niche

This thesis work shows that LN-332 inhibits Wnt signaling whereas LN-511 promotes Tgf- $\beta$  signaling *in vitro*. The predominant presence of LN-332 during catagen-telogen transition might therefore inhibit Wnt signaling and terminate hair growth. In addition, its high expression in the IFE might prevent these cells from acquiring a HF fate. The mechanism of how LN-332 inhibits Wnt is not clear. One option is that it regulates the bioavailability of Wnt antagonists, such as Dkk. Interestingly, the diffusion of secreted Dkk1 is involved in regulation of HF spacing (Sick et al., 2006). Another scenario is the involvement of syndecans. LN-332 interacts with syndecan-1 and syndecan-4 (Rousselle and Beck, 2013), HSPGs that bind Wnt and thereby regulate Wnt signaling (Astudillo et al., 2014; Liu et al., 2003).

How LN-511 regulates Tgf- $\beta$  signaling is also an interesting open question. Tgf- $\beta$  is secreted in a large latent complex that needs to be activated for Tgf- $\beta$  to bind its receptors. LN-511 contains a HSPG-binding domain that is known to interact with perlecan (Yu and Talts, 2003). Interestingly, perlecan can interact with fibrillin-1 (Tiedemann et al., 2005), which directly interacts with LTBP1 (Massam-Wu et al., 2010), thus providing a potential mechanism by which LN-511 could mediate Tgf- $\beta$  activation.

## **5.6 Aberrant SC activation causes replication stress and predisposition to skin carcinogenesis**

An imbalance between SC quiescence and activation can lead to the generation of tumor-initiating cells (Beck and Blanpain, 2013). SC quiescence has been proposed to act as a tumor suppressing mechanism in hematopoietic SCs (Bakker and Passegue, 2013). Loss of cell cycle regulator p21 in hematopoietic SCs leads to increased proliferation and SC exhaustion with the accumulation of DNA damage due to replication stress (Cheng et al., 2000). Furthermore quiescent bulge SCs respond to DNA damage by increasing levels of the anti-apoptotic gene Bcl-2 and a faster DNA repair machinery (Sotiropoulou et al., 2010). In line with these observations and in agreement with the loss of HFSC quiescence, the amount of DNA damage within ILK-K5 skin was significantly increased already in P21 HFs.

8-week old ILK-K5 mice, despite having lost most of the HFs, still showed elevated Wnt/ $\beta$ -catenin pathway activity accompanied by a hyperproliferative epidermis. Again, increased DNA damage was observed. When subjected to a two-stage carcinogenesis experiment ILK-K5 mice showed higher tumor incidence and tumor multiplicity. As no difference in tumor size, proliferation, or apoptosis was observed, we hypothesize that the increased replicative stress and DNA damage predisposes ILK-deficient skin to malignant transformation, whereas later on the tumor cells do not benefit from the absence of ILK expression.

However, due to skin health conditions of ILK-K5 mice, investigating tumor progression and malignant conversion was not possible. Using a genetic cancer mouse model in combination with an inducible deletion of ILK would be the best way to continue these studies in the future. This would not only circumvent the skin health problems generated by deletion of ILK during embryogenesis, but the genetic tumor

model would also prevent additional induction of oxidative and replicative stress that is caused by DMBA and TPA (DiGiovanni, 1992). The conditional expression of oncogenic mutant KRas (such as lox-STOP-lox KRas G12D) in an inducible ILK-deficient epidermis would provide such a model (O'Hagan and Heyer, 2011). The SC-specific Lgr5 mouse model in combination with the keratinocyte-specific expression of oncogenic KRas would serve as an excellent model to study HFSC tumor development and the impact of ILK as a potential tumor suppressor by balancing SC differentiation and maintenance.

To conclude, the thesis work has identified mechanisms by which ILK regulates ECM remodeling and the BM niche and how the composition of this niche feeds back on cellular behavior. Together with other work in the field it highlights the role of tissue architecture in coordinating cellular behaviors and protecting it from malignant transformation. Future work should be aimed at precise molecular characterization of the ECM of the various SC niches, for example, by mass-spectrometry. Furthermore, investigating the topography and stiffness of the various ECM niches would generate important insights into the molecular mechanisms of SC-niche interactions.

## References

Abel, E.L., Angel, J.M., Kiguchi, K., and DiGiovanni, J. (2009). Multi-stage chemical carcinogenesis in mouse skin: fundamentals and applications. *Nature protocols* *4*, 1350-1362.

Astudillo, P., Carrasco, H., and Larrain, J. (2014). Syndecan-4 inhibits Wnt/beta-catenin signaling through regulation of low-density-lipoprotein receptor-related protein (LRP6) and R-spondin 3. *The international journal of biochemistry & cell biology* *46*, 103-112.

Aumailley, M. (2013). The laminin family. *Cell adhesion & migration* *7*, 48-55.

Aumailley, M., Bruckner-Tuderman, L., Carter, W.G., Deutzmann, R., Edgar, D., Ekblom, P., Engel, J., Engvall, E., Hohenester, E., Jones, J.C., *et al.* (2005). A simplified laminin nomenclature. *Matrix biology : journal of the International Society for Matrix Biology* *24*, 326-332.

Aumailley, M., and Gayraud, B. (1998). Structure and biological activity of the extracellular matrix. *Journal of molecular medicine* *76*, 253-265.

Bakker, S.T., and Passegue, E. (2013). Resilient and resourceful: genome maintenance strategies in hematopoietic stem cells. *Experimental hematology* *41*, 915-923.

Baneyx, G., Baugh, L., and Vogel, V. (2002). Fibronectin extension and unfolding within cell matrix fibrils controlled by cytoskeletal tension. *Proc Natl Acad Sci U S A* *99*, 5139-5143.

Barker, N., van Es, J.H., Kuipers, J., Kujala, P., van den Born, M., Cozijnsen, M., Haegbarth, A., Korving, J., Begthel, H., Peters, P.J., *et al.* (2007). Identification of stem cells in small intestine and colon by marker gene *Lgr5*. *Nature* *449*, 1003-1007.

Baudoin, C., Fantin, L., and Meneguzzi, G. (2005). Proteolytic processing of the laminin alpha3 G domain mediates assembly of hemidesmosomes but has no role on keratinocyte migration. *J Invest Dermatol* *125*, 883-888.

Beck, B., and Blanpain, C. (2013). Unravelling cancer stem cell potential. *Nature reviews Cancer* *13*, 727-738.

Behrens, D.T., Villone, D., Koch, M., Brunner, G., Sorokin, L., Robenek, H., Bruckner-Tuderman, L., Bruckner, P., and Hansen, U. (2012). The epidermal basement membrane is a composite of separate laminin- or collagen IV-containing networks connected by aggregated perlecan, but not by nidogens. *J Biol Chem* *287*, 18700-18709.

Belvindrah, R., Nalbant, P., Ding, S., Wu, C., Bokoch, G.M., and Muller, U. (2006). Integrin-linked kinase regulates Bergmann glial differentiation during cerebellar development. *Molecular and cellular neurosciences* *33*, 109-125.

- Blanpain, C., and Fuchs, E. (2006). Epidermal stem cells of the skin. *Annual review of cell and developmental biology* 22, 339-373.
- Blumbach, K., Zweers, M.C., Brunner, G., Peters, A.S., Schmitz, M., Schulz, J.N., Schild, A., Denton, C.P., Sakai, T., Fassler, R., *et al.* (2010). Defective granulation tissue formation in mice with specific ablation of integrin-linked kinase in fibroblasts - role of TGFbeta1 levels and RhoA activity. *Journal of cell science* 123, 3872-3883.
- Botchkarev, V.A., Botchkareva, N.V., Nakamura, M., Huber, O., Funa, K., Lauster, R., Paus, R., and Gilchrist, B.A. (2001). Noggin is required for induction of the hair follicle growth phase in postnatal skin. *FASEB journal : official publication of the Federation of American Societies for Experimental Biology* 15, 2205-2214.
- Botchkarev, V.A., and Paus, R. (2003). Molecular biology of hair morphogenesis: development and cycling. *Journal of experimental zoology Part B, Molecular and developmental evolution* 298, 164-180.
- Boudeau, J., Miranda-Saavedra, D., Barton, G.J., and Alessi, D.R. (2006). Emerging roles of pseudokinases. *Trends Cell Biol* 16, 443-452.
- Bouvard, D., Pouwels, J., De Franceschi, N., and Ivaska, J. (2013). Integrin inactivators: balancing cellular functions in vitro and in vivo. *Nature reviews Molecular cell biology* 14, 430-442.
- Breitkreutz, D., Koxholt, I., Thiemann, K., and Nischt, R. (2013). Skin basement membrane: the foundation of epidermal integrity--BM functions and diverse roles of bridging molecules nidogen and perlecan. *BioMed research international* 2013, 179784.
- Bruckner, P. (2010). Suprastructures of extracellular matrices: paradigms of functions controlled by aggregates rather than molecules. *Cell and tissue research* 339, 7-18.
- Bruckner-Tuderman, L., and Has, C. (2012). Molecular heterogeneity of blistering disorders: the paradigm of epidermolysis bullosa. *J Invest Dermatol* 132, E2-5.
- Bulow, H.E., and Hobert, O. (2006). The molecular diversity of glycosaminoglycans shapes animal development. *Annual review of cell and developmental biology* 22, 375-407.
- Campbell, I.D., and Humphries, M.J. (2011). Integrin structure, activation, and interactions. *Cold Spring Harb Perspect Biol* 3.
- Chen, M., Tian, S., Yang, X., Lane, A.P., Reed, R.R., and Liu, H. (2014). Wnt-responsive Lgr5(+) globose basal cells function as multipotent olfactory epithelium progenitor cells. *The Journal of neuroscience : the official journal of the Society for Neuroscience* 34, 8268-8276.
- Chen, S., Guttridge, D.C., You, Z., Zhang, Z., Fribley, A., Mayo, M.W., Kitajewski, J., and Wang, C.Y. (2001). Wnt-1 signaling inhibits apoptosis by activating beta-catenin/T cell factor-mediated transcription. *J Cell Biol* 152, 87-96.

## References

- Cheng, T., Rodrigues, N., Shen, H., Yang, Y., Dombkowski, D., Sykes, M., and Scadden, D.T. (2000). Hematopoietic stem cell quiescence maintained by p21<sup>cip1</sup>/waf1. *Science* 287, 1804-1808.
- Chiswell, B.P., Zhang, R., Murphy, J.W., Boggon, T.J., and Calderwood, D.A. (2008). The structural basis of integrin-linked kinase-PINCH interactions. *Proc Natl Acad Sci U S A* 105, 20677-20682.
- Choi, Y.S., Zhang, Y., Xu, M., Yang, Y., Ito, M., Peng, T., Cui, Z., Nagy, A., Hadjantonakis, A.K., Lang, R.A., *et al.* (2013). Distinct functions for Wnt/beta-catenin in hair follicle stem cell proliferation and survival and interfollicular epidermal homeostasis. *Cell stem cell* 13, 720-733.
- Clark, K., Pankov, R., Travis, M.A., Askari, J.A., Mould, A.P., Craig, S.E., Newham, P., Yamada, K.M., and Humphries, M.J. (2005). A specific alpha5beta1-integrin conformation promotes directional integrin translocation and fibronectin matrix formation. *Journal of cell science* 118, 291-300.
- Clayton, E., Doupe, D.P., Klein, A.M., Winton, D.J., Simons, B.D., and Jones, P.H. (2007). A single type of progenitor cell maintains normal epidermis. *Nature* 446, 185-189.
- Clevers, H., and Nusse, R. (2012). Wnt/beta-catenin signaling and disease. *Cell* 149, 1192-1205.
- Colognato, H., Winkelmann, D.A., and Yurchenco, P.D. (1999). Laminin polymerization induces a receptor-cytoskeleton network. *J Cell Biol* 145, 619-631.
- Conti, F.J., Rudling, R.J., Robson, A., and Hodivala-Dilke, K.M. (2003). alpha3beta1-integrin regulates hair follicle but not interfollicular morphogenesis in adult epidermis. *Journal of cell science* 116, 2737-2747.
- Cotsarelis, G., Sun, T.T., and Lavker, R.M. (1990). Label-retaining cells reside in the bulge area of pilosebaceous unit: implications for follicular stem cells, hair cycle, and skin carcinogenesis. *Cell* 61, 1329-1337.
- Daley, W.P., and Yamada, K.M. (2013). ECM-modulated cellular dynamics as a driving force for tissue morphogenesis. *Current opinion in genetics & development* 23, 408-414.
- DeRouen, M.C., Zhen, H., Tan, S.H., Williams, S., Marinkovich, M.P., and Oro, A.E. (2010). Laminin-511 and integrin beta-1 in hair follicle development and basal cell carcinoma formation. *BMC developmental biology* 10, 112.
- Deschene, E.R., Myung, P., Rompolas, P., Zito, G., Sun, T.Y., Taketo, M.M., Saotome, I., and Greco, V. (2014). beta-Catenin activation regulates tissue growth non-cell autonomously in the hair stem cell niche. *Science* 343, 1353-1356.
- DiGiovanni, J. (1992). Multistage carcinogenesis in mouse skin. *Pharmacology & therapeutics* 54, 63-128.

- Dong, C., Zhu, S., Wang, T., Yoon, W., and Goldschmidt-Clermont, P.J. (2002). Upregulation of PAI-1 is mediated through TGF-beta/Smad pathway in transplant arteriopathy. *J Heart Lung Transplant* *21*, 999-1008.
- Driskell, R.R., Clavel, C., Rendl, M., and Watt, F.M. (2011). Hair follicle dermal papilla cells at a glance. *Journal of cell science* *124*, 1179-1182.
- Eckes, B., and Krieg, T. (2004). Regulation of connective tissue homeostasis in the skin by mechanical forces. *Clinical and experimental rheumatology* *22*, S73-76.
- El-Aouni, C., Herbach, N., Blattner, S.M., Henger, A., Rastaldi, M.P., Jarad, G., Miner, J.H., Moeller, M.J., St-Arnaud, R., Dedhar, S., *et al.* (2006). Podocyte-specific deletion of integrin-linked kinase results in severe glomerular basement membrane alterations and progressive glomerulosclerosis. *Journal of the American Society of Nephrology : JASN* *17*, 1334-1344.
- Elias, J., Dimitrio, L., Clairambault, J., and Natalini, R. (2014). The p53 protein and its molecular network: modelling a missing link between DNA damage and cell fate. *Biochim Biophys Acta* *1844*, 232-247.
- Esko, J.D., Kimata, K., and Lindahl, U. (2009). Proteoglycans and Sulfated Glycosaminoglycans. In *Essentials of Glycobiology*, A. Varki, R.D. Cummings, J.D. Esko, H.H. Freeze, P. Stanley, C.R. Bertozzi, G.W. Hart, and M.E. Etzler, eds. (Cold Spring Harbor (NY)).
- Fan, G., Xiao, L., Cheng, L., Wang, X., Sun, B., and Hu, G. (2000). Targeted disruption of NDST-1 gene leads to pulmonary hypoplasia and neonatal respiratory distress in mice. *FEBS Lett* *467*, 7-11.
- Fässler, R., Pfaff, M., Murphy, J., Noegel, A.A., Johansson, S., Timpl, R., and Albrecht, R. (1995). Lack of beta 1 integrin gene in embryonic stem cells affects morphology, adhesion, and migration but not integration into the inner cell mass of blastocysts. *J Cell Biol* *128*, 979-988.
- Fico, A., Maina, F., and Dono, R. (2011). Fine-tuning of cell signaling by glypicans. *Cell Mol Life Sci* *68*, 923-929.
- Foitzik, K., Lindner, G., Mueller-Roever, S., Maurer, M., Botchkareva, N., Botchkarev, V., Handjiski, B., Metz, M., Hibino, T., Soma, T., *et al.* (2000). Control of murine hair follicle regression (catagen) by TGF-beta1 in vivo. *FASEB journal : official publication of the Federation of American Societies for Experimental Biology* *14*, 752-760.
- Frank, D.E., and Carter, W.G. (2004). Laminin 5 deposition regulates keratinocyte polarization and persistent migration. *Journal of cell science* *117*, 1351-1363.
- Frantz, C., Stewart, K.M., and Weaver, V.M. (2010). The extracellular matrix at a glance. *Journal of cell science* *123*, 4195-4200.
- Friedrich, E.B., Liu, E., Sinha, S., Cook, S., Milstone, D.S., MacRae, C.A., Mariotti, M., Kuhlencordt, P.J., Force, T., Rosenzweig, A., *et al.* (2004). Integrin-linked kinase

## References

regulates endothelial cell survival and vascular development. *Molecular and cellular biology* 24, 8134-8144.

Fujiwara, H., Ferreira, M., Donati, G., Marciano, D.K., Linton, J.M., Sato, Y., Hartner, A., Sekiguchi, K., Reichardt, L.F., and Watt, F.M. (2011). The basement membrane of hair follicle stem cells is a muscle cell niche. *Cell* 144, 577-589.

Fukuda, K., Gupta, S., Chen, K., Wu, C., and Qin, J. (2009). The pseudoactive site of ILK is essential for its binding to alpha-Parvin and localization to focal adhesions. *Mol Cell* 36, 819-830.

Gao, J., DeRouen, M.C., Chen, C.H., Nguyen, M., Nguyen, N.T., Ido, H., Harada, K., Sekiguchi, K., Morgan, B.A., Miner, J.H., *et al.* (2008). Laminin-511 is an epithelial message promoting dermal papilla development and function during early hair morphogenesis. *Genes Dev* 22, 2111-2124.

Gat, U., DasGupta, R., Degenstein, L., and Fuchs, E. (1998). De Novo hair follicle morphogenesis and hair tumors in mice expressing a truncated beta-catenin in skin. *Cell* 95, 605-614.

Gattazzo, F., Urciuolo, A., and Bonaldo, P. (2014). Extracellular matrix: a dynamic microenvironment for stem cell niche. *Biochim Biophys Acta* 1840, 2506-2519.

George, E.L., Georges-Labouesse, E.N., Patel-King, R.S., Rayburn, H., and Hynes, R.O. (1993). Defects in mesoderm, neural tube and vascular development in mouse embryos lacking fibronectin. *Development* 119, 1079-1091.

Georges-Labouesse, E., Messaddeq, N., Yehia, G., Cadalbert, L., Dierich, A., and Le Meur, M. (1996a). Absence of integrin alpha 6 leads to epidermolysis bullosa and neonatal death in mice. *Nat Genet* 13, 370-373.

Georges-Labouesse, E.N., George, E.L., Rayburn, H., and Hynes, R.O. (1996b). Mesodermal development in mouse embryos mutant for fibronectin. *Dev Dyn* 207, 145-156.

Ghatak, S., Morgner, J., and Wickström, S.A. (2013). ILK: a pseudokinase with a unique function in the integrin-actin linkage. *Biochem Soc Trans* 41, 995-1001.

Gheyara, A.L., Vallejo-Illarramendi, A., Zang, K., Mei, L., St-Arnaud, R., Dedhar, S., and Reichardt, L.F. (2007). Deletion of integrin-linked kinase from skeletal muscles of mice resembles muscular dystrophy due to alpha 7 beta 1-integrin deficiency. *The American journal of pathology* 171, 1966-1977.

Gkretsi, V., Mars, W.M., Bowen, W.C., Barua, L., Yang, Y., Guo, L., St-Arnaud, R., Dedhar, S., Wu, C., and Michalopoulos, G.K. (2007). Loss of integrin linked kinase from mouse hepatocytes in vitro and in vivo results in apoptosis and hepatitis. *Hepatology* 45, 1025-1034.

Gordon, M.K., and Hahn, R.A. (2010). Collagens. *Cell and tissue research* 339, 247-257.

- Gorska, M., Popowska, U., Sielicka-Dudzin, A., Kuban-Jankowska, A., Sawczuk, W., Knap, N., Cicero, G., and Wozniak, F. (2012). Geldanamycin and its derivatives as Hsp90 inhibitors. *Frontiers in bioscience* *17*, 2269-2277.
- Grashoff, C., Aszodi, A., Sakai, T., Hunziker, E.B., and Fässler, R. (2003). Integrin-linked kinase regulates chondrocyte shape and proliferation. *EMBO reports* *4*, 432-438.
- Greco, V., Chen, T., Rendl, M., Schober, M., Pasolli, H.A., Stokes, N., Dela Cruz-Racelis, J., and Fuchs, E. (2009). A two-step mechanism for stem cell activation during hair regeneration. *Cell stem cell* *4*, 155-169.
- Hannigan, G.E., Leung-Hagesteijn, C., Fitz-Gibbon, L., Coppelino, M.G., Radeva, G., Filmus, J., Bell, J.C., and Dedhar, S. (1996). Regulation of cell adhesion and anchorage-dependent growth by a new beta 1-integrin-linked protein kinase. *Nature* *379*, 91-96.
- Harburger, D.S., and Calderwood, D.A. (2009). Integrin signalling at a glance. *Journal of cell science* *122*, 159-163.
- Higginson, J.R., and Winder, S.J. (2005). Dystroglycan: a multifunctional adaptor protein. *Biochem Soc Trans* *33*, 1254-1255.
- Hinz, B. (2007). Formation and function of the myofibroblast during tissue repair. *J Invest Dermatol* *127*, 526-537.
- Hohenester, E., and Yurchenco, P.D. (2013). Laminins in basement membrane assembly. *Cell adhesion & migration* *7*, 56-63.
- Horsley, V., Aliprantis, A.O., Polak, L., Glimcher, L.H., and Fuchs, E. (2008). NFATc1 balances quiescence and proliferation of skin stem cells. *Cell* *132*, 299-310.
- Hsu, Y.C., and Fuchs, E. (2012). A family business: stem cell progeny join the niche to regulate homeostasis. *Nature reviews Molecular cell biology* *13*, 103-114.
- Hsu, Y.C., Li, L., and Fuchs, E. (2014). Transit-amplifying cells orchestrate stem cell activity and tissue regeneration. *Cell* *157*, 935-949.
- Hsu, Y.C., Pasolli, H.A., and Fuchs, E. (2011). Dynamics between stem cells, niche, and progeny in the hair follicle. *Cell* *144*, 92-105.
- Huelsken, J., Vogel, R., Erdmann, B., Cotsarelis, G., and Birchmeier, W. (2001). beta-Catenin controls hair follicle morphogenesis and stem cell differentiation in the skin. *Cell* *105*, 533-545.
- Huet-Calderwood, C., Brahme, N.N., Kumar, N., Stiegler, A.L., Raghavan, S., Boggon, T.J., and Calderwood, D.A. (2014). Differential binding to the ILK complex determines kindlin isoform adhesion localization and integrin activation. *Journal of cell science*.
- Humphries, J.D., Byron, A., and Humphries, M.J. (2006). Integrin ligands at a glance. *Journal of cell science* *119*, 3901-3903.

## References

- Huveneers, S., Truong, H., Fassler, R., Sonnenberg, A., and Danen, E.H. (2008). Binding of soluble fibronectin to integrin alpha5 beta1 - link to focal adhesion redistribution and contractile shape. *Journal of cell science* *121*, 2452-2462.
- Hynes, R.O. (2002). Integrins: bidirectional, allosteric signaling machines. *Cell* *110*, 673-687.
- Imanishi, H., Tsuruta, D., Tateishi, C., Sugawara, K., Kobayashi, H., Ishii, M., and Kishi, K. (2014). Spatial and temporal control of laminin-332 and -511 expressions during hair morphogenesis. *Medical molecular morphology* *47*, 38-42.
- Ito, S., Takahara, Y., Hyodo, T., Hasegawa, H., Asano, E., Hamaguchi, M., and Senga, T. (2010). The roles of two distinct regions of PINCH-1 in the regulation of cell attachment and spreading. *Molecular biology of the cell* *21*, 4120-4129.
- Ivanova, N.B., Dimos, J.T., Schaniel, C., Hackney, J.A., Moore, K.A., and Lemischka, I.R. (2002). A stem cell molecular signature. *Science* *298*, 601-604.
- Jaks, V., Barker, N., Kasper, M., van Es, J.H., Snippert, H.J., Clevers, H., and Toftgard, R. (2008). Lgr5 marks cycling, yet long-lived, hair follicle stem cells. *Nat Genet* *40*, 1291-1299.
- Jones, P., and Simons, B.D. (2008). Epidermal homeostasis: do committed progenitors work while stem cells sleep? *Nature reviews Molecular cell biology* *9*, 82-88.
- Jones, P.H., Simons, B.D., and Watt, F.M. (2007). Sic transit gloria: farewell to the epidermal transit amplifying cell? *Cell stem cell* *1*, 371-381.
- Judah, D., Rudkouskaya, A., Wilson, R., Carter, D.E., and Dagnino, L. (2012). Multiple roles of integrin-linked kinase in epidermal development, maturation and pigmentation revealed by molecular profiling. *PLoS One* *7*, e36704.
- Kadler, K.E., Baldock, C., Bella, J., and Boot-Handford, R.P. (2007). Collagens at a glance. *Journal of cell science* *120*, 1955-1958.
- Kandyba, E., Leung, Y., Chen, Y.B., Widelitz, R., Chuong, C.M., and Kobiela, K. (2013). Competitive balance of intrabulge BMP/Wnt signaling reveals a robust gene network ruling stem cell homeostasis and cyclic activation. *Proc Natl Acad Sci U S A* *110*, 1351-1356.
- Kerever, A., Schnack, J., Vellinga, D., Ichikawa, N., Moon, C., Arikawa-Hirasawa, E., Efir, J.T., and Mercier, F. (2007). Novel extracellular matrix structures in the neural stem cell niche capture the neurogenic factor fibroblast growth factor 2 from the extracellular milieu. *Stem cells* *25*, 2146-2157.
- Kikkawa, Y., Yu, H., Genersch, E., Sanzen, N., Sekiguchi, K., Fassler, R., Campbell, K.P., Talts, J.F., and Ekblom, P. (2004). Laminin isoforms differentially regulate adhesion, spreading, proliferation, and ERK activation of beta1 integrin-null cells. *Experimental cell research* *300*, 94-108.

- Kinsey, R., Williamson, M.R., Chaudhry, S., Mellody, K.T., McGovern, A., Takahashi, S., Shuttleworth, C.A., and Kielty, C.M. (2008). Fibrillin-1 microfibril deposition is dependent on fibronectin assembly. *Journal of cell science* *121*, 2696-2704.
- Kobielak, K., Stokes, N., de la Cruz, J., Polak, L., and Fuchs, E. (2007). Loss of a quiescent niche but not follicle stem cells in the absence of bone morphogenetic protein signaling. *Proc Natl Acad Sci U S A* *104*, 10063-10068.
- Krieg, T., and Aumailley, M. (2011). The extracellular matrix of the dermis: flexible structures with dynamic functions. *Experimental dermatology* *20*, 689-695.
- Lange, A., Wickström, S.A., Jakobson, M., Zent, R., Sainio, K., and Fässler, R. (2009). Integrin-linked kinase is an adaptor with essential functions during mouse development. *Nature* *461*, 1002-1006.
- Larsen, M., Artym, V.V., Green, J.A., and Yamada, K.M. (2006). The matrix reorganized: extracellular matrix remodeling and integrin signaling. *Current opinion in cell biology* *18*, 463-471.
- Larson, R.S., Corbi, A.L., Berman, L., and Springer, T. (1989). Primary structure of the leukocyte function-associated molecule-1 alpha subunit: an integrin with an embedded domain defining a protein superfamily. *J Cell Biol* *108*, 703-712.
- LeBleu, V.S., Macdonald, B., and Kalluri, R. (2007). Structure and function of basement membranes. *Experimental biology and medicine* *232*, 1121-1129.
- Lechler, T., and Fuchs, E. (2005). Asymmetric cell divisions promote stratification and differentiation of mammalian skin. *Nature* *437*, 275-280.
- Legate, K.R., Wickström, S.A., and Fässler, R. (2009). Genetic and cell biological analysis of integrin outside-in signaling. *Genes Dev* *23*, 397-418.
- Li, J., Tzu, J., Chen, Y., Zhang, Y.P., Nguyen, N.T., Gao, J., Bradley, M., Keene, D.R., Oro, A.E., Miner, J.H., *et al.* (2003). Laminin-10 is crucial for hair morphogenesis. *EMBO J* *22*, 2400-2410.
- Lien, W.H., Polak, L., Lin, M., Lay, K., Zheng, D., and Fuchs, E. (2014). In vivo transcriptional governance of hair follicle stem cells by canonical Wnt regulators. *Nature cell biology* *16*, 179-190.
- Lin, X., Wei, G., Shi, Z., Dryer, L., Esko, J.D., Wells, D.E., and Matzuk, M.M. (2000). Disruption of gastrulation and heparan sulfate biosynthesis in EXT1-deficient mice. *Developmental biology* *224*, 299-311.
- Liu, B.Y., Kim, Y.C., Leatherberry, V., Cowin, P., and Alexander, C.M. (2003). Mammary gland development requires syndecan-1 to create a beta-catenin/TCF-responsive mammary epithelial subpopulation. *Oncogene* *22*, 9243-9253.
- Liu, E., Sinha, S., Williams, C., Cyrille, M., Heller, E., Snapper, S.B., Georgopoulos, K., St-Arnaud, R., Force, T., Dedhar, S., *et al.* (2005). Targeted deletion of integrin-

## References

linked kinase reveals a role in T-cell chemotaxis and survival. *Molecular and cellular biology* 25, 11145-11155.

Lorenz, K., Grashoff, C., Torka, R., Sakai, T., Langbein, L., Bloch, W., Aumailley, M., and Fässler, R. (2007). Integrin-linked kinase is required for epidermal and hair follicle morphogenesis. *J Cell Biol* 177, 501-513.

Lowry, W.E., Blanpain, C., Nowak, J.A., Guasch, G., Lewis, L., and Fuchs, E. (2005). Defining the impact of beta-catenin/Tcf transactivation on epithelial stem cells. *Genes Dev* 19, 1596-1611.

Lukas, J., Lukas, C., and Bartek, J. (2011). More than just a focus: The chromatin response to DNA damage and its role in genome integrity maintenance. *Nature cell biology* 13, 1161-1169.

Mackinnon, A.C., Qadota, H., Norman, K.R., Moerman, D.G., and Williams, B.D. (2002). *C. elegans* PAT-4/ILK functions as an adaptor protein within integrin adhesion complexes. *Current biology : CB* 12, 787-797.

Mak, K.K., and Chan, S.Y. (2003). Epidermal growth factor as a biologic switch in hair growth cycle. *J Biol Chem* 278, 26120-26126.

Margadant, C., Monsuur, H.N., Norman, J.C., and Sonnenberg, A. (2011). Mechanisms of integrin activation and trafficking. *Current opinion in cell biology* 23, 607-614.

Marinkovich, M.P., Keene, D.R., Rimberg, C.S., and Burgeson, R.E. (1993). Cellular origin of the dermal-epidermal basement membrane. *Dev Dyn* 197, 255-267.

Massam-Wu, T., Chiu, M., Choudhury, R., Chaudhry, S.S., Baldwin, A.K., McGovern, A., Baldock, C., Shuttleworth, C.A., and Kielty, C.M. (2010). Assembly of fibrillin microfibrils governs extracellular deposition of latent TGF beta. *Journal of cell science* 123, 3006-3018.

McKee, K.K., Capizzi, S., and Yurchenco, P.D. (2009). Scaffold-forming and Adhesive Contributions of Synthetic Laminin-binding Proteins to Basement Membrane Assembly. *J Biol Chem* 284, 8984-8994.

McMillan, J.R., Akiyama, M., and Shimizu, H. (2003). Epidermal basement membrane zone components: ultrastructural distribution and molecular interactions. *J Dermatol Sci* 31, 169-177.

McQuade, K.J., Beauvais, D.M., Burbach, B.J., and Rapraeger, A.C. (2006). Syndecan-1 regulates alpha5beta1 integrin activity in B82L fibroblasts. *Journal of cell science* 119, 2445-2456.

Merrill, B.J., Gat, U., DasGupta, R., and Fuchs, E. (2001). Tcf3 and Lef1 regulate lineage differentiation of multipotent stem cells in skin. *Genes Dev* 15, 1688-1705.

Millar, S.E. (2002). Molecular mechanisms regulating hair follicle development. *J Invest Dermatol* 118, 216-225.

- Mills, J., Niewmierzycka, A., Oloumi, A., Rico, B., St-Arnaud, R., Mackenzie, I.R., Mawji, N.M., Wilson, J., Reichardt, L.F., and Dedhar, S. (2006). Critical role of integrin-linked kinase in granule cell precursor proliferation and cerebellar development. *The Journal of neuroscience : the official journal of the Society for Neuroscience* 26, 830-840.
- Miner, J.H., Cunningham, J., and Sanes, J.R. (1998). Roles for laminin in embryogenesis: exencephaly, syndactyly, and placentopathy in mice lacking the laminin alpha5 chain. *J Cell Biol* 143, 1713-1723.
- Mokkapatil, S., Baranowsky, A., Mirancea, N., Smyth, N., Breitkreutz, D., and Nischt, R. (2008). Basement membranes in skin are differently affected by lack of nidogen 1 and 2. *J Invest Dermatol* 128, 2259-2267.
- Moll, R., Franke, W.W., Schiller, D.L., Geiger, B., and Krepler, R. (1982). The catalog of human cytokeratins: patterns of expression in normal epithelia, tumors and cultured cells. *Cell* 31, 11-24.
- Montanez, E., Wickström, S.A., Altstatter, J., Chu, H., and Fässler, R. (2009). Alpha-parvin controls vascular mural cell recruitment to vessel wall by regulating RhoA/ROCK signalling. *EMBO J* 28, 3132-3144.
- Morris, R.J., Liu, Y., Marles, L., Yang, Z., Trempus, C., Li, S., Lin, J.S., Sawicki, J.A., and Cotsarelis, G. (2004). Capturing and profiling adult hair follicle stem cells. *Nature biotechnology* 22, 411-417.
- Morse, E.M., Brahme, N.N., and Calderwood, D.A. (2014). Integrin cytoplasmic tail interactions. *Biochemistry* 53, 810-820.
- Muller-Rover, S., Tokura, Y., Welker, P., Furukawa, F., Wakita, H., Takigawa, M., and Paus, R. (1999). E- and P-cadherin expression during murine hair follicle morphogenesis and cycling. *Experimental dermatology* 8, 237-246.
- Munger, J.S., Harpel, J.G., Giancotti, F.G., and Rifkin, D.B. (1998). Interactions between growth factors and integrins: latent forms of transforming growth factor-beta are ligands for the integrin alphavbeta1. *Molecular biology of the cell* 9, 2627-2638.
- Murga, M., Bunting, S., Montana, M.F., Soria, R., Mulero, F., Canamero, M., Lee, Y., McKinnon, P.J., Nussenzweig, A., and Fernandez-Capetillo, O. (2009). A mouse model of ATR-Seckel shows embryonic replicative stress and accelerated aging. *Nat Genet* 41, 891-898.
- Murillas, R., Larcher, F., Conti, C.J., Santos, M., Ullrich, A., and Jorcano, J.L. (1995). Expression of a dominant negative mutant of epidermal growth factor receptor in the epidermis of transgenic mice elicits striking alterations in hair follicle development and skin structure. *EMBO J* 14, 5216-5223.
- Murray, P., and Edgar, D. (2000). Regulation of programmed cell death by basement membranes in embryonic development. *J Cell Biol* 150, 1215-1221.

## References

- Naba, A., Clauser, K.R., Hoersch, S., Liu, H., Carr, S.A., and Hynes, R.O. (2012). The matrisome: in silico definition and in vivo characterization by proteomics of normal and tumor extracellular matrices. *Mol Cell Proteomics* *11*, M111 014647.
- Nakrieko, K.A., Rudkouskaya, A., Irvine, T.S., D'Souza, S.J., and Dagnino, L. (2011). Targeted inactivation of integrin-linked kinase in hair follicle stem cells reveals an important modulatory role in skin repair after injury. *Molecular biology of the cell* *22*, 2532-2540.
- Nakrieko, K.A., Welch, I., Dupuis, H., Bryce, D., Pajak, A., St Arnaud, R., Dedhar, S., D'Souza, S.J., and Dagnino, L. (2008). Impaired hair follicle morphogenesis and polarized keratinocyte movement upon conditional inactivation of integrin-linked kinase in the epidermis. *Molecular biology of the cell* *19*, 1462-1473.
- Ng, A., Tan, S., Singh, G., Rizk, P., Swathi, Y., Tan, T.Z., Huang, R.Y., Leushacke, M., and Barker, N. (2014). *Lgr5* marks stem/progenitor cells in ovary and tubal epithelia. *Nature cell biology* *16*, 745-757.
- Nguyen, H., Rendl, M., and Fuchs, E. (2006). *Tcf3* governs stem cell features and represses cell fate determination in skin. *Cell* *127*, 171-183.
- Niewmierzycka, A., Mills, J., St-Arnaud, R., Dedhar, S., and Reichardt, L.F. (2005). Integrin-linked kinase deletion from mouse cortex results in cortical lamination defects resembling cobblestone lissencephaly. *The Journal of neuroscience : the official journal of the Society for Neuroscience* *25*, 7022-7031.
- Nikolopoulos, S.N., and Turner, C.E. (2000). Actopaxin, a new focal adhesion protein that binds paxillin LD motifs and actin and regulates cell adhesion. *J Cell Biol* *151*, 1435-1448.
- Nishiuchi, R., Murayama, O., Fujiwara, H., Gu, J., Kawakami, T., Aimoto, S., Wada, Y., and Sekiguchi, K. (2003). Characterization of the ligand-binding specificities of integrin alpha3beta1 and alpha6beta1 using a panel of purified laminin isoforms containing distinct alpha chains. *Journal of biochemistry* *134*, 497-504.
- Nistala, H., Lee-Arteaga, S., Smaldone, S., Siciliano, G., Carta, L., Ono, R.N., Sengle, G., Arteaga-Solis, E., Levasseur, R., Ducy, P., *et al.* (2010). Fibrillin-1 and -2 differentially modulate endogenous TGF-beta and BMP bioavailability during bone formation. *J Cell Biol* *190*, 1107-1121.
- Nowak, J.A., Polak, L., Pasolli, H.A., and Fuchs, E. (2008). Hair follicle stem cells are specified and function in early skin morphogenesis. *Cell stem cell* *3*, 33-43.
- O'Hagan, R.C., and Heyer, J. (2011). KRAS Mouse Models: Modeling Cancer Harboring KRAS Mutations. *Genes & cancer* *2*, 335-343.
- Ohashi, T., Kiehart, D.P., and Erickson, H.P. (2002). Dual labeling of the fibronectin matrix and actin cytoskeleton with green fluorescent protein variants. *Journal of cell science* *115*, 1221-1229.

- Okina, E., Manon-Jensen, T., Whiteford, J.R., and Couchman, J.R. (2009). Syndecan proteoglycan contributions to cytoskeletal organization and contractility. *Scandinavian journal of medicine & science in sports* *19*, 479-489.
- Olorundare, O.E., Peyruchaud, O., Albrecht, R.M., and Mosher, D.F. (2001). Assembly of a fibronectin matrix by adherent platelets stimulated by lysophosphatidic acid and other agonists. *Blood* *98*, 117-124.
- Olski, T.M., Noegel, A.A., and Korenbaum, E. (2001). Parvin, a 42 kDa focal adhesion protein, related to the alpha-actinin superfamily. *Journal of cell science* *114*, 525-538.
- Oshimori, N., and Fuchs, E. (2012). Paracrine TGF-beta signaling counterbalances BMP-mediated repression in hair follicle stem cell activation. *Cell stem cell* *10*, 63-75.
- Owens, P., Han, G., Li, A.G., and Wang, X.J. (2008). The role of Smads in skin development. *J Invest Dermatol* *128*, 783-790.
- Oxvig, C., and Springer, T.A. (1998). Experimental support for a beta-propeller domain in integrin alpha-subunits and a calcium binding site on its lower surface. *Proc Natl Acad Sci U S A* *95*, 4870-4875.
- Pankov, R., Cukierman, E., Katz, B.Z., Matsumoto, K., Lin, D.C., Lin, S., Hahn, C., and Yamada, K.M. (2000). Integrin dynamics and matrix assembly: tensin-dependent translocation of alpha(5)beta(1) integrins promotes early fibronectin fibrillogenesis. *J Cell Biol* *148*, 1075-1090.
- Paus, R., and Foitzik, K. (2004). In search of the "hair cycle clock": a guided tour. *Differentiation* *72*, 489-511.
- Pelham, R.J., Jr., and Wang, Y. (1997). Cell locomotion and focal adhesions are regulated by substrate flexibility. *Proc Natl Acad Sci U S A* *94*, 13661-13665.
- Piwko-Czuchra, A., Koegel, H., Meyer, H., Bauer, M., Werner, S., Brakebusch, C., and Fassler, R. (2009). Beta1 integrin-mediated adhesion signalling is essential for epidermal progenitor cell expansion. *PLoS One* *4*, e5488.
- Plikus, M.V., Mayer, J.A., de la Cruz, D., Baker, R.E., Maini, P.K., Maxson, R., and Chuong, C.M. (2008). Cyclic dermal BMP signalling regulates stem cell activation during hair regeneration. *Nature* *451*, 340-344.
- Potten, C.S. (1981). Cell replacement in epidermis (keratopoiesis) via discrete units of proliferation. *International review of cytology* *69*, 271-318.
- Radovanac, K., Morgner, J., Schulz, J.N., Blumbach, K., Patterson, C., Geiger, T., Mann, M., Krieg, T., Eckes, B., Fässler, R., *et al.* (2013). Stabilization of integrin-linked kinase by the Hsp90-CHIP axis impacts cellular force generation, migration and the fibrotic response. *EMBO J* *32*, 1409-1424.

## References

- Ramalho-Santos, M., Yoon, S., Matsuzaki, Y., Mulligan, R.C., and Melton, D.A. (2002). "Stemness": transcriptional profiling of embryonic and adult stem cells. *Science* 298, 597-600.
- Ramirez, A., Page, A., Gandarillas, A., Zanet, J., Pibre, S., Vidal, M., Tusell, L., Genesca, A., Whitaker, D.A., Melton, D.W., *et al.* (2004). A keratin K5Cre transgenic line appropriate for tissue-specific or generalized Cre-mediated recombination. *Genesis* 39, 52-57.
- Ramirez, F., and Dietz, H.C. (2007). Fibrillin-rich microfibrils: Structural determinants of morphogenetic and homeostatic events. *Journal of cellular physiology* 213, 326-330.
- Ramirez, F., and Sakai, L.Y. (2010). Biogenesis and function of fibrillin assemblies. *Cell and tissue research* 339, 71-82.
- Rhee, H., Polak, L., and Fuchs, E. (2006). Lhx2 maintains stem cell character in hair follicles. *Science* 312, 1946-1949.
- Ricard-Blum, S. (2011). The collagen family. *Cold Spring Harb Perspect Biol* 3, a004978.
- Rompolas, P., Mesa, K.R., and Greco, V. (2013). Spatial organization within a niche as a determinant of stem-cell fate. *Nature* 502, 513-518.
- Rousselle, P., and Beck, K. (2013). Laminin 332 processing impacts cellular behavior. *Cell adhesion & migration* 7, 122-134.
- Rudkouskaya, A., Welch, I., and Dagnino, L. (2014). ILK modulates epithelial polarity and matrix formation in hair follicles. *Molecular biology of the cell* 25, 620-632.
- Ryan, M.C., Lee, K., Miyashita, Y., and Carter, W.G. (1999). Targeted disruption of the LAMA3 gene in mice reveals abnormalities in survival and late stage differentiation of epithelial cells. *J Cell Biol* 145, 1309-1323.
- Sakai, T., Larsen, M., and Yamada, K.M. (2003a). Fibronectin requirement in branching morphogenesis. *Nature* 423, 876-881.
- Sakai, T., Li, S., Docheva, D., Grashoff, C., Sakai, K., Kostka, G., Braun, A., Pfeifer, A., Yurchenco, P.D., and Fässler, R. (2003b). Integrin-linked kinase (ILK) is required for polarizing the epiblast, cell adhesion, and controlling actin accumulation. *Genes Dev* 17, 926-940.
- Sarrazin, S., Lamanna, W.C., and Esko, J.D. (2011). Heparan sulfate proteoglycans. *Cold Spring Harb Perspect Biol* 3.
- Scadden, D.T. (2006). The stem-cell niche as an entity of action. *Nature* 441, 1075-1079.
- Schepeler, T., Page, M.E., and Jensen, K.B. (2014). Heterogeneity and plasticity of epidermal stem cells. *Development* 141, 2559-2567.

- Schiller, H.B., and Fässler, R. (2013). Mechanosensitivity and compositional dynamics of cell-matrix adhesions. *EMBO reports* *14*, 509-519.
- Schlake, T. (2007). Determination of hair structure and shape. *Seminars in cell & developmental biology* *18*, 267-273.
- Schmidt-Ullrich, R., and Paus, R. (2005). Molecular principles of hair follicle induction and morphogenesis. *BioEssays : news and reviews in molecular, cellular and developmental biology* *27*, 247-261.
- Schneider, M.R., Schmidt-Ullrich, R., and Paus, R. (2009). The hair follicle as a dynamic miniorgan. *Current biology : CB* *19*, R132-142.
- Schofield, R. (1978). The relationship between the spleen colony-forming cell and the haemopoietic stem cell. *Blood cells* *4*, 7-25.
- Schwarzbauer, J.E., and DeSimone, D.W. (2011). Fibronectins, their fibrillogenesis, and in vivo functions. *Cold Spring Harb Perspect Biol* *3*.
- Sechler, J.L., Cumiskey, A.M., Gazzola, D.M., and Schwarzbauer, J.E. (2000). A novel RGD-independent fibronectin assembly pathway initiated by alpha4beta1 integrin binding to the alternatively spliced V region. *Journal of cell science* *113* ( Pt 8), 1491-1498.
- Sennett, R., and Rendl, M. (2012). Mesenchymal-epithelial interactions during hair follicle morphogenesis and cycling. *Seminars in cell & developmental biology* *23*, 917-927.
- Shi, F., Hu, L., and Edge, A.S. (2013). Generation of hair cells in neonatal mice by beta-catenin overexpression in Lgr5-positive cochlear progenitors. *Proc Natl Acad Sci U S A* *110*, 13851-13856.
- Sick, S., Reinker, S., Timmer, J., and Schlake, T. (2006). WNT and DKK determine hair follicle spacing through a reaction-diffusion mechanism. *Science* *314*, 1447-1450.
- Sinclair, R., Jolley, D., Mallari, R., Magee, J., Tosti, A., Piracinni, B.M., Vincenzi, C., Happle, R., Ferrando, J., Grimalt, R., *et al.* (2003). Morphological approach to hair disorders. *The journal of investigative dermatology Symposium proceedings / the Society for Investigative Dermatology, Inc [and] European Society for Dermatological Research* *8*, 56-64.
- Soriano, P. (1999). Generalized lacZ expression with the ROSA26 Cre reporter strain. *Nat Genet* *21*, 70-71.
- Sotiropoulou, P.A., Candi, A., Mascré, G., De Clercq, S., Youssef, K.K., Lapouge, G., Dahl, E., Semeraro, C., Denecker, G., Marine, J.C., *et al.* (2010). Bcl-2 and accelerated DNA repair mediates resistance of hair follicle bulge stem cells to DNA-damage-induced cell death. *Nature cell biology* *12*, 572-582.
- Stanchi, F., Grashoff, C., Nguemeni Yonga, C.F., Grall, D., Fässler, R., and Van Obberghen-Schilling, E. (2009). Molecular dissection of the ILK-PINCH-parvin triad

## References

- reveals a fundamental role for the ILK kinase domain in the late stages of focal-adhesion maturation. *Journal of cell science* *122*, 1800-1811.
- Steinert, P.M., and Marekov, L.N. (1995). The proteins elafin, filaggrin, keratin intermediate filaments, loricrin, and small proline-rich proteins 1 and 2 are isodipeptide cross-linked components of the human epidermal cornified cell envelope. *J Biol Chem* *270*, 17702-17711.
- Stephens, L.E., Sutherland, A.E., Klimanskaya, I.V., Andrieux, A., Meneses, J., Pedersen, R.A., and Damsky, C.H. (1995). Deletion of beta 1 integrins in mice results in inner cell mass failure and peri-implantation lethality. *Genes Dev* *9*, 1883-1895.
- Stiegler, A.L., Grant, T.D., Luft, J.R., Calderwood, D.A., Snell, E.H., and Boggon, T.J. (2013). Purification and SAXS analysis of the integrin linked kinase, PINCH, parvin (IPP) heterotrimeric complex. *PLoS One* *8*, e55591.
- Sugawara, K., Tsuruta, D., Kobayashi, H., Ikeda, K., Hopkinson, S.B., Jones, J.C., and Ishii, M. (2007). Spatial and temporal control of laminin-332 (5) and -511 (10) expression during induction of anagen hair growth. *The journal of histochemistry and cytochemistry : official journal of the Histochemistry Society* *55*, 43-55.
- Tamkun, J.W., DeSimone, D.W., Fonda, D., Patel, R.S., Buck, C., Horwitz, A.F., and Hynes, R.O. (1986). Structure of integrin, a glycoprotein involved in the transmembrane linkage between fibronectin and actin. *Cell* *46*, 271-282.
- Tateishi, C., Tsuruta, D., Sugawara, K., Yoshizato, K., Imanishi, H., Nishida, K., Ishii, M., and Kobayashi, H. (2010). Spatial and temporal control of laminin-511 and -332 expressions during catagen. *J Dermatol Sci* *58*, 55-63.
- Terpstra, L., Prud'homme, J., Arabian, A., Takeda, S., Karsenty, G., Dedhar, S., and St-Arnaud, R. (2003). Reduced chondrocyte proliferation and chondrodysplasia in mice lacking the integrin-linked kinase in chondrocytes. *J Cell Biol* *162*, 139-148.
- Tiedemann, K., Sasaki, T., Gustafsson, E., Gohring, W., Batge, B., Notbohm, H., Timpl, R., Wedel, T., Schlotzer-Schrehardt, U., and Reinhardt, D.P. (2005). Microfibrils at basement membrane zones interact with perlecan via fibrillin-1. *J Biol Chem* *280*, 11404-11412.
- Tomasek, J.J., Gabbiani, G., Hinz, B., Chaponnier, C., and Brown, R.A. (2002). Myofibroblasts and mechano-regulation of connective tissue remodelling. *Nature reviews Molecular cell biology* *3*, 349-363.
- Torkamani, N., Rufaut, N.W., Jones, L., and Sinclair, R.D. (2014). Beyond goosebumps: does the arrector pili muscle have a role in hair loss? *International journal of trichology* *6*, 88-94.
- Tseng, Q., Wang, I., Duchemin-Pelletier, E., Azioune, A., Carpi, N., Gao, J., Filhol, O., Piel, M., Thery, M., and Balland, M. (2011). A new micropatterning method of soft substrates reveals that different tumorigenic signals can promote or reduce cell contraction levels. *Lab on a chip* *11*, 2231-2240.

- Tu, Y., Huang, Y., Zhang, Y., Hua, Y., and Wu, C. (2001). A new focal adhesion protein that interacts with integrin-linked kinase and regulates cell adhesion and spreading. *J Cell Biol* 153, 585-598.
- Turksen, K., Kupper, T., Degenstein, L., Williams, I., and Fuchs, E. (1992). Interleukin 6: insights to its function in skin by overexpression in transgenic mice. *Proc Natl Acad Sci U S A* 89, 5068-5072.
- Vaezi, A., Bauer, C., Vasioukhin, V., and Fuchs, E. (2002). Actin cable dynamics and Rho/Rock orchestrate a polarized cytoskeletal architecture in the early steps of assembling a stratified epithelium. *Dev Cell* 3, 367-381.
- van Genderen, C., Okamura, R.M., Farinas, I., Quo, R.G., Parslow, T.G., Bruhn, L., and Grosschedl, R. (1994). Development of several organs that require inductive epithelial-mesenchymal interactions is impaired in LEF-1-deficient mice. *Genes Dev* 8, 2691-2703.
- Vicente-Manzanares, M., and Horwitz, A.R. (2011). Adhesion dynamics at a glance. *Journal of cell science* 124, 3923-3927.
- Vidal, V.P., Chaboissier, M.C., Lutzkendorf, S., Cotsarelis, G., Mill, P., Hui, C.C., Ortonne, N., Ortonne, J.P., and Schedl, A. (2005). Sox9 is essential for outer root sheath differentiation and the formation of the hair stem cell compartment. *Current biology : CB* 15, 1340-1351.
- Wang, H.V., Chang, L.W., Brixius, K., Wickström, S.A., Montanez, E., Thievensen, I., Schwander, M., Muller, U., Bloch, W., Mayer, U., *et al.* (2008). Integrin-linked kinase stabilizes myotendinous junctions and protects muscle from stress-induced damage. *J Cell Biol* 180, 1037-1049.
- Watt, F.M., and Fujiwara, H. (2011). Cell-extracellular matrix interactions in normal and diseased skin. *Cold Spring Harb Perspect Biol* 3.
- Watt, F.M., and Green, H. (1982). Stratification and terminal differentiation of cultured epidermal cells. *Nature* 295, 434-436.
- Wennerberg, K., Lohikangas, L., Gullberg, D., Pfaff, M., Johansson, S., and Fassler, R. (1996). Beta 1 integrin-dependent and -independent polymerization of fibronectin. *J Cell Biol* 132, 227-238.
- Wickström, S.A., Lange, A., Montanez, E., and Fässler, R. (2010). The ILK/PINCH/parvin complex: the kinase is dead, long live the pseudokinase! *EMBO J* 29, 281-291.
- Wickström, S.A., Radovanac, K., and Fässler, R. (2011). Genetic analyses of integrin signaling. *Cold Spring Harb Perspect Biol* 3.
- Winter, H., and Schweizer, J. (1983). Keratin synthesis in normal mouse epithelia and in squamous cell carcinomas: evidence in tumors for masked mRNA species coding for high molecular weight keratin polypeptides. *Proc Natl Acad Sci U S A* 80, 6480-6484.

## References

- Yamaji, S., Suzuki, A., Sugiyama, Y., Koide, Y., Yoshida, M., Kanamori, H., Mohri, H., Ohno, S., and Ishigatsubo, Y. (2001). A novel integrin-linked kinase-binding protein, affixin, is involved in the early stage of cell-substrate interaction. *J Cell Biol* *153*, 1251-1264.
- Yan, D., and Lin, X. (2009). Shaping morphogen gradients by proteoglycans. *Cold Spring Harb Perspect Biol* *1*, a002493.
- Yang, J.T., Bader, B.L., Kreidberg, J.A., Ullman-Cullere, M., Trevithick, J.E., and Hynes, R.O. (1999). Overlapping and independent functions of fibronectin receptor integrins in early mesodermal development. *Developmental biology* *215*, 264-277.
- Yang, J.T., Rayburn, H., and Hynes, R.O. (1993). Embryonic mesodermal defects in alpha 5 integrin-deficient mice. *Development* *119*, 1093-1105.
- Yang, J.T., Rayburn, H., and Hynes, R.O. (1995). Cell adhesion events mediated by alpha 4 integrins are essential in placental and cardiac development. *Development* *121*, 549-560.
- Yang, Y., Wang, X., Hawkins, C.A., Chen, K., Vaynberg, J., Mao, X., Tu, Y., Zuo, X., Wang, J., Wang, Y.X., *et al.* (2009). Structural basis of focal adhesion localization of LIM-only adaptor PINCH by integrin-linked kinase. *J Biol Chem* *284*, 5836-5844.
- Yu, H., and Talts, J.F. (2003). Beta1 integrin and alpha-dystroglycan binding sites are localized to different laminin-G-domain-like (LG) modules within the laminin alpha5 chain G domain. *Biochem J* *371*, 289-299.
- Yurchenco, P.D. (2011). Basement membranes: cell scaffoldings and signaling platforms. *Cold Spring Harb Perspect Biol* *3*.
- Yurchenco, P.D., Quan, Y., Colognato, H., Mathus, T., Harrison, D., Yamada, Y., and O'Rear, J.J. (1997). The alpha chain of laminin-1 is independently secreted and drives secretion of its beta- and gamma-chain partners. *Proc Natl Acad Sci U S A* *94*, 10189-10194.
- Zaidel-Bar, R., and Geiger, B. (2010). The switchable integrin adhesome. *Journal of cell science* *123*, 1385-1388.
- Zaidel-Bar, R., Itzkovitz, S., Ma'ayan, A., Iyengar, R., and Geiger, B. (2007). Functional atlas of the integrin adhesome. *Nature cell biology* *9*, 858-867.
- Zamir, E., and Geiger, B. (2001). Molecular complexity and dynamics of cell-matrix adhesions. *Journal of cell science* *114*, 3583-3590.
- Zamir, E., Katz, M., Posen, Y., Erez, N., Yamada, K.M., Katz, B.Z., Lin, S., Lin, D.C., Bershadsky, A., Kam, Z., *et al.* (2000). Dynamics and segregation of cell-matrix adhesions in cultured fibroblasts. *Nature cell biology* *2*, 191-196.
- Zervas, C.G., Gregory, S.L., and Brown, N.H. (2001). *Drosophila* integrin-linked kinase is required at sites of integrin adhesion to link the cytoskeleton to the plasma membrane. *J Cell Biol* *152*, 1007-1018.

- Zhang, Y., Chen, K., Tu, Y., Velyvis, A., Yang, Y., Qin, J., and Wu, C. (2002). Assembly of the PINCH-ILK-CH-ILKBP complex precedes and is essential for localization of each component to cell-matrix adhesion sites. *Journal of cell science* *115*, 4777-4786.
- Zhang, Y., Yu, J., Shi, C., Huang, Y., Wang, Y., Yang, T., and Yang, J. (2013). Lef1 contributes to the differentiation of bulge stem cells by nuclear translocation and cross-talk with the Notch signaling pathway. *International journal of medical sciences* *10*, 738-746.
- Zhu, J., Luo, B.H., Xiao, T., Zhang, C., Nishida, N., and Springer, T.A. (2008). Structure of a complete integrin ectodomain in a physiologic resting state and activation and deactivation by applied forces. *Mol Cell* *32*, 849-861.

## Appendix

Primer sequences used for qRT-PCR

Gene/oligo	Sequence 5' – 3'	Amplicon length (bp)
mβAct fw	TCAAGATCATTGCTC	106
mβAct rev	TACTTCTGCTTGCTGATCCAC	
mAxin2 fw	AGCGCCAACGACAGCGAGTT	188
mAxin2 rev	AGGCGGTGGGTTCTCGGAAA	
mBambi fw	CTTTGGAATGCTGTCACGAA	149
mBambi rev	GGAAGTCAGCTCCTGCATCT	
mBgn fw	TCCGCACTCCAACAACATCA	204
mBgn rev	GGCAACCACTGCCTCTACTT	
mCD44 fw	AGCCCTCCTGAAGAAGACT	116
mCD44 rev	ACTCGCCCTTCTTGCTGTAG	
mDkk3 fw	ATGCTATGCACCCGAGACAG	159
mDkk3 rev	GAACAGCAGGCCTCTTTGGA	
mGrem1 fw	CCACGGAAGTGACAGAATGA	141
mGrem1 rev	TTGTGCTGAGCCTTGTCAGG	
mId2 fw	ATCCCCAGAACAAGAAGGT	128
mId2 rev	TGTCCAGGTCTCTGGTGATG	
mIL1b fw	CGACCCCAAAGATGAAGGGCTGC	99
mIL1b rev	GCTCTTGTTGATGTGCTGCTGCG	
mIL6 fw	ACACATGTTCTCTGGGAAATC	84
mIL6 rev	AAGTGCATCATCGTTGTTTCATACA	
mLef1 fw	CGGAACCTGCGCCACCGAT	177
mLef1 rev	TGACCACCTCATGCCCGTTGC	
mLhx2 fw	CCTACTACAACGGCGTGGGCACTGT	137
mLhx2 rev	GTCACGATCCAGGTGTTTCAGCATCG	
mLgr5 fw	CCAATGGAATAAAGACGACGGCAACA	128
mLgr5 rev	GGGCCTTCAGGTCTTCTCAAAGTCA	
mNfatc1 fw	GGTGCTGTCTGGCCATAACT	128
mNfatc1 rev	CCAGGGAATTTGGCTTGCAC	
mp21 fw	GGCAGACCAGCCTGACAGAT	69
mp21 rev	TTCAGGGTTTTCTCTTGCAGAAG	
mPai1 fw	GACACCCTCAGCATGTTCATC	218
mPai1 rev	AGGGTTGCACTAAACATGTCAG	
mS26 fw	CGTCTTCGACGCCTACGTGCT	180
mS26 rev	CGGCCTCTTACATGGGCTTTGGT	
mSfrp1 fw	GCAAGCGAGTTTGCCTGAGGATGA	101
mSfrp1 rev	GGCCCAGCTTCAAGGGTTTCTTCT	
mTcf3 fw	CTCAGCAGCAAATCCAAGAGGCAGAG	109
mTcf3 rev	TGGGAAGACGCAGGGCTATCACAAG	
mTgfb1 fw	ACCCTGCCCCTATATTTGGA	63
mTgfb1 rev	TGGTTGTAGAGGGCAAGGAC	
mTNFa fw	GACCCTCACACTCAGATCATCTTCT	80
mTNFa rev	CCTCCACTTGGTGGTTTGCT	

## Abbreviations

AdMIDAS	adjacent to MIDAS
Akt	RAC-alpha serine/threonineprotein kinase
ANK	ankyrin repeat
Arp2/3	actin related protein 2/3complex
Axin2	axis inhibition protein 2
Bgn	biglycan
BrdU	5-bromo-2'-deoxyuridine
Cdc42	cell division cycle 42
CH	calponin homology
Cre	cyclization recombinase
Ctgf	connective tissue growth factor
Col	collagen
DAG	diacylglycerol
Dkk3	Dickkopf 3
DMBA	7,12-Dimethylbenz(a)anthracene
E	embryonic day
ECM	extracellular matrix
EdU	5-ethynyl-2'-deoxyuridine
EGF	epidermal growth factor
EGFP	Enhanced Green Fluorescent Protein
EGFR	epidermal growth factor receptor
ERK	extracellular signal-regulated kinase
FA	focal adhesion
FB	fibrillar adhesion

FC	focal complex
FN	fibronectin
FAK	focal adhesion kinase
GAP	GTP-ase activating protein
GEF	guanine nucleotide exchange factor
GPCRs	G proteins coupled receptors
GSK3 $\beta$	glycogen synthase kinase 3 $\beta$
HF	hair follicle
Id2	inhibitor of differentiation 2
IF	immunofluorescence
Ig	immunoglobulin
IL	interleukin
ILK	integrin linked kinase
IPP	ILK-PINCH-Parvin
IP3	inositol triphosphate
JAK	Janus kinase
K	keratin
KD	kinase domain
LAP	latency-associated peptide
Lhx2	LIM homeobox protein 2
LEF	lymphoid enhancer-binding factor
Lgr 5	leucine-rich repeat-containing G-protein coupled receptor 5
LN	laminin
LTBP	latent TGF- $\beta$ binding protein
MAPK	mitogen-activated protein kinase

MIDAS	metal-ion-dependent adhesion site
MLC	myosin light chain
MMP	matrix metalloproteinase
NFATc1	nuclear factor of activated T cells cytoplasmic 1
P	postnatal day
pFAK	phosphoFAK
Pai-1	plasmonogen activator inhibitor-1
PI3K	phosphatidylinositol 3-kinase
PINCH	Particularly interesting new Cys-His protein
PKC	protein kinase C
PH	pleckstrin homology
PLC	phospholipase C
PtdIns	phosphatidylinositol
PtdIns-4,5-P2	PtdIns4,5-bisphosphate
Rac1	ras-related C3 botulinum toxin substrate 1
Rap1	RAS-related protein-1
Ras	rat sarcoma viral oncogene homolog
rcf	relative centrifugal force
RGD	arginine, glycine, aspartate
RhoA	ras homolog gene family, member A
RIAM	Rap1-interacting adaptor molecule
ROCK	Rho-associated protein kinase
rpm	rounds per minute
RSU1	Ras suppressor protein 1
RT	room temperature

SC	stem cell
Sfrp1	secreted frizzled related protein 1
Smad	Similar to mothers against decapentaplegic
Sox 9	(sex determining region Y)-box 9
Src	Rous sarcoma oncogene
SyMBS	synergistic metal ion binding site
TCF	T cell-specific transcription factor
TGF- $\beta$	transforming growth factor $\beta$
TESK1	testis-specific kinase 1
TPA	12- <i>O</i> -Tetradecanoylphorbol-13-acetate
WASP	Wiscott-Aldrich Syndrome protein
WAVE	WASP-family verprolin homologue
Wnt	wingless-type MMTV integration site family member

## Acknowledgements

This thesis would have never been possible without the support of many people.

First of all, I would like to thank Dr. Sara Wickström for her great supervision, for giving me the opportunity to work on interesting projects and for the great experience to set up a new lab and to see how a group grows together.

I would like to thank Dr. Matthias Hammerschmidt, Dr. Mats Paulsson and Dr. Beate Eckes for being my PhD committee. I thank Dr. Monique Aumailley for her support on this project.

I want to express my gratitude to all present and former lab members of the Wickström lab. Thanks to Torsten Bücher, Kristina Behrendt and Juliana Du for sharing the good and bad times of everyday lab life. I would like to thank Sushmita Ghatak for cheering me up and celebrating the glorious moments, Huy Le Quang for making working at weekends a good time, Carlos Chacon for balancing me with his tranquility, David Schneider for bringing me closer to the “nerd world”, Chloé Yeung for bringing joy inside and outside the lab and her great help while writing this thesis.

I would like to thank the members of the Department for Dermatology at the University of Cologne, which gave me a warm and easy welcome, and I am proud to call some of them my friends.

I would like to thank the members of the Niessen lab and Iden lab for adopting our lab for science and fun times.

I am grateful to my friends and family who were accepting of all my excuses and forgiving me every time that I spent in lab instead of being with them.

However, the absolutely utmost and without any doubts most unselfish support was provided by my partner, Eva, and there are not enough words that are able to express my deepest gratitude to her!

## **Publications**

Radovanac, K.\*, Morgner, J.\*, Schulz, J.N., Blumbach, K., Patterson, C., Geiger, T., Mann, M., Krieg, T., Eckes, B., Fässler, R., and S. A. Wickström (2013). Stabilization of integrin- linked kinase by the Hsp90-CHIP axis impacts cellular force generation, migration and the fibrotic response. *EMBO J* 32, 1409-1424.

Morgner, J. and S. A. Wickström (2013). "The weakest link: a new paradigm for stabilizing the integrin-actin connection." *Cell Cycle* 12(18): 2929-2930.

Ghatak, S., Morgner, J., and Wickström, S.A. (2013). ILK: a pseudokinase with a unique function in the integrin-actin linkage. *Biochem Soc Trans* 41, 995-1001.

## **Erklärung**

Ich versichere, dass ich die von mir vorgelegte Dissertation selbständig angefertigt, die benutzten Quellen und Hilfsmittel vollständig angegeben und die Stellen der Arbeit – einschließlich Tabellen, Karten und Abbildungen –, die anderen Werken im Wortlaut oder dem Sinn nach entnommen sind, in jedem Einzelfall als Entlehnung kenntlich gemacht habe; dass diese Dissertation noch keiner anderen Fakultät oder Universität zur Prüfung vorgelegen hat; dass sie – abgesehen von unten angegebenen Teilpublikationen – noch nicht veröffentlicht worden ist sowie, dass ich eine solche Veröffentlichung vor Abschluss des Promotionsverfahrens nicht vornehmen werde. Die Bestimmungen der Promotionsordnung sind mir bekannt. Die von mir vorgelegte Dissertation ist von Frau Dr. Sara A. Wickström betreut worden.

Köln, den

# Lebenslauf

---

## Persönliche Angaben

Name: Jessica Morgner  
Geburtsort/ Geburtstag: Düsseldorf, den 22. Februar 1980  
Nationalität: deutsch

---

## Schulbildung

1986 – 1990 Gemeinschaftsgrundschule Knittkuhl, Düsseldorf  
1990 – 1999 Gymnasium Gerresheim, Düsseldorf; Allgemeine Hochschulreife (Abitur)

## Ausbildung

08/1999 – 06/2002 **Ausbildung zur Chemielaborantin**  
Schwarz Pharma AG, Monheim am Rhein  
07/2002 – 09/2005 **Chemielaborantin**  
Schwarz BioSciences, Monheim am Rhein, Abteilung Medicinal Chemistry

## Studium

10/2005 – 09/2008 **Bachelor of Science In Medizinische Biologie**  
Universität Duisburg-Essen, Bachelorarbeit in der Abteilung Entwicklungsbiologie, Prof. Andrea Vortkamp, Universität Duisburg-Essen  
10/2008-09/2010 **Master of Science in Medizinische Biologie**  
Universität Duisburg-Essen, Masterarbeit am Institut für Zellbiologie, Arbeitsgruppe Molecular Cell Biology, Prof. Verena Jendrossek, Universität Duisburg-Essen  
Seit 10/2010 **Doktorarbeit**  
Max Planck Institut für Biologie des Alterns unter der Anleitung von Dr. Sara A. Wickström  
Thema: „Role of Integrin-linked kinase in extracellular matrix remodeling and cell fate decisions“

## Publikationen

Morgner, J. and S. A. Wickstrom (2013). "The weakest link: a new paradigm for stabilizing the integrin-actin connection." Cell Cycle 12(18): 2929-2930.

Ghatak, S., Morgner, J., and Wickstrom, S.A. (2013). ILK: a pseudokinase with a unique function in the integrin-actin linkage. Biochem Soc Trans 41, 995-1001.

Traub, S., Morgner, J., Martino, M.M., Honing, S., Swartz, M.A., Wickstrom, S.A., Hubbell, J.A., and Eming, S.A. (2013). The promotion of endothelial cell attachment and spreading using FNIII10 fused to VEGF-A165. *Biomaterials* 34, 5958-5968.

Radovanac, K.\*, Morgner, J.\*, Schulz, J.N., Blumbach, K., Patterson, C., Geiger, T., Mann, M., Krieg, T., Eckes, B., Fassler, R., et al. (2013). Stabilization of integrin-linked kinase by the Hsp90-CHIP axis impacts cellular force generation, migration and the fibrotic response. *EMBO J* 32, 1409-1424.

Kessler, D., Gruen, G.C., Heider, D., Morgner, J., Reis, H., Schmid, K.W., and Jendrossek, V. (2012). The action of small GTPases Rab11 and Rab25 in vesicle trafficking during cell migration. *Cell Physiol Biochem* 29, 647-656.

Schroder, E., Gebel, L., Ereemeev, A.A., Morgner, J., Grum, D., Knauer, S.K., Bayer, P., and Mueller, J.W. (2012). Human PAPS synthase isoforms are dynamically regulated enzymes with access to nucleus and cytoplasm. *PLoS One* 7, e29559.

\* these authors contributed equally to this work